Re-Assessment of the Late Jurassic Eusauropod Dinosaur Hudiesaurus sinojapanorum Dong, 1997, from the Turpan Basin, China, and the Evolution of Hyper-Robust Antebrachia in Sauropods

Authors: Upchurch, Paul, Mannion, Philip D., Xu, Xing, and Barrett, Paul M.

Check for updates

ARTICLE

RE-ASSESSMENT OF THE LATE JURASSIC EUSAUROPOD DINOSAUR *HUDIESAURUS SINOJAPANORUM* DONG, 1997, FROM THE TURPAN BASIN, CHINA, AND THE EVOLUTION OF HYPER-ROBUST ANTEBRACHIA IN SAUROPODS

PAUL UPCHURCH, [1*] PHILIP D. MANNION, [1] XING XU,[2,3] and PAUL M. BARRETT [1,4]
[1]Department of Earth Sciences, University College London, Gower Street, London WC1E 6BT, U.K., p.upchurch@ucl.ac.uk,
philipdmannion@gmail.com;
[2]Key Laboratory of Evolutionary Systematics of Vertebrates, Institute of Vertebrate Paleontology & Paleoanthropology, Chinese
Academy of Sciences, Beijing 100044, China, xu.xing@ivpp.ac.cn;
[3]CAS Center of Excellence in Life and Paleoenvironment, Beijing, 100044, China;
[4]Department of Earth Sciences, Natural History Museum, Cromwell Road, London SW7 5BD, U.K., p.barrett@nhm.ac.uk

ABSTRACT—*Hudiesaurus sinojapanorum* is a Late Jurassic sauropod from northwestern China that was erected on the basis of a cervicodorsal vertebra, four teeth, and a nearly complete forelimb. However, re-evaluation of this material, and comparisons with other taxa, indicate that there are few grounds for regarding these specimens as congeneric. Consequently, although we retain the vertebra as the holotype specimen of *Hudiesaurus*, the forelimb is assigned to a new taxon—*Rhomaleopakhus turpanensis*, gen. et sp. nov. The teeth previously referred to *Hudiesaurus* are poorly preserved but resemble those of several other 'core *Mamenchisaurus*-like taxa' (CMTs) from East Asia, such as *Mamenchisaurus sinocanadorum*. Phylogenetic analyses confirm that *Hudiesaurus* is a CMT and the sister taxon of *Xinjiangtitan*. Despite some uniquely shared features, their large size, and close geographic provenance, *Hudiesaurus* and *Xinjiangtitan* are retained as distinct genera based on their stratigraphic separation and numerous anatomical differences. *Rhomaleopakhus* is also shown to be a CMT in all analyses, being most closely related to *Chuanjiesaurus* and *Analong*. We link the convergent evolution of robust antebrachia and an enlarged olecranon in CMTs, titanosaurs, and some ornithischians (e.g., ceratopsids) to a more flexed orientation of the forearm, an enhanced role for the forelimb in locomotion, and an anterior shift in the whole-body center of mass. CMTs and titanosaurs potentially converged on a feeding strategy in which the ability to increase browse height via bipedal rearing was sacrificed in return for more efficient locomotion that improved travel between patchily distributed food sources.

http://zoobank.org/urn:lsid:zoobank.org:pub:A42348FE-ECE6-4524-B536-857AFFD22DB2

SUPPLEMENTAL DATA—Supplemental materials are available for this article for free at www.tandfonline.com/UJVP.

Citation for this article: Upchurch, P., P. D. Mannion, X. Xu, and P. M. Barrett. 2021. Re-assessment of the Late Jurassic eusauropod dinosaur *Hudiesaurus sinojapanorum* Dong, 1997, from the Turpan Basin, China, and the evolution of hyper-robust antebrachia in sauropods. Journal of Vertebrate Paleontology. DOI: 10.1080/02724634.2021.1994414

INTRODUCTION

The Kalazha Formation (also referred to as the Karaza, Kalaza, or Hongshan Formation; see Dong [1992] and Eberth et al. [2001]) is exposed in the Qiketai (sometimes referred to as Qiketia or Qikatai) area of Shanshan County, Turpan Basin, Xinjiang Uyghur Autonomous Region, in northwestern China (Zhao, 1980; Dong, 1992, 1997) (Fig. 1). This unit comprises thick red sandstones and mudstones deposited in a terrestrial (possibly fluvial) environment. The formation has been suggested to be Late Jurassic in age, based on invertebrate remains (Zhao, 1980; Dong, 1992) and, more

specifically, late Kimmeridgian–Tithonian based on regional stratigraphic correlations and sedimentology (Eberth et al., 2001; Deng et al., 2015; Fang et al., 2016; N.B., these studies examined the Kalazha Formation in the Junggar Basin, north of the Turpan Basin). This part of the Turpan Basin, in Qiketai, has yielded the remains of several different dinosaurs, including a sauropod tooth originally described as '*Chiayusaurus lacustris*' (Bohlin, 1953) (now regarded as Eusauropoda indet.; Barrett et al., 2002) and part of a left maxilla of a 'megalosaurid', although it is uncertain which bed yielded the latter specimen (Dong, 1992). New sauropod material was collected from the Kalazha Formation in 1993 as part of the Sino-Japanese Silk Road Dinosaur Expedition (Dong, 1997). This material consists of a presacral vertebra (IVPP V11120), a complete right forelimb (IVPP V11121-1), and four teeth (IVPP V11121-2). Dong (1997) proposed the name *Hudiesaurus sinojapanorum*, with the vertebra designated as the holotype, and referred the teeth and forelimb to this taxon, despite these elements coming from different locations and having no anatomical overlap between them. The generic name was derived from 'Hudie' (the Mandarin Pinyin for butterflies, reflecting the purported 'wing'-like processes on the neural
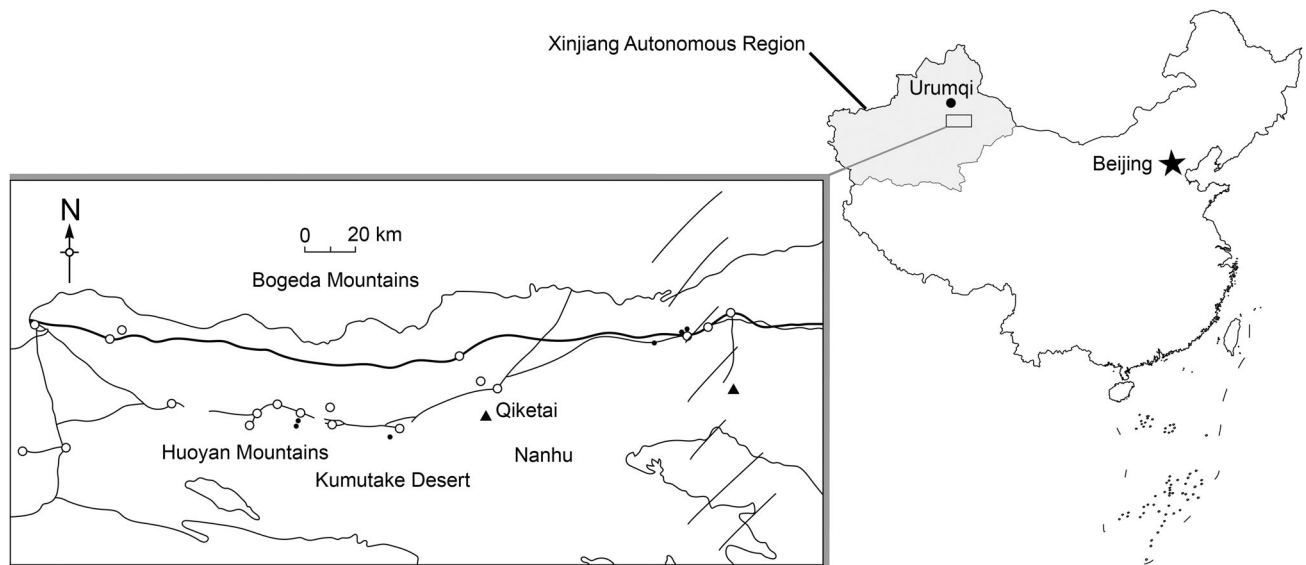
FIGURE 1. Map showing Xinjiang Autonomous Region in China, with a magnified inset showing the approximate location of the *Hudiesaurus* specimens within Shanshan County.

spine) and the specific name was in honor of the expedition. Dong (1997) provided a diagnosis and description of the material, and referred it to Mamenchisauridae Young and Zhao, 1972 based on a few similarities with other members of that family (see also Maisch and Matzke, 2019). Dong (1997) also estimated the body length of the animal to have been 29–30 m, which would have made it the largest sauropod known from Asia at that time.

Hudiesaurus has been overlooked by many systematic studies, despite a growing record of 'core *Mamenchisaurus*-like taxa' (CMTs, see below and definition in Moore et al., 2020) from the Jurassic–Early Cretaceous of East Asia (e.g., Wu et al., 2013; Xing et al., 2015). To date, no phylogenetic analysis has included *Hudiesaurus* and it has been considered as Eusauropoda incertae sedis (Upchurch et al., 2004a). Here, we re-describe this material, present photographs to supplement those provided by Dong (1997), revise the taxonomy and nomenclature of *Hudiesaurus*, evaluate the phylogenetic affinities of each of the specimens, and examine the potential function and ecological significance of robust antebrachia in CMTs and other sauropods. We propose that the taxon proposed by Dong (1997) is a chimera and assign the referred forelimb to a new sauropod taxon.

Anatomical Abbreviations—We use the nomenclature and abbreviations for vertebral laminae and fossae proposed by Wilson (1999) and Wilson et al. (2011), with some additions and modifications. Namely, we follow Tschopp and Mateus (2013) in preferring 'interprezygapophyseal lamina' and 'interpostzygapophyseal lamina' rather than Wilson's (1999) 'intraprezygapophyseal lamina' and 'intrapostzygapophyseal lamina'. Anatomical abbreviations are either listed here, defined on first usage in the text, or as required in the figure legends. **Cv**, cervical vertebra; **Dv**, dorsal vertebra.

Institutional Abbreviations—**CCG**, Chengdu University of Technology, Chengdu, China; **CM**, Carnegie Museum of Natural History, Pittsburgh, Pennsylvania, U.S.A.; **CPT**, Museo de la Fundación Conjunto Paleontológico de Teruel-Dinópolis, Teruel, Spain; **IVPP**, Institute of Vertebrate Paleontology and Paleoanthropology, Beijing, China; **MfN**, Museum für Naturkunde, Berlin, Germany; **MNN**, Musée National du Niger, Niger (specimens mentioned in this work with this institutional abbreviation are currently housed at the University of Chicago); **NHMUK**, Natural History Museum, London, United Kingdom; **UNPSJB-PV**, Universidad Nacional de la Patagonia 'San Juan Bosco'- Paleovertebrados, Comodoro Rivadavia, Argentina; **USNM**, United States National Museum of Natural History, Smithsonian Institution, Washington D.C., U.S.A.; **ZDM**, Zigong Dinosaur Museum, Zigong, China.

Other Abbreviations—**CMT**, core *Mamenchisaurus*-like taxa (sensu Moore et al., 2020, see below); **EIW**, extended implied weighting; **EWP**, equal weights parsimony; **MPT**, most parsimonious tree; **OTU**, operational taxonomic unit.

A NOTE ON THE TERM 'MAMENCHISAURIDAE'

Although its exact constituents and nomenclature are debated, most workers recognize the presence of a monophyletic group of predominantly Middle and Late Jurassic East Asian non-neosauropod eusauropods that includes *Mamenchisaurus* (e.g., Upchurch, 1998; Wilson, 2002; Upchurch et al., 2004a; Sekiya, 2011; Xing et al., 2015; Xu et al., 2018; Mannion et al., 2019a; Moore et al., 2020). Such taxa have typically been assigned to the family Mamenchisauridae and include several genera with an increased number of cervical vertebrae (usually 16–18) relative to most other sauropods (Young and Chao, 1972; Sekiya, 2011; Xing et al., 2015; Moore et al., 2020). Given the provenance of *Hudiesaurus*, and a preliminary survey of its anatomy, our starting hypothesis is that the specimens belong to Mamenchisauridae, and this is reflected in our focus on comparisons with other 'mamenchisaurids' and sauropods from the Jurassic of East Asia generally. Moore et al. (2020) noted a systematic problem created by the definition of this clade name in conjunction with the phylogenetic topologies favored by that study. The type species of *Mamenchisaurus* (*M. constructus*) often fell outside of the clade that contained most other typical *Mamenchisaurus*-like taxa, including several species of *Mamenchisaurus* (e.g., *M. hochuanensis*, *M. youngi*), *Klamelisaurus*, and *Qijianglong*. As an interim measure pending further work, Moore et al. (2020) used the term 'core *Mamenchisaurus*-like taxa' (CMTs) to refer to this group rather than introduce a new name, and we follow this practice in our main text here. However, in our Systematic Paleontology sections, we continue to use the term Mamenchisauridae because we do not wish to

list 'core *Mamenchisaurus*-like taxon' as part of a formal taxonomic hierarchy.

COMMENTS ON THE ASSOCIATION AND PROVENANCE OF THE *HUDIESAURUS* SPECIMENS

Xing et al. (2015) suggested that *Hudiesaurus* was recovered from the Middle Jurassic Qigu Formation, and cited Wings et al. (2011, 2012) in support of this contention. However, although Wings et al. (2011) mentioned the Qigu Formation in the Junggar Basin in passing, they did not discuss the provenance of *Hudiesaurus*. Wings et al. (2012) noted that the Qigu Formation has been dated at ~164.6 Ma in the Junggar Basin (Wang and Gao, 2012); however, the former study also pointed out that there is currently no explicit evidence that the putative outcrops of the Qigu Formation in the Turpan Basin correlate with those in the Junggar Basin (N.B., the same issue also affects correlation of the Kalazha Formation across these two basins). We have not been able to establish the basis for Xing et al.'s (2015) assertion that the *Hudiesaurus* specimens were found in the Qigu rather than the Kalazha Formation, and the former formation has been regarded as Late Jurassic (Oxfordian–early Kimmeridgian) by more recent studies (Deng et al., 2015; Fang et al., 2016; Maisch and Matzke, 2019). In short, the evidence that the Qigu Formation in the Turpan Basin is late Middle Jurassic in age must be regarded as somewhat tentative and, currently, no evidence for *Hudiesaurus* having been recovered from this formation has been presented. We therefore regard *Hudiesaurus* and the other sauropod specimens described by Dong (1997) as occurring in the latest Jurassic Kalazha Formation, as originally suggested, pending further discoveries and stratigraphic work.

Before re-describing and re-evaluating the specimens assigned to *Hudiesaurus* (sensu Dong, 1997), it is necessary to determine whether all of this material belongs to a single taxon. Although the right forelimb was apparently collected from the same horizon as the holotypic vertebra of *Hudiesaurus*, Dong (1997:104) stated that " … the quarry [that yielded the forelimb] is about 1.1 km from the quarry of the type specimen." Moreover, he noted that " … the four teeth were also found in the same beds yielding the forelimb," although he did not elaborate on whether they were found in association with these specimens. The history of sauropod discoveries during the past 200 years presents numerous examples where isolated, fragmentary specimens from the same horizon have been assigned to a single genus or species, which have been shown subsequently to belong to a variety of distinct, distantly related taxa (e.g., the taxonomic histories of Morrison Formation sauropods—Ostrom and McIntosh [1966]; material referred to *Cetiosaurus*—Upchurch and Martin [2003]; and British Wealden sauropods—Upchurch et al. [2011, 2015]). In order to avoid the creation of chimeric taxa, the referral of material from distant localities should be based on the presence of putative autapomorphies that can be observed on both the holotype and the overlapping portions of referred specimens (e.g., Nesbitt and Stocker, 2008). Thus, given the lack of anatomical overlap and the spatial separation of quarries yielding the forelimb and holotypic vertebra, we suggest that there is no compelling evidence supporting the assignment of these specimens to a single genus (see also Upchurch et al., 2004a). Similarly, the referral of the isolated teeth to *Hudiesaurus* is unsupported. Therefore, we restrict the binomial *Hudiesaurus sinojapanorum* to the holotypic vertebra, and the forelimb and teeth are treated separately.

SYSTEMATIC PALEONTOLOGY

DINOSAURIA Owen, 1842
SAUROPODOMORPHA von Huene, 1932
SAUROPODA Marsh, 1878
EUSAUROPODA Upchurch, 1995
MAMENCHISAURIDAE Young and Chao, 1972
HUDIESAURUS SINOJAPANORUM Dong, 1997
(Figs. 2–4)

Original Diagnosis—Re-written from Dong (1997:102): (1) top of neural spine of anterior dorsal vertebra forms a 'U'-shaped shallow cleft; (2) wing-like process between bases of postzygapophyses and lateral margin of neural spine; (3) anteriorly directed laterally compressed 'sword-like' process on anterior face of neural spine; (4) deep pleurocoels on lateral faces of the centrum; (5) midline keel on the ventral surface of the centrum.

Comments on Original Diagnosis—The original diagnosis provided by Dong (1997) can now be shown to be inadequate. Putative autapomorphies 1, 4, and 5 are present in several other sauropod genera. For example, shallow 'U'-shaped bifurcation of the posterior cervical and anterior dorsal neural spines also occurs in *Mamenchisaurus* (Young and Chao, 1972), *Klamelisaurus* (Zhao, 1993; Moore et al., 2020), *Euhelopus* (Wiman, 1929; Wilson and Upchurch, 2009), several turiasaurians (Royo-Torres et al., 2006, 2017; Britt et al., 2017), *Camarasaurus* (Osborn and Mook, 1921; Gilmore, 1925), and *Opisthocoelicaudia* (Borsuk-Białynicka, 1977), among others. Deep lateral pneumatic openings (= 'pleurocoels') are widespread in the presacral centra of many eusauropods (Upchurch et al., 2004a), and a ventral keel is also present in the cervicodorsal region of several other taxa, including *Mamenchisaurus hochuanensis* (CCG V 20401; PU and PMB pers. observ. 2010), *Klamelisaurus* (Moore et al., 2020), and *Euhelopus* (Wilson and Upchurch, 2009). It is not entirely clear what Dong (1997) meant by the 'wing-like' processes (putative autapomorphy '2'), as their location was neither fully described nor annotated in his figures. However, it seems likely that these are merely the typical posterolateral projection of the postzygapophyses, rather than unusual processes. Finally, the 'sword-like' anterior process is not part of a novel articulation with the hyposphene of a preceding vertebra (contra Dong, 1997: see Description, below); rather, it appears to be a transversely compressed sheet of ossified intervertebral ligament. Ossification of such ligaments and tendons is rare, but not unheard of, among sauropods (e.g., *Camarasaurus* [= '*Cathetosaurus*'] *lewisi* [Jensen, 1988]; *Diplodocus* [USNM 10865; Gilmore, 1932; PU pers. observ., 1991]; see also Cerda, 2009; Klein et al., 2012; Cerda et al., 2015). Thus, the presence of such a feature is more likely to represent individual variation, pathology, and/or unusual preservation, rather than an autapomorphy. If this feature is to be accepted as having some diagnostic value, this must wait until it is found repeatedly in other individuals of *Hudiesaurus*.

TABLE 1. Measurements of the posterior cervical vertebra of *Hudiesaurus sinojapanorum* (IVPP V11120). All measurements in mm.

Description	Measurement
Anteroposterior length of centrum (including condyle)	466
Anteroposterior length of centrum (excluding condyle)	376
Dorsoventral height of centrum (posterior surface)	351
Transverse width of centrum (posterior surface)	398
Maximum transverse width across prezygapophyses	539
Maximum transverse width across postzygapophyses	439
Height of postzygapophyses above dorsal margin of centrum	295
Transverse width across prezygapophyseal articular surface	178
Transverse width across metapophyses	177

FIGURE 2. Posterior cervical vertebra of *Hudiesaurus sinojapanorum* (IVPP V11120; holotype). **A**, right lateral view; **B**, left lateral view; **C**, anterior view; **D**, posterior view. **Abbreviations**: **acc.proc**, accessory process; **ACDL**, anterior centrodiapophyseal lamina; **CPOF**, centropostzygapophyseal fossa; **CPOL**, centropostzygapophyseal lamina; **CPRF**, centroprezygapophyseal fossa; **CPRL**, centroprezygapophyseal lamina; **dia**, diapophysis; **lig**, ossified intervertebral ligament; **mp**, metapophysis; **mt**, median tubercle; **PCDL**, posterior centrodiapophyseal lamina; **POCDF**, postzygapophyseal centrodiapophyseal fossa; **PODL**, postzygodiapophyseal lamina; **poz**, postzygapophysis; **pp**, parapophysis; **PRCDF**, prezygocentrodiapophyseal fossa; **PRDL**, prezygodiapophyseal lamina; **PRDL.k**, kink in PRDL; **prz**, prezygapophysis; **SDF**, spinodiapophyseal fossa; **SPOF**, spinopostzygapophyseal fossa; **SPOL**, spinopostzygapophyseal lamina; **SPRL**, spinoprezygapophyseal lamina; **TPOL**, interpostzygapophyseal lamina; **TPRL**, interprezygapophyseal lamina. Scale bars equal 100 mm.
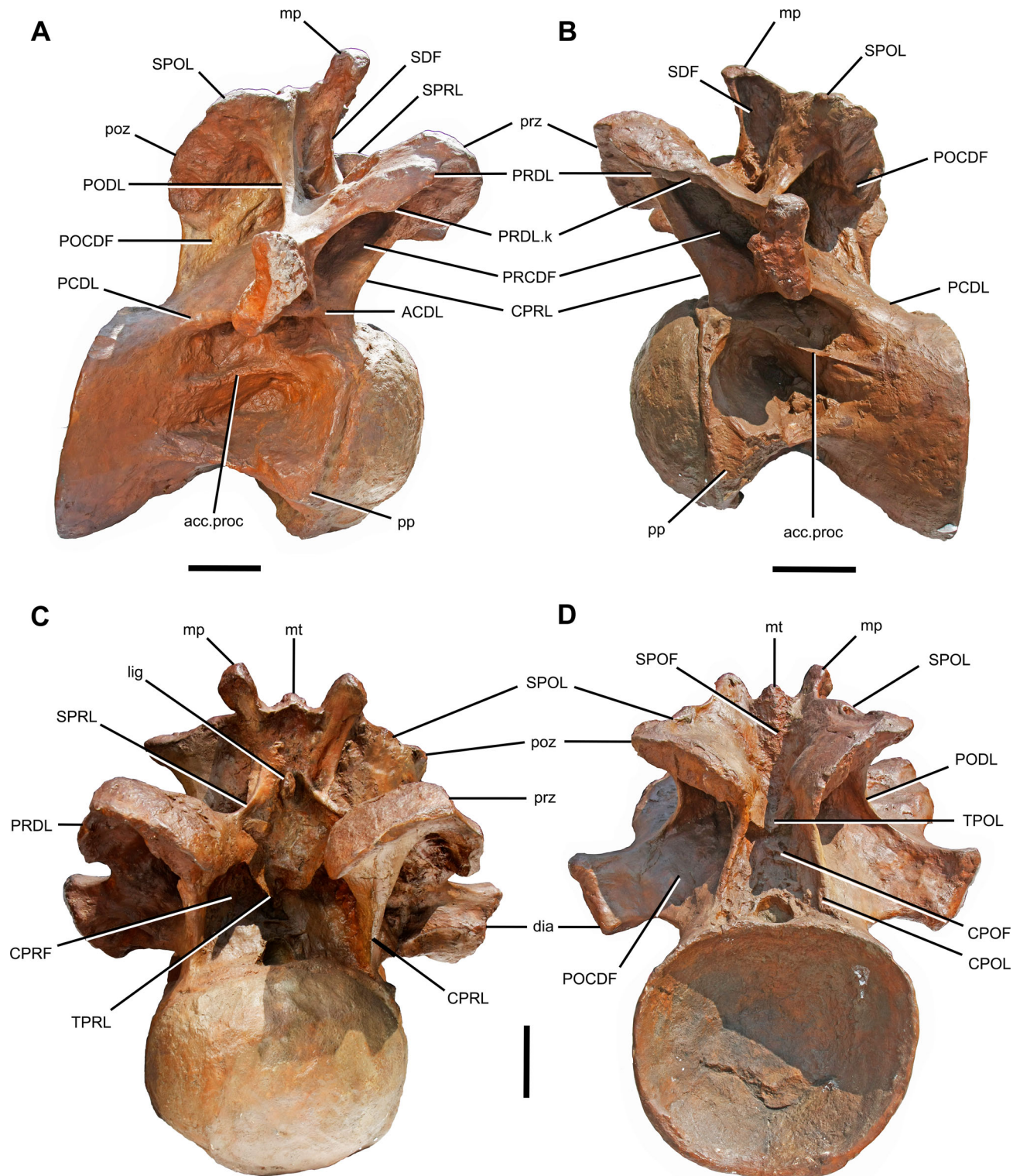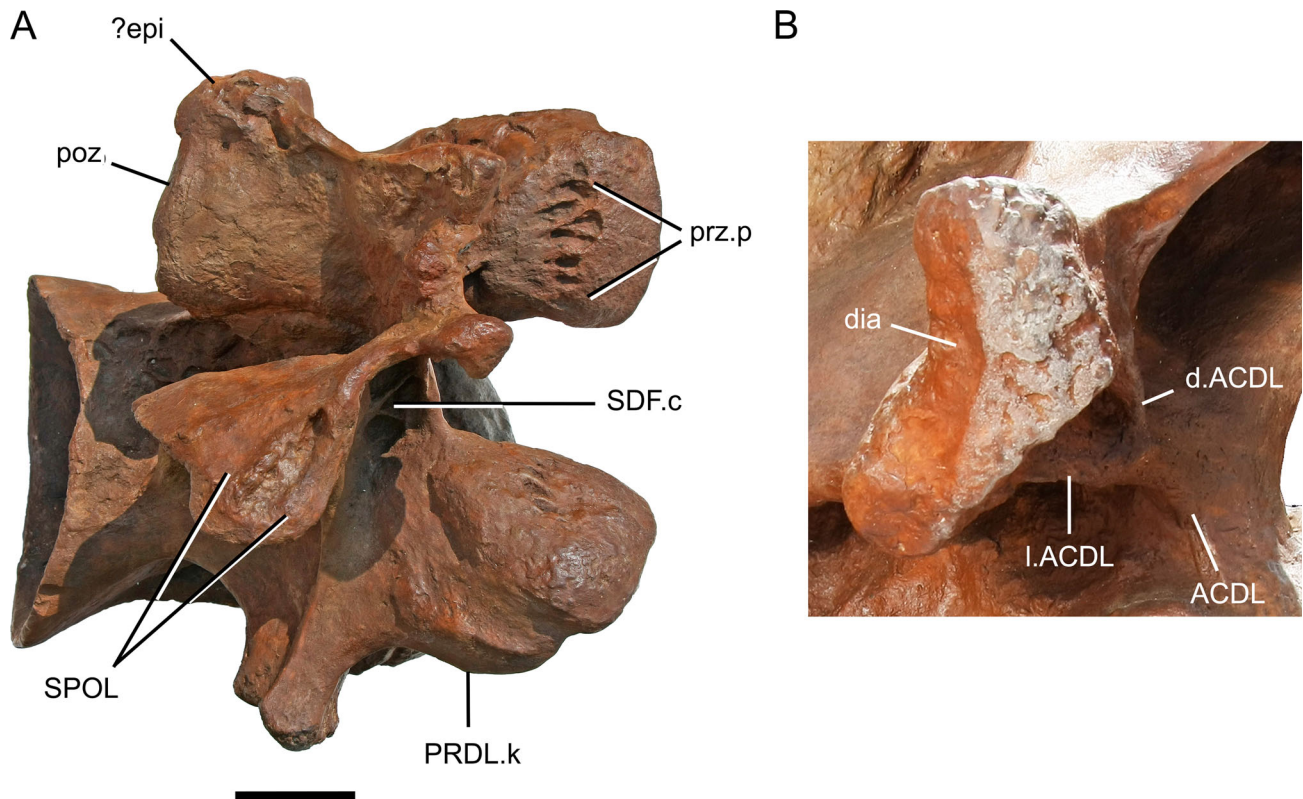
FIGURE 3. Posterior cervical vertebra of *Hudiesaurus sinojapanorum* (IVPP V11120; holotype). **A**, dorsal view; **B**, close up on anterior vertebral laminae supporting the diapophysis in right lateral view (not to scale). **Abbreviations**: **ACDL**, anterior centrodiapophyseal lamina; **d.ACDL**, dorsal branch of ACDL; **l.ACDL**, lateral branch of ACDL; **dia**, diapophysis; **?epi**, epipophysis; **poz**, postzygapophysis; **PRDL.k**, kink in PRDL; **prz.p**, pits on dorsal surface of prezygapophysis; **SDF.c**, pneumatic coel within spinodiapophyseal fossa; **SPOL**, spinopostzygapophyseal lamina. Scale bar equals 100 mm.

Revised Diagnosis—*Hudiesaurus* can be diagnosed on the basis of the following autapomorphies: (1) small projection on neurocentral junction above lateral pneumatic opening; (2) ACDL splits into upper and lower branches (the former extends to anterodorsal margin of the diapophysis, and the latter to posteroventral margin of the diapophysis, where it meets the anterior end of the PCDL); (3) approximately transverse row of 5–6 small coels on dorsal surface of prezygapophyseal process, immediately posterior to articular facet; (4) SPRLs bifurcate close to the base of the metapophysis, with one branch extending up anterior surface and fading out before reaching the summit, and the other branch forming a thin sheet that extends along the anterolateral margin of the metapophysis to the summit; and (5) SPOL bifurcates into two distinct ridges immediately above postzygapophysis (or this could be described as a short lamina extending dorsomedially from the PODL to the SPOL). N.B., portions of the PRDLs and diapophyses have been heavily restored with plaster, so autapomorphy 2 should be treated with caution.

Holotype—A nearly complete vertebra from the cervicodorsal region (estimated to be the last cervical vertebra; IVPP V11120) (Figs. 2–4; Table 1). N.B., Dong (1997) identified this specimen as an anterior dorsal vertebra, but we regard it as being more probably a posterior cervical vertebra (see below).

Locality and Horizon—Lower part of the Kalazha Formation (Upper Jurassic: upper Kimmeridgian–Tithonian) of Qiketai, Shanshan County, Turpan Basin, Xinjiang Uyghur Autonomous Region, China (Dong, 1997; Deng et al., 2015; Fang et al., 2016; Fig. 1).

Description and Comparisons

Dong (1997) identified the holotype of *Hudiesaurus* as an anterior dorsal vertebra; however, it also resembles a posterior-most cervical vertebra in several features. Even with well-preserved presacral series, it is often difficult to define the point where the neck meets the trunk in sauropods: this is because the morphology of the posterior cervical vertebrae gradually transforms into that of the most anterior dorsal vertebrae (Wilson and Upchurch, 2009; Moore et al., 2020). Despite some occasional doubts and apparent inconsistencies, we have generally accepted the identifications of the cervical-dorsal junction proposed by previous workers for other taxa. However, in the case of *Mamenchisaurus hochuanensis* (CCG V 20401), we note that the suggested 19 cervical and 12 dorsal vertebrae (Young and Chao, 1972) is likely to be incorrect. This is because 'Dv2' possesses a hyposphene (PU and PMB pers. observ., 2010), which would be atypical for such an anterior dorsal vertebra: a hyposphene does not usually appear until Dv3 or Dv4 in sauropods (Upchurch et al., 2004a). We therefore propose provisionally that *Mamenchisaurus hochuanensis* had 18 cervical and 13 dorsal vertebrae. Given the difficulties of pinpointing the cervical-dorsal junction in even well preserved and complete presacral series, identifying the precise position of an isolated vertebra (such as *Hudiesaurus*) is even more problematic. Below, we compare the *Hudiesaurus* vertebra with both the posterior cervical and anterior dorsal vertebrae of other sauropods. The majority of features support a position as either the last cervical or the first dorsal vertebra, with the former being
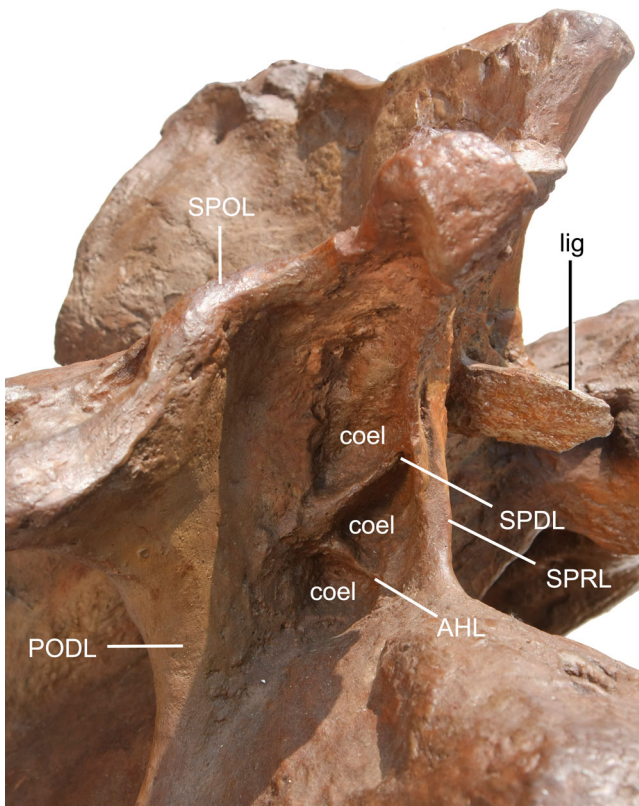
FIGURE 4. Posterior cervical vertebra of *Hudiesaurus sinojaponorum* (IVPP V11120; holotype). Close-up on the right lateral side of the neural spine in dorsolateral view to show pneumatic coels and accessory laminae within the spinodiapophyseal fossa (not to scale). **Abbreviations**: **AHL**, accessory horizontal lamina; **lig**, ossified intervertebral ligament; **PODL**, postzygodiapophyseal lamina; **SPOL**, spinopostzygapophyseal lamina; **SPRL**, spinoprezygapophyseal lamina.

more probable based on some features that are uniquely shared by *Hudiesaurus* and the last cervical vertebra (Cv18) of *Xinjiangtitan*. This identification, of course, depends on the assumption that Zhang et al. (2020) were correct when they placed the cervical-dorsal junction of *Xinjiangtitan* between the 18th and 19th presacral vertebrae (counting from the head).

The *Hudiesaurus* vertebra is relatively complete, although the PRDLs and transverse processes have been partly reconstructed (see also Dong, 1997). As in the cervical and anterior dorsal vertebrae of most eusauropods, it has a strongly opisthocoelous centrum (Dong, 1997) (Fig. 2), differing from the amphiplatyan/amphicoelous presacral vertebrae of most non-gravisaurian sauropodomorphs (Upchurch, 1995; Wilson, 2002; Upchurch et al., 2007a; Yates, 2007; Allain and Aquesbi, 2008; McPhee et al., 2014). In anterior or posterior view, the centrum is subcircular in outline, being slightly wider transversely than dorsoventrally (Table 1), as is typical for the cervicodorsal vertebrae of neosauropods (Mannion et al., 2019a) and some earlier-branching forms such as *Qijianglong*, *Mamenchisaurus youngi*, and *Bellusaurus* (Moore et al., 2020 and references therein). This contrasts with the transversely compressed middle–posterior cervical centra of many other East Asian eusauropods, including *Shunosaurus*, *Erketu*, *Euhelopus*, *Mamenchisaurus hochuanensis* (CCG V 20401), and *Xinjiangtitan* (Upchurch, 1998; Mannion et al., 2013; Moore et al., 2020; Zhang et al., 2020; PU and PMB pers. observ., 2010), as well as most rebbachisaurids (Mannion et al., 2019a). The Functional (i.e., excluding the

anterior convexity) Average Elongation Index (FAEI) is 1.0 in the *Hudiesaurus* vertebra. FAEIs tend to decrease towards the cervical-dorsal junction compared with those for middle cervical vertebrae, and a value close to 1.0 is compatible with a position either as the last cervical or one of the first two dorsal vertebrae of a non-diplodocine sauropod (Table S1 in Supplemental Data 1). As in *Mamenchisaurus hochuanensis* (CCG V 20401; PU and PMB pers. observ., 2010), *Klamelisaurus* (Moore et al., 2020; contra Zhao, 1993), *Euhelopus* (Wilson and Upchurch, 2009), and many flagellicaudatans (Upchurch et al., 2004a), the ventral surface of the *Hudiesaurus* centrum is strongly concave transversely as well as anteroposteriorly over its whole length, and is bounded by ventrolaterally directed ridges (Dong, 1997). A prominent midline ridge is present within the ventral concavity, as also found in dicraeosaurids (Upchurch, 1998; Wilson, 2002), Cv17–Dv1 of *Euhelopus* (Wilson and Upchurch, 2009), posterior cervicals to Dv2 in *Klamelisaurus* (Moore et al., 2020), Cv13–18 in *Xinjiangtitan* (Zhang et al., 2020), and Dv1 (= 'Cv19') in *Mamenchisaurus hochuanensis* (CCG V 20401; PU and PMB pers. observ., 2010).

The parapophysis is located at the anteroventral corner of the lateral surface of the centrum (Fig. 2). This position is typical for sauropod cervical vertebrae, although it also occurs in Dv1 in most taxa (Upchurch et al., 2004a), including *Klamelisaurus* (Moore et al., 2020), *Mamenchisaurus hochuanensis* (CCG V 20401; PU and PMB pers. observ., 2010), and *Xinjiangtitan* (Zhang et al., 2020), and in Dv1 and 2 in *Euhelopus* (Wilson and Upchurch, 2009) and *Apatosaurus ajax* (Upchurch et al., 2004b). In *Hudiesaurus*, there is no indication that the shallowly concave articular surface of the parapophysis was fused to a rib: this is more consistent with this specimen being a dorsal, rather than cervical, vertebra (Hatcher, 1901; Gilmore, 1936; McIntosh, 1990; Upchurch, 1998; Upchurch et al., 2004a; Zhang et al., 2020). However, rib–vertebra fusion is not an infallible indicator that a vertebra is a cervical (Moore et al., 2020): for example, the ribs of Cv17 and 18 of *Mamenchisaurus hochuanensis* (CCG V 20401) are not fused to the parapophyses (PU and PMB pers. observ., 2010). The dorsal surface of the parapophysis is excavated in *Hudiesaurus*, and this depression is continuous with the lateral pneumatic opening, as seen in the cervical vertebrae of many non-neosauropod eusauropods, such as *Cetiosaurus* and *Chebsaurus* (Upchurch and Martin, 2002, 2003; Upchurch et al., 2004a; Mahammed et al., 2005). Many neosauropods also have dorsally excavated cervical parapophyses, but such taxa typically possess a ridge that divides this depression from the lateral pneumatic opening (Upchurch, 1998; Upchurch and Martin, 2002, 2003). The lateral pneumatic opening of *Hudiesaurus* is small and deep, with a rounded, wide anterior margin that is positioned dorsal to the parapophysis (Fig. 2). Posteriorly, this opening is bounded dorsally by a sharp ridge that runs posteroventrally, giving the posterior margin an acute profile. Such a ridge is unusual in sauropods, only being reported previously in Cv17 and 18 of *Xinjiangtitan* (Zhang et al., 2020:figs. 15, 16, and 18), and confirmed as absent in *Mamenchisaurus youngi* by the latter study. Dorsal vertebrae 1 and 2 of *Apatosaurus ajax* have a ridge bounding the lateral pneumatic opening dorsally (Upchurch et al., 2004b), but this differs from the condition in *Hudiesaurus* and *Xinjiangtitan* by extending further anteriorly (i.e., to the anterior end of the opening) and being horizontal rather than posteroventrally inclined. In *Hudiesaurus*, this ridge merges into the centrum-arch junction, where there is a small, laterally extending projection on each side (Fig. 2): the latter is unique and is regarded as an autapomorphy. The presence of lateral pneumatic openings with oval outlines (i.e., strongly rounded and dorsoventrally wide anterior margins and acute posterior ends) in anterior dorsal vertebrae has frequently been regarded as a derived character state uniting Macronaria or a slightly less inclusive clade (e.g., Upchurch, 1998; Mannion et al., 2013). However, they are also seen in Dv1

and 2 of *Klamelisaurus* (Moore et al., 2020), the anterior dorsal vertebrae of *Bellusaurus* and *Haplocanthosaurus priscus* (Mannion et al., 2019a), and indeterminate cervicodorsal vertebrae from the Late Jurassic Shishugou Formation of China (Moore et al., 2020). In *Hudiesaurus*, the lateral pneumatic opening is not as elongate as those found in either the cervical centra of *Cetiosaurus* (Upchurch and Martin, 2002) or several Jurassic Chinese taxa (such as *Dashanpusaurus* and *Daanosaurus*; Peng et al., 2005; Ye et al., 2005). Indeed, *Hudiesaurus* possesses a lateral pneumatic opening that is largely restricted to the anterior two-thirds of the centrum (excluding the anterior articular convexity), a derived condition seen in the cervical vertebrae of many CMTs (e.g., *Klamelisaurus*, *Mamenchisaurus youngi*, *Qijianglong*, *Xinjiangtitan*), *Euhelopus*, and several titanosauriforms (Whitlock, 2011; Moore et al., 2020). However, the relatively small size and anterior location of the lateral pneumatic opening is also consistent with the *Hudiesaurus* vertebra being from the anterior dorsal region. The oblique accessory lamina that divides the lateral pneumatic opening into anterior and posterior sections in the cervical vertebrae of several non-neosauropod eusauropods (e.g., *Mamenchisaurus*, *Klamelisaurus*, *Xinjiangtitan*) and many neosauropods (Wilson, 2002; Upchurch et al., 2004a; Moore et al., 2020) is not present in *Hudiesaurus* (Fig. 2). While its absence is more compatible with an identification of the *Hudiesaurus* specimen as being an anterior dorsal vertebra, the oblique lamina is also sometimes absent in posterior-most cervical vertebrae, such as Cv18 of *Mamenchisaurus hochuanensis* (CCG V 20401; PU and PMB pers. observ., 2010), Cv17 and 18 of *Xinjiangtitan* (Zhang et al., 2020), and Cv17 of *Euhelopus* (Wilson and Upchurch, 2009). The lateral pneumatic opening becomes shallower posteriorly in *Hudiesaurus*, as is typical for most sauropod cervical vertebrae (e.g., *Cetiosaurus*, *Patagosaurus*, and the CCG V 20401 specimen of *Mamenchisaurus hochuanensis*: Bonaparte, 1986; Upchurch and Martin, 2002, 2003; PU and PMB pers. observ., 2010).

Measured on the anterior surface, the ratio of the dorsoventral height of the neural arch (from the dorsal surface of the centrum to the ventromedial tips of the prezygapophyses) to centrum height is low (~0.35) in *Hudiesaurus*. With the exception of comparably low neural arches in some somphospondylans and *Omeisaurus tianfuensis*, this ratio is ≥0.5 in the posterior cervical vertebrae of other eusauropods (Bonaparte et al., 2006; Mannion et al., 2013). In *Hudiesaurus*, the prezygapophyses project forward to a point beyond the anterior end of the condyle (Fig. 2). Such projection is typical for the posterior cervical and anterior dorsal vertebrae of many sauropods: for example, in *Klamelisaurus* it is only posterior to Dv5 that the prezygapophyses no longer project beyond the anterior articulation of the centrum (Moore et al., 2020). However, this contrasts with the condition in taxa like *Apatosaurus ajax*, where the prezygapophyses no longer project beyond the anterior end of the centrum from Cv12 rearwards (Upchurch et al., 2004b). In *Hudiesaurus*, the prezygapophyses are large and broad, with transversely convex articular surfaces (Fig. 3A). Sauropods typically have flat prezygapophyseal articular surfaces plesiomorphically, but the derived, strongly convex condition is also present in the cervical vertebrae of diplodocines (Upchurch, 1995; Tschopp et al., 2015a) and the CMTs *Klamelisaurus* (Moore et al., 2020) and *Xinjiangtitan* (Zhang et al., 2020), as well as the anterior dorsal vertebrae of *Mamenchisaurus hochuanensis* (CCG V 20401; PU and PMB pers. observ., 2010). The zygapophyses have several small, irregularly shaped coels on their dorsal surfaces (Dong, 1997). In the case of the prezygapophyses, these coels form a line of 5–6 adjacent pits, separated from each other by small anteroposteriorly directed ridges, located immediately posterior to the articular facet (Fig. 3A). These might represent a pneumatized internal tissue structure that has been revealed by erosion of the surface bone: however, their presence

in the same position on both prezygapophyses suggests that they are not taphonomic artifacts. We therefore regard these coels as external pneumatic features and as autapomorphic for *Hudiesaurus*. The thin, medial edges of the prezygapophyses descend steeply to meet each other on the midline and form a single lamina extending down to the top of the small, subcircular neural canal (Fig. 2C); this is probably the "well developed medial lamina" of Dong (1997:103), here termed the interprezygapophyseal lamina (TPRL) according to a revised version of Wilson's (1999) system (see Tschopp and Mateus, 2013). This TPRL partially subdivides the centroprezygapophyseal fossa (CPRF) into left and right subfossae. A TPRL is absent from the posterior cervical vertebrae of *Euhelopus* (Wilson and Upchurch, 2009) and *Xinjiangtitan* (Zhang et al., 2020), and the anterior dorsal vertebrae of *Klamelisaurus* and *Mamenchisaurus youngi* (Moore et al., 2020), although it is present in several other sauropods (e.g., there is a short, stout version on the posterior cervical vertebrae of *Apatosaurus ajax*; Upchurch et al., 2004b). The centroprezygapophyseal laminae (CPRLs) of *Hudiesaurus* are large and stout (as in *Cetiosaurus*; Upchurch and Martin, 2003) and do not bifurcate at their dorsal ends, unlike those of the cervical vertebrae of several diplodocids (Upchurch, 1998) and many non-neosauropod eusauropods (Moore et al., 2020), such as those on Cv18 in *Xinjiangtitan* (Zhang et al., 2020). The stout, single CPRLs of *Hudiesaurus* more closely resemble those of anterior dorsal vertebrae in taxa such as *Klamelisaurus*, although the former lacks the accessory laminae seen in the PRCDF of the latter taxon (Moore et al., 2020). In lateral view, the CPRLs slope anterodorsally and are subparallel with the PCDLs (Fig. 2A, B), a configuration also seen in the cervical and anterior-most dorsal vertebrae (i.e., Dv1 and 2) of many sauropods. By contrast, in Dv3 and 4 of most taxa, these laminae become more vertical, and are fully vertical from around Dv5 onwards, as seen in *Klamelisaurus* (Moore et al., 2020). Thus, the orientation of the CPRLs further supports the view that the *Hudiesaurus* vertebra is either a cervical or one of the most anterior dorsal vertebrae. As in the cervical vertebrae of some non-neosauropod eusauropods (including *Shunosaurus*, *Omeisaurus tianfuensis*, *Chuanjiesaurus*, and *Cetiosaurus*) and many diplodocoids, pre-epipophyses are absent in *Hudiesaurus*. This contrasts with most CMTs, such as *Klamelisaurus* and *Mamenchisaurus youngi*, as well as *Bellusaurus*, *Euhelopus*, and many other neosauropods, in which these projections are well-developed (Wilson and Upchurch, 2009; Mannion et al., 2013, 2019a; Moore et al., 2020). However, pre-epipophyses are typically absent in the dorsal vertebrae of sauropods (Wilson and Upchurch, 2009), so the condition in *Hudiesaurus* might merely reflect a location in the anterior dorsal series.

The transverse processes are short and project laterally and slightly ventrally (Dong, 1997), although it is difficult to ascertain how genuine this morphology is, given the degree of plaster restoration. If the transverse processes are truly pendant, then this is consistent with this specimen being either a cervical or very anterior dorsal vertebra (Upchurch et al., 2004a). For example, the shift from pendant to horizontal transverse processes occurs between Cv18 and Dv2 in *Mamenchisaurus hochuanensis* (CCG V 20401; PU and PMB pers. observ., 2010), from Cv17 to Dv2 in *Euhelopus* (Wilson and Upchurch, 2009), and more abruptly between Cv18 and Dv1 in *Xinjiangtitan* (Wu et al., 2013; Zhang et al., 2020). In *Hudiesaurus*, the transverse process lies some distance below the level of the zygapophyses (Fig. 2), as is typical for posterior cervical and the most anterior dorsal vertebrae (Moore et al., 2020). Prominent anterior and posterior centrodiapophyseal laminae (ACDLs, PCDLs) extend anteroventrally and posteroventrally, respectively, at approximately 45° to the horizontal (Fig. 2). The presence of an ACDL is consistent with this specimen being either a cervical or anterior dorsal vertebra: for example, in *Klamelisaurus*, the

ACDL is present in Dv1 and 2 as a separate lamina, and in Dv3 and 4 merges into the CPRL (Moore et al., 2020; see also Wilson, 1999). As the ACDL approaches the transverse process in *Hudiesaurus*, it bifurcates to form two laminae that extend along the ventral and anterior surfaces of the transverse process (potentially as far as the distal articular end) (Fig. 3B). The more posterior of these laminae merges into the posteroventral margin of the transverse process, where it meets the anterodorsal end of the PCDL. This posteriorly bifurcate ACDL appears to be unique to *Hudiesaurus*. The relatively steeply inclined PCDL is consistent with the identification of the *Hudiesaurus* vertebra as a posterior-most cervical or an anterior dorsal vertebra: this lamina is typically close to horizontal in cervical vertebrae but tends to become more steeply inclined in the cervicodorsal region (Wilson and Upchurch, 2009). Sauropods display some variation in this regard, although this might also reflect inconsistent identification of the cervical-dorsal junction. For example, PCDLs remain shallowly inclined even in the most posterior cervical vertebrae of *Qijianglong* (Xing et al., 2015:fig. 12F), but they become increasingly steep from Cv16 to 18 in *Mamenchisaurus hochuanensis* (CCG V 20401; PU and PMB pers. observ., 2010). In *Hudiesaurus*, the prezygodiapophyseal lamina (PRDL) extends anterodorsally from the transverse process to the prezygapophysis at a moderate angle (c. 30°) to the horizontal, whereas the postzygodiapophyseal lamina (PODL) is nearly vertical (Fig. 2). The anterior margin of the PRDL forms a convex projection or 'kink' (Figs. 2, 3) that is potentially homologous with the apomorphically convex ventral margin seen in the middle and posterior cervical vertebrae of several CMTs (Moore et al., 2020). Unlike the condition in the cervicodorsal vertebrae of *Euhelopus*, *Klamelisaurus*, and some additional CMT specimens (Moore et al., 2020), the PODL is not bifid ventrally.

The posterior margins of the postzygapophyses terminate some distance anterior to the posterior margin of the centrum (Fig. 2). This condition is a derived state when it occurs in posterior cervical vertebrae, which is seen in several non-neosauropod eusauropods (e.g., *Omeisaurus tianfuensis*—He et al., 1988:fig. 23; *Mamenchisaurus youngi*—Ouyang and Ye, 2002:fig. 18C; *Chuanjiesaurus*—Sekiya, 2011:fig. 14; *Qijianglong*—Xing et al., 2015:fig. 12F; *Xinjiangtitan*—Zhang et al., 2020:figs. 15 and 16; *Jobaria*—Mannion et al., 2017), and early diverging macronarians (e.g., *Camarasaurus*; Osborn and Mook, 1921:pl. LXVII), but is typically absent in many diplodocoids, including *Apatosaurus ajax* (Upchurch et al., 2004b), *Dicraeosaurus* (Janensch, 1929, 1936:table I, fig. 11a), and *Limaysaurus* (Calvo and Salgado, 1995:fig. 8B) (see also Tschopp and Mateus, 2013; Tschopp et al., 2015a; Poropat et al., 2016). Epipophyses are greatly reduced or absent in *Hudiesaurus*, perhaps being represented by small tab-like processes above the postzygapophyses (Fig. 3). Such a condition is typical for the posterior-most cervical vertebrae of sauropods, except *Euhelopus* (Wilson and Upchurch, 2009), *Jobaria* (MNN specimens; PDM pers. observ., 2012), *Nigersaurus* (MNN specimens; PDM pers. observ., 2010), and diplodocines (Tschopp and Mateus, 2013). For example, epipophyses are present in Cv2–16 in *Xinjiangtitan*, but are absent in Cv17 and 18 (Zhang et al., 2020). Their absence is also consistent with the *Hudiesaurus* vertebra being an anterior dorsal, since it is even rarer for well-developed epipophyses to be present on such vertebrae (to date they have only been reported in anterior dorsal vertebrae of some turiasaurians (Britt et al., 2017; Mannion, 2019; Mannion et al., 2019a), although they can be traced into the dorsal series as the homologs of the tips of the aliform processes in *Euhelopus* (Wilson and Upchurch, 2009). Given the uncertainty in the position of the *Hudiesaurus* vertebra, and the subtlety of its putative epipophyses, we score this character (i.e., presence/absence of epipophyses) as a '?' in our phylogenetic data matrices. The postzygapophyses of *Hudiesaurus* are relatively large, with concave articular surfaces facing

downwards and outwards (Fig. 2D). Their ventral margins merge into the dorsal parts of well-developed centropostzygapophyseal laminae (CPOLs) that descend separately without meeting on the midline; however, the detailed anatomy of this region is obscured by damage and reconstruction. Nevertheless, despite Dong's (1997) assertion of its presence, there is no hyposphene-hypantrum articulation (see above). On the left side at least, and possibly also the right, the CPOLs bifurcate dorsally, creating a small subtriangular fossa that faces mainly posteriorly (Fig. 2D). A dorsally bifurcated CPOL is sporadically present in the middle and posterior cervical vertebrae of eusauropods (e.g., *Cetiosaurus*, *Patagosaurus*, *Camarasaurus*, *Giraffatitan*, *Rapetosaurus*, and some flagellicaudatans), and is generally absent in CMTs apart from the 'Phu Kradung taxon' (Tschopp et al., 2015a; Carballido et al., 2017; Moore et al., 2020). However, the medial branch of the bifid CPOL of *Hudiesaurus* supports the postzygapophysis rather than curving medially to meet its partner on the midline as occurs in other taxa. Similarly, no single vertical midline interpostzygapophyseal lamina (TPOL) can be observed, although it is not clear whether this represents genuine absence or the effects of poor preservation.

The spinoprezygapophyseal laminae (SPRLs) are low ridges that extend medially from the middle of the posterior margins of the prezygapophyses to the anterior bases of the metapophyses (Figs. 2, 4). At this point, each SPRL autapomorphically splits into two branches: one ascends the anterior surface of the metapophysis and fades out at about midheight; the other becomes a thin flange-like ridge that extends along the anterolateral margin of the metapophysis and reaches the summit. These anterolateral flanges are potentially homologous with the 'scabrous' projections observed in the middle–posterior cervical vertebrae of *Klamelisaurus* (which become less 'ragged' in the most posterior cervical vertebrae), and the dorsolaterally flattened SPRLs seen in the middle and posterior cervical vertebrae of *Bellusaurus* (Moore et al., 2020). In *Hudiesaurus*, there is a large flat space on the anterior surface of the neural spine between the SPRLs and below the bifurcated summit. Near the top of this area, along the midline, is the base of a transversely compressed process (Figs. 2, 4): this is the feature that Dong (1997) described as an 84 mm long, anteriorly directed, 'swordlike' process (for which he used the term 'prepophysis'). We observed this process in our first examination of this specimen in 1995, but by our second examination, in 2007, we found that the process had been broken and lost, so that now only its base is preserved. Dong (1997) suggested that this structure might be for the insertion of muscles, or for articulation with the hyposphene of the preceding vertebra; however, the latter proposal would seem to be impossible because the location of the process on the spine means that it would project into the spinopostzygapophyseal fossa (SPOF: = postspinal fossa) of the preceding vertebra. Moreover, hyposphene-hypantrum articulations have not been observed in the posterior cervical or anterior-most dorsal vertebrae of any sauropod: such structures are restricted to middle and posterior dorsal vertebrae (Upchurch et al., 2004a). We instead interpret this structure to be part of an ossified ligament (see above).

The posterior margin of the neural spine slopes strongly forward in lateral view, and the spine is slightly anterodorsally directed (though not to the same extent as in *Dicraeosaurus*; Janensch, 1929). The neural spine of Cv16 in *Mamenchisaurus hochuanensis* (CCG V 20401; PU and PMB pers. observ., 2010) has a nearly vertical anterior margin and gently sloping posterior one, resembling that of *Hudiesaurus*. This contrasts with the posterior-most cervical vertebrae of some taxa, such as *Qijianglong* (Xing et al., 2015:fig. 12E, F), in which the neural spine has a fairly symmetrical lateral profile, with posterodorsally sloping anterior and anterodorsally sloping posterior margins. As in the cervicodorsal vertebrae of CMTs, turiasaurians, *Camarasaurus*, and some titanosaurs, the

neural spine is relatively low in *Hudiesaurus*, projecting only slightly above the level of the postzygapophyses (Mannion et al., 2019a; Moore et al., 2020). The neural spine is bifurcated (Fig. 2C, D), as in the presacral vertebrae of numerous other eusauropods (*Klamelisaurus*, *Mamenchisaurus*, *Qijianglong*, some turiasaurians, flagellicaudatans, *Camarasaurus*, *Euhelopus*, and several somphospondylans; Wiman, 1929; Young, 1954; Borsuk-Białynicka, 1977; Zhao, 1993; Wilson, 2002; Harris and Dodson, 2004; Upchurch et al., 2004a; Royo-Torres et al., 2006; Ksepka and Norell, 2006; D'Emic et al., 2013; Mannion et al., 2019a; Moore et al., 2020). In anterior and posterior views (Fig. 2C, D), the metapophyses are divergent, as in diplodocids and most other taxa with bifid neural spines, but unlike the derived condition seen in dicraeosaurids, in which these structures are subparallel or converge towards their summits (Rauhut et al., 2005; Xu et al., 2018). In *Hudiesaurus*, the notch between the metapophyses is moderately deep and 'U'-shaped, with a median tubercle at its base (Fig. 2C, D). Such a tubercle is variably present in other sauropods with bifid presacral spines: for example, it occurs in the last two cervical vertebrae and Dv1–4 of *Euhelopus*, where it is drawn out into a large process that is as prominent as the metapophyses (Wilson and Upchurch, 2009); it is present as a low rounded process in the last two cervical vertebrae and Dv1–3 of *Barosaurus* (Zhang et al., 2020); it is a small bump on the posterodorsal margin of the notch in *Klamelisaurus* (Moore et al., 2020); it is variably absent/present in specimens of *Camarasaurus* (Tsuihiji, 2004); and it is absent in *Mamenchisaurus*, *Qijianglong*, *Suuwassea*, and *Amargasaurus* (Wilson, 2002; Harris and Dodson, 2004; Xing et al., 2015). The metapophyses of *Hudiesaurus* are knob-like and subtriangular in dorsal view, robust rather than compressed transversely, and relatively short dorsoventrally (not elongated as in derived dicraeosaurids: Janensch, 1929; Xu et al., 2018).

The spinodiapophyseal fossa (SDF), posterior to the SPRL and anterior to the SPOL, is divided into three subtriangular coels by two accessory laminae or ridges (Fig. 4). Dong (1997:103) described these structures as forming "a V-shaped posterolaterally projecting lamina": in lateral view, the two laminae meet each other at their posterior ends and diverge anteriorly. This 'V' is created from a lower horizontal lamina that extends from the PODL to the base of the SPRL, and an upper anterodorsally directed lamina that extends from the posterior end of the horizontal lamina to the posterior margin of the anterolateral branch of the SPRL (see above). Although both of these ridges are found separately on the presacral vertebrae of many sauropods (see below), the presence of both of them in this 'V'-shaped configuration is only known in Cv18 of *Xinjiangtitan* (Zhang et al., 2020:figs. 16A, 17B) and *Hudiesaurus*. The lower, horizontal, lamina is reminiscent of the 'epipophyseal-prezygapophyseal lamina' (EPRL) that occurs in the cervical vertebrae of several sauropods, such as *Nigersaurus* (Sereno et al., 2007) and *Euhelopus* (Wilson and Upchurch, 2009), as well as some other dinosaurs (Moore et al., 2020). Occasionally, this structure can also occur in the anterior-most dorsal vertebrae, such as Dv1 and 2 in *Euhelopus*, where it partially divides the SDF into lower and upper portions (Wilson and Upchurch, 2009), and Dv1 of *Klamelisaurus* (Moore et al., 2020). However, Moore et al. (2020) demonstrated that simply identifying this structure as the EPRL is problematic because it can be formed by either one or both of two separate components. One component is a more anteriorly placed ridge (termed the horizontal accessory lamina) that lies fully within the SDF and was probably formed by pneumatization. The other component is a more posteriorly placed 'anterior epipophyseal' epaxial muscle scar that lies on the lateral surface of the postzygapophyseal process and may project anteriorly into the posterior part of the SDF. Here, we identify the lower strut in *Hudiesaurus* as the horizontal accessory lamina formed by pneumatization. Moore et al.'s (2020) survey of these structures among sauropods suggests that, when considering just posterior cervical vertebrae, the pneumatic strut is currently only known in

rebbachisaurids (e.g., *Nigersaurus*, *Limaysaurus*), *Euhelopus* (where it lies below, and separate from, the anterior epipophyseal muscle scar), and some CMTs such as *Klamelisaurus* and *Mamenchisaurus hochuanensis* (CCG V 20401; PU and PMB pers. observ., 2010). It can be confirmed as being absent in the posterior cervical vertebrae of some non-neosauropods such as *Mamenchisaurus youngi* (where it only occurs in middle cervical vertebrae: Zhang et al., 2020), as well as several macronarians in which it has previously been identified, including *Camarasaurus lewisi*, *Europasaurus*, *Giraffatitan*, and *Uberabatitan*. The anterodorsally directed ridge within the SDFs of *Hudiesaurus* and *Xinjiangtitan* is potentially a SPDL, though it contacts the PODL rather than the diapophysis directly. The SPDLs in Dv4 of *Klamelisaurus* and Dv3 of *Euhelopus* resemble this anterodorsal lamina, but no such structure occurs in the more anterior dorsal or posterior cervical vertebrae of these taxa (Wilson and Upchurch, 2009; Moore et al., 2020). Despite the presence of two ridges produced by pneumatization within the SDF (i.e., the ?SPDL and horizontal accessory lamina), *Hudiesaurus* lacks the 3–4 irregular coels in this region seen in several early-branching titanosauriforms and many CMTs (Mannion et al., 2017; Moore et al., 2020). In *Hudiesaurus*, the SDF is not roofed dorsally by a horizontal rugose line of epaxial muscle scars immediately below the spine summit, unlike the condition in some non-neosauropod sauropods (e.g., *Klamelisaurus*, *Jobaria*, *Mierasaurus*, and *Moabosaurus*), as well as most diplodocids and many non-titanosaurian macronarians (Tschopp and Mateus, 2013; Mannion et al., 2019a; Moore et al., 2020). The prominent SPOLs of *Hudiesaurus* extend anteromedially and dorsally to the summit of each metapophysis (Fig. 2). At its posteroventral end (above the postzygapophysis), the SPOL splits into two ridges, with a small subtriangular fossa (SPOL-F) between them (Fig. 4). Such a bifurcated SPOL and cavity is not known in the posterior cervical vertebrae of other sauropods, but SPOL bifurcation in dorsal vertebrae has been listed as a synapomorphy of a clade of eusauropods comprising *Barapasaurus*, *Omeisaurus*, *Mamenchisaurus*, *Patagosaurus*, *Jobaria*, and neosauropods (Wilson, 2002). However, the SPOL bifurcation noted by Wilson typically occurs in the middle and posterior dorsal vertebrae and has a very different structure. In the *Barapasaurus* + Neosauropoda clade, each SPOL is a single structure close to the postzygapophysis and then bifurcates into a lateral SPOL (which usually merges with the SPDL) and a medial SPOL (which usually meets its partner on the midline within the SPOF: Wilson, 1999, 2002). Aside from occurring in a more anteriorly placed presacral vertebra, the condition in *Hudiesaurus* also differs from other eusauropods in that the SPOL is single over most of the spine length and then bifurcates as it approaches the postzygapophysis. As such, irrespective of whether the *Hudiesaurus* specimen is a posterior cervical or anterior dorsal vertebra, it appears to possess an autapomorphic condition with regard to its SPOL bifurcation. The SPOF is large, 'U'-shaped in transverse cross-section, and opens posterodorsally.

We could not observe the internal tissue structure of the vertebra. As such, we cannot determine whether the vertebra is camerate, as is the case in most eusauropods (Wedel, 2003), or pneumatized by camellae, which characterizes the presacral vertebrae of titanosauriforms (Wilson, 2002; Wedel, 2003) and many CMTs (Young and Chao, 1972; Moore et al., 2020).

EUSAUROPODA Upchurch, 1995
(?)MAMENCHISAURIDAE Young and Chao, 1972
GEN. ET SP. INDET.
(Fig. 5)

Material—Four teeth, IVPP V11121-2 (Fig. 5; Table 2).
Locality and Horizon—Lower part of the Kalazha Formation (Upper Jurassic: upper Kimmeridgian–Tithonian) of Qiketai, Shanshan County, Turpan Basin, Xinjiang Uyghur Autonomous
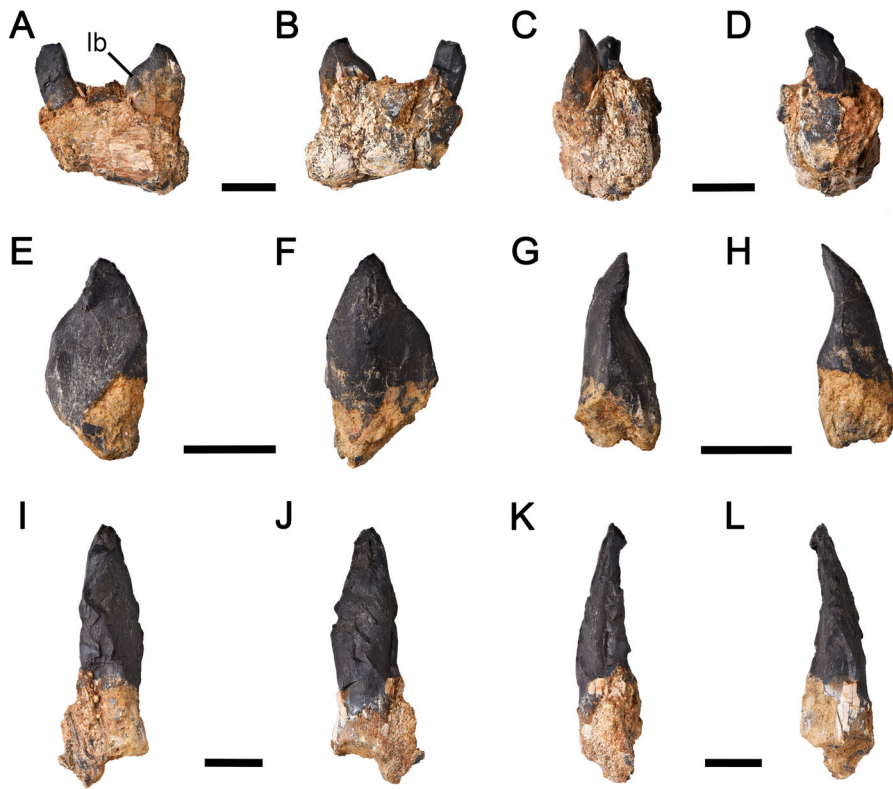
FIGURE 5. Teeth previously referred to *Hudiesaurus sinojaponorum* (IVPP 11121-2) but regarded as ?Mamenchisauridae indet. herein. **A–D**, Two tooth crowns within a broken jaw element in lingual (**A**), labial (**B**), distal (**C**), and mesial (**D**) views. **E–H**, Isolated tooth crown in lingual (**E**), labial (**F**), distal (**G**), and mesial (**H**) views. **I–L**, isolated tooth crown in lingual (**I**), labial (**J**), distal (**K**), and mesial (**L**) views. **Abbreviation**: **lb**, lingual boss. Scale bars equal 10 mm.

TABLE 2. Measurements of the teeth (IVPP V11121-2). **Abbreviations**: **e**, estimated value; **SI**, slenderness index (sensu Upchurch, 1998). All measurements are in mm.

Specimen	Crown apicobasal length	Crown maximum mesiodistal width	SI value
1	–	–	–
2	15+	10.5	1.5–2.0e
3	–	12	–
4	40e	11e	3.0–3.5e

Region, China (Dong, 1997; Deng et al., 2015; Fang et al., 2016) (Fig. 1). Exact locality unknown (see Introduction, above).

Description

The four teeth are not labelled with unique specimen numbers and so are referred to as specimens 1–4 herein. Two of the teeth (identified as premaxillary teeth by Dong [1997]) are embedded in a fragment of very worn, indeterminate bone, and the other two teeth are loose and were interpreted by Dong (1997) as maxillary teeth. It is not possible to determine which elements yielded these teeth, but it seems likely that the three smaller, low-crowned teeth were from the posterior part of the tooth row, whereas the single larger, higher-crowned tooth would have been more anteriorly positioned. No useful morphology can be gleaned from the bone fragment, although it is unlikely to have been the premaxilla on the basis of tooth size. Two of the teeth are quite similar in morphology: these are the larger tooth in the bone fragment (tooth 2) and the smaller of the two loose teeth (tooth 3). These specimens resemble the low broad teeth of *Jobaria* (Sereno et al., 1999; Chure et al., 2010), *Turiasaurus* (Royo-Torres and Upchurch, 2012), and *Zby* (Mateus et al., 2014), whereas the other two teeth (teeth 1 and 4) are more slender (Table 2).

Tooth 1 (smaller tooth in bone fragment: Fig. 5A–D) has been badly damaged and is missing most of the original surface, so its true shape cannot be determined. No informative character states can be observed.

Tooth 2 (larger tooth in bone fragment: Fig. 5A–D) lacks denticles and wear facets. There is no sign of wrinkled enamel texture on either the labial or lingual surface, suggesting some general surficial wear either during life or after the tooth was shed. The apex of the tooth is pointed and is deflected distally: this suggests that it is either an upper right or lower left tooth. The labial surface is gently convex mesiodistally and apicobasally, with the part of the crown mesial to the apex more strongly convex than that section distal to it, creating an asymmetrical 'D'-shaped cross-section. Mesial and distal grooves appear to be absent on the labial surface. The crown is mesiodistally expanded with respect to the tooth base, but the crown–root junction cannot be precisely determined because most of the tooth below this expansion is obscured by bone. The mesial margin is smoothly convex from apex to base, whereas the distal margin is first concave, then convex, producing a mildly sinuous profile in labial and lingual views (Fig. 5A, B). Most of the lingual surface of the crown is concave mesiodistally and apicobasally: the base of this concavity lies at a point approximately level with the maximum mesiodistal width of the tooth. Basal to this point, the lingual crown surface is swollen and mesiodistally convex. The crown margins are both slightly swollen, with the distal margin possessing a small, low, and elliptical boss that is level with the point of greatest mesiodistal expansion. This boss is in the same position as similar structures in *Euhelopus* (Wilson and Upchurch, 2009). There is no true lingual ridge,

but a slight eminence extends from the tooth apex for a very short distance basally, before merging into the surface of the lingual concavity.

Tooth 3 (the smaller of the isolated teeth: Fig. 5E–H) has the same morphology, in most respects, as tooth 2. The enamel surface is better preserved and has a wrinkled texture. The lingual 'boss' is less distinct and is a simple swelling of the distal margin, situated at a point level with the greatest mesiodistal expansion. As in tooth 2, there are no true mesial or distal grooves on the labial surface, but a distinct change in slope distal to the apical swelling does create the impression of a groove in the distal position (the cross-sectional asymmetry mentioned above). The root–crown junction cannot be observed because of breakage. Neither 'shoulder-like' nor apical macrowear are present.

Tooth 4 (largest tooth: Fig. 5I–L) is badly abraded and the enamel surface texture cannot be observed. There is also some damage to the crown margins. No wear facets or serrations can be identified. This tooth is much longer than the others, with a maximum length of 40 mm (Table 2): however, it is not possible to judge the position of the root–crown boundary because of the absence of enamel. It appears to be much slenderer than the other teeth, with a maximum mesiodistal width of 11 mm, and thus a Slenderness Index (SI: sensu Upchurch, 1998; Chure et al., 2010) that is potentially >3, but the true value cannot be determined because of the lack of accurate information on the location of the crown–root junction. The crown has a 'D'-shaped cross-section but has only a very shallow lingual concavity. There is no sign of a lingual ridge, lingual bosses, or labial grooves, but these absences could be the result of poor preservation.

Comparisons and Identification

The teeth are too incomplete to be usefully incorporated into a formal phylogenetic analysis. Instead, we assess their affinities by evaluating the potential significance of the putative synapomorphies and symplesiomorphies that they display. Possession of crowns that are basally constricted mesiodistally is a derived state characteristic of Sauropodomorpha (Yates, 2007; McPhee et al., 2014; Peyre de Fabrègues et al., 2015; Apaldetti et al., 2018; Chapelle and Choiniere, 2018), although this is lost in the elongated 'pencil-like' teeth of most diplodocoids and derived somphospondylans (Upchurch, 1998; Upchurch et al., 2004a). The labial profile of the IVPP V11121-2 teeth, with convex mesial and sigmoid distal margins, is characteristic of most spatulate sauropod teeth (Carballido and Pol, 2010). Only tooth 3 confirms the presence of wrinkled tooth enamel, but its absence on the other three crowns appears to be the result of poor preservation. Such enamel texturing is absent in the earliest branching sauropodomorphs (e.g., *Efraasia*), occurs in small patches of fine wrinkles in more derived non-sauropods (such as massospondylids, *Melanorosaurus*), and occurs over the entire crown as coarse anastamosing ridges and grooves in 'true' sauropods (e.g., *Pulanesaura*, *Gongxianosaurus*, *Tazoudasaurus*, and eusauropods) (Yates, 2007; Carballido and Pol, 2010; McPhee et al., 2015; Apaldetti et al., 2018; Chapelle and Choiniere, 2018). The presence of a lingual concavity on tooth crowns is generally regarded as a synapomorphy pertaining to a node between Sauropoda and Eusauropoda (Upchurch, 1995; Yates, 2007; Peyre de Fabrègues et al., 2015; Apaldetti et al., 2018; Chapelle and Choiniere, 2018). For example, this feature occurs in the teeth of all eusauropods (except diplodocoids and those somphospondylans with 'pencil-like' teeth), as well as some non-eusauropod sauropods such as *Gongxianosaurus* and *Tazoudasaurus*, but is rudimentary in *Chinshakiangosaurus* and *Pulanesaura* (Barrett et al., 2002; Upchurch et al., 2007a; Mannion et al., 2013; McPhee et al. 2015). Labial grooves are a synapomorphy of

Eusauropoda, being present in *Shunosaurus*, *Barapasaurus*, *Omeisaurus*, *Patagosaurus*, and many other forms, including most neosauropods (except some diplodocoids and titanosaurs with cylindrical teeth). By contrast, with the exception of *Pulanesaura* (McPhee et al., 2015), such grooves are absent in non-eusauropod sauropods (e.g., *Tazoudasaurus*) and non-sauropod sauropodomorphs such as *Plateosaurus* and *Anchisaurus* (Upchurch, 1995; Yates, 2007; Peyre de Fabrègues et al., 2015; Apaldetti et al., 2018; Chapelle and Choiniere, 2018). There is some evidence that the distal labial groove evolved before the mesial one, since the teeth of *Chinshakiangosaurus* and *Amygdalodon* either possess only the latter, or the distal groove is more marked than the mesial one (Upchurch et al., 2007a; Carballido and Pol, 2010). This character state distribution could be taken as evidence that the IVPP V11121-2 teeth did not belong to a eusauropod: however, *Mamenchisaurus sinocanadorum* (IVPP V10603) also lacks both mesial and distal grooves (PMB and PU pers. observ., 2010), and this feature might sometimes reflect individual variation and/or position in the jaws (Holwerda et al., 2015). Non-sauropod sauropodomorphs typically have SI values in the range of 1.5–2.0, with some taxa (such as *Thecodontosaurus* and *Anchisaurus*) having SIs around 2.2 (Chure et al., 2010). Most sauropods, except diplodocoids and titanosaurs, have SI values between 2.0–2.5, although a few forms (such as *Amygdalodon*, *Patagosaurus*, *Jobaria*, and turiasaurians) have unusually low SIs in the range of 1.3–1.6 (Barrett et al., 2002; Chure et al., 2010). Thus, although caution is warranted given their incomplete preservation, the SI of 1.5 (tooth 2) to ~3.0 (tooth 4) estimated for the IVPP V11121-2 teeth (Table 2) is consistent with a phylogenetic position anywhere within Sauropodomorpha apart from Diplodocoidea and Somphospondyli. Dong (1997) stated that the teeth of *Hudiesaurus* are serrated, but we found no such structures on any of the four crowns. Virtually all non-sauropod sauropodomorphs, and many non-eusauropod sauropods, have relatively large serrations on both the mesial and distal margins of their tooth crowns (Upchurch, 1998; Wilson and Sereno, 1998; Upchurch et al., 2004a, 2007a, b; Yates, 2007; Apaldetti et al., 2018; Chapelle and Choiniere, 2018). Well-developed serrations are also present on both mesial and distal crown margins in some non-neosauropod eusauropods, such as the CMT *Klamelisaurus* (Moore et al., 2020). In a few early-branching eusauropods (e.g., *Barapasaurus*, *Omeisaurus tianfuensis*, a referred specimen of *Mamenchisaurus hochuanensis*), serrations are retained on the mesial margins and lost on the distal margins (Ye et al., 2001; Yates, 2007; Moore et al., 2020). Variation can even occur along the length of the jaw of a single individual: for example, the anterior dentary teeth of *Mamenchisaurus sinocanadorum* lack serrations, whereas they are present as relatively small projections on just the mesial/apical margins of the posterior teeth (Moore et al., 2020). Thus, the absence of serrations in the IVPP V11121-2 teeth is more typical of a neosauropod (or close relative such as a turiasaurian) (Upchurch et al., 2004a; Royo-Torres and Upchurch, 2012), though this is also seen in *Amygdalodon*, *Shunosaurus*, and teeth referred to *Kotasaurus* (Carballido and Pol, 2010). Given this variation, however, the absence/presence of serrations probably provides only weak evidence of phylogenetic affinities (Upchurch, 1998; Barrett and Upchurch, 2005; Upchurch et al., 2007b; Carballido and Pol, 2010). An apicobasally oriented ridge within the lingual concavity is present in nearly all known spatulate sauropod teeth (Barrett et al., 2002; Mannion et al., 2013), and might be homologous with the mesiodistally convex lingual surface of the crowns of many diplodocoids and somphospondylans (Upchurch et al., 2004a, 2011). The absence of this ridge in the IVPP V11121-2 teeth is shared with just three other taxa with spatulate teeth: *Oplosaurus armatus* from the Early Cretaceous of England (Upchurch et al., 2004a, 2011), *Jobaria* from the Middle Jurassic of Niger (Mannion et al., 2017), and *Klamelisaurus gobiensis* from the Middle Jurassic of China (Zhao, 1993; Moore et al., 2020). However, in most other respects the teeth of the former two taxa

are very different from those of IVPP V11121-2 (Upchurch et al., 2011; Mannion et al., 2017). In particular, the lingual surfaces of the IVPP V11121-2 crowns are nearly flat mesiodistally, whereas this surface is concave in *Oplosaurus* and *Jobaria*. Perhaps the most informative character state in the IVPP V11121-2 teeth is the presence of a boss on the distal margin of the crown. These resemble those seen in *Euhelopus* (Wilson and Sereno, 1998; Wilson and Upchurch, 2009). Over the past decade, nearly all studies have recovered *Euhelopus* within Macronaria, usually as an early-branching somphospondylan (e.g., Wilson and Sereno, 1998; Wilson, 2002; Wilson and Upchurch, 2009; D'Emic, 2012; Mannion et al., 2013; Gorscak and O'Connor, 2019; Carballido et al., 2020). Consequently, the presence of these bosses in IVPP V11121-2 specimens 2 and 3 would previously have been interpreted as indicative of macronarian affinities and potential membership of an Early Cretaceous somphospondylan euhelopodid radiation (sensu D'Emic, 2012; see also Canudo et al. [2002] and Barrett and Wang [2007]). However, Moore et al. (2020) found that most of their phylogenetic analyses placed *Euhelopus* within CMTs, well outside Neosauropoda. Moreover, the distolingual boss is also present on the dentary teeth of *Mamenchisaurus sinocanadorum* (Suteethorn et al., 2013; Moore et al., 2020), although it also characterizes the teeth of the Early Cretaceous Chinese taxon *Yongjinglong*, which has been recovered as a somphospondylan in previous studies (Li et al., 2014; Mannion et al., 2019b).

In summary, the character states present in the teeth of IVPP V11121-2 support their identification as those of a non-neosauropod eusauropod (though somphospondylan affinities cannot be ruled out) and are consistent with Dong's (1997) suggestion that they belonged to a mamenchisaurid. Indeed, apart from the absence of the lingual apicobasal ridge in IVPP V11121-2, these teeth most closely resemble those of *Mamenchisaurus sinocanadorum*. IVPP V11121-2 lacks any true autapomorphies but does possess a unique combination of features: it is the only taxon currently known that lacks both the apicobasal lingual ridge and clear labial grooves, while also possessing a distolingual boss. Given the inadvisability of naming new taxa on such scant material (e.g., the danger of historical obsolescence described by Wilson and Upchurch [2003]), we refrain from erecting a new genus or species at this time, pending further discoveries.

<div align="center">

EUSAUROPODA Upchurch, 1995
MAMENCHISAURIDAE Young and Chao, 1972
RHOMALEOPAKHUS, gen. nov.

</div>

Diagnosis—As for type species.

<div align="center">

RHOMALEOPAKHUS TURPANENSIS, sp. nov.
(Figs. 6–10; Tables 3 and 4)

</div>

Nomenclatural Acts—The electronic edition of this article conforms to the requirements of the amended International Code of Zoological Nomenclature, and hence the new names contained herein are available under that Code from the electronic edition of this article. This published work and the nomenclatural acts it contains have been registered in ZooBank, the online registration system for the ICZN. The ZooBank LSIDs (Life Science Identifiers) can be resolved and the associated information viewed through any standard web browser by appending the LSID to the prefix 'http://zoobank.org/.' The LSID for this publication is: urn:lsid:zoobank.org:pub:A42348FE-ECE6-4524-B536-857AFFD22DB2. The electronic edition of this work was published in a journal with an ISSN, and has been archived and is available from the following digital repositories: CLOCKSS.

Species Diagnosis—*Rhomaleopakhus turpanensis* is diagnosed on the basis of three autapomorphies: (1) humeral deltopectoral crest terminates distally in a transversely narrow ridge that is separated from the main body of the crest by distinct lateral and medial grooves; (2) prominent (100 mm long) ridge, projecting posteromedially, on posterior surface of radial shaft, a short distance below the proximal end; and (3) radial distal articular surface markedly concave in central and medial portions. In addition, *Rhomaleopakhus turpanensis* possesses one of the most robust ulnae of any known sauropod (maximum proximal end width to proximodistal length ratio is 0.50; Table S2 in Supplemental Data 1), and is currently the only known non-somphospondylan eusauropod with the long-axes of the proximal and distal surfaces of the radius twisted through ~90° with respect to each other.

Holotype—A right forelimb, IVPP V11121-1 (Figs. 6–10; Tables 3 and 4), consisting of the humerus, ulna, radius, one carpal, and virtually complete manus of a single individual.

Etymology—*Rhomaleos* (ancient Greek, masculine) equals 'robust' (pertaining to the body), and *pakhus* (ancient Greek, masculine) equals 'forearm.' The species name refers to the Turpan Basin, China, where the holotype was found.

Locality and Horizon—Lower part of the Kalazha Formation (Upper Jurassic: upper Kimmeridgian–Tithonian) of Qiketai, Shanshan County, Turpan Basin, Xinjiang Uyghur Autonomous Region, China (Dong, 1997; Deng et al., 2015; Fang et al., 2016).

Description and Comparisons

Humerus—The right humerus is nearly complete, apart from a portion of the proximomedial expansion (Dong, 1997) and a small part of the proximolateral corner (Figs. 6, 7A, 8A). The posterior surface of this element could not be examined fully due to its large size and storage within a protective cradle. It is a relatively robust element, with an estimated Humeral Robusticity Index (sensu Wilson and Upchurch, 2003) of 0.35, similar to those of other heavily built taxa such as *Mamenchisaurus youngi*, *Apatosaurus*, dicraeosaurids, and *Opisthocoelicaudia* (Upchurch et al., 2015:table 2). Proximally, the humerus expands laterally relative to the shaft, giving it an hourglass-shaped outline in anterior view; this is the plesiomorphic sauropod condition, contrasting with the more asymmetrical humeri of most titanosauriforms and turiasaurians (Tschopp et al., 2015a; Poropat et al., 2016). The anterior surface of the humerus is too damaged proximally to determine whether a tuberosity for the attachment of the M. coracobrachialis was present.

The deltopectoral crest of *Rhomaleopakhus* is more prominent than those of most sauropods and is similar to those in *Turiasaurus* (Royo-Torres et al., 2006) and brachiosaurids (Wilson and Sereno, 1998). The crest lies entirely on the anterolateral margin of the humeral shaft: it does not expand or project medially across the anterior surface (Fig. 7A), unlike those in many titanosauriforms (Wilson, 2002; Mannion et al., 2013). It terminates at ~44% of humerus length from the proximal end: by comparison, values among other sauropods range between 35–50% (Upchurch et al., 2015:table 2). In this respect, *Rhomaleopakhus* is almost identical to several other CMTs: for example, these values are 44% in *Anhuilong* and *Omeisaurus tianfuensis*, and 43% in *Huangshanlong* (Ren et al., 2018). In anterior view, the anterolateral margin of the deltopectoral crest has a sigmoid profile and is relatively narrow throughout its length. One unusual feature of the deltopectoral crest is that its distal terminus forms a narrow ridge that is offset medially and laterally from the rest of the crest surface by deep, dorsoventrally oriented grooves or breaks-in-slope: this is provisionally regarded as autapomorphic. *Rhomaleopakhus* lacks prominent ridges or bulges on the posterolateral surface of the shaft, at the level of the deltopectoral crest. Such projections occur in many titanosaurs, including *Alamosaurus*, *Opisthocoelicaudia*, *Patagotitan*, and *Saltasaurus*, and have been interpreted as the insertion sites of a number of muscles, including the M. latissimus dorsi, M. scapulohumeralis

FIGURE 6. Holotype right forelimb of *Rhomaleopakhus turpanensis* gen. et sp. nov. (IVPP V11121-1; holotype) with individual elements in approximate anatomical position, shown in anterior view. Scale bar equals 200 mm.

anterior, and M. deltoideus clavicularis, although these interpretations are debated (e.g., Borsuk-Białynicka, 1977; Otero, 2010, 2018; Upchurch et al., 2015; Moore et al., 2020; Otero et al.,

2020; Voegele et al., 2020). In *Rhomaleopakhus*, as in most sauropods (Wilson, 2002; Mannion et al., 2013; Upchurch et al., 2015), the humeral shaft is wider transversely than anteroposteriorly, producing an elliptical horizontal cross-section at midlength. The transverse width of the shaft at midlength to proximodistal length ratio is estimated at 0.17–0.18. There is a small amount of torsion in the shaft, such that the long-axes of the proximal and distal end surfaces are slightly rotated relative to each other, but *Rhomaleopakhus* lacks the marked torsion (c. 40°) seen in many diplodocids (Tschopp et al., 2015a) and some CMTs (e.g., at least 30° in *Klamelisaurus* [Moore et al., 2020] and 25° in *Huangshanlong* [Huang et al., 2014] and *Anhuilong* (Ren et al., 2018]). Huang et al. (2014) regarded such humeral torsion as a synapomorphy of Mamenchisauridae, but there is clearly some variation among CMTs and homoplasy within Sauropoda, especially given that a strong degree of torsion of the humeral shaft is the plesiomorphic sauropodomorph condition that is lost in early sauropods (e.g., Yates, 2007; McPhee et al., 2014).

The distal end of the humerus is relatively wide transversely compared with the width of the shaft at midlength, largely because it projects a considerable distance medially (Fig. 7A). The ratio of distal end transverse width to humerus proximodistal length is 0.38, which is equaled or exceeded only by *Apatosaurus* and a few titanosaurs (Poropat et al., 2016; Table S2 in Supplemental Data 1). Distally, the anterior surface of the humerus is flat, apart from the relatively large lateral and medial anterodistal processes (sensu Upchurch et al., 2015) (Fig. 8B). Although the relative size of these anterodistal processes is difficult to quantify, they are very reduced or absent in *Chubutisaurus* and titanosaurs (D'Emic, 2012), and are particularly large in several CMTs (Remes, 2008), such as *Chuanjiesaurus* (Sekiya, 2011) and *Huangshanlong* (Huang et al., 2014). Enlarged (Huang et al., 2014) and/or anteriorly directed (Ren et al., 2018) anterodistal processes have been regarded as a synapomorphy of Mamenchisauridae: however, reduction and loss of these processes appears to be the derived state (D'Emic, 2012), and increased process size requires quantification and more comparative work before it can provide support for mamenchisaurid affinities. In *Rhomaleopakhus*, the distal articular surface is rugose and does not expand up onto the anterior face of the shaft, unlike the humeri of some titanosaurs (Wilson and Carrano, 1999; Wilson, 2002). The ulnar and radial condyles are not strongly divided from each other, and the former is somewhat larger than the latter. Remes (2008) suggested that mamenchisaurids possess a unique distal humeral configuration. In *Klamelisaurus*, *Omeisaurus tianfuensis*, and *Mamenchisaurus youngi*, the lateral condyle (which Remes [2008] termed the 'radial' condyle, but which has become the ulnar condyle in sauropods because of the rotation of the antebrachium [Bonnan, 2003]), is larger than the radial one. Moreover, the ulnar and radial condylar surfaces have long axes that are at ~90° to each other in distal end view, with the former directed anterolaterally. This results in the lateral part of the distal end having a distinct subtriangular profile, formed by fairly straight anterolateral and posterolateral margins that meet each other at an acute angle (e.g., He et al., 1988:fig. 44B; Ouyang and Ye, 2002:fig. 35F; Sekiya, 2011:figs. 38C, 39C). In many other sauropods, this lateral portion is more semicircular or subquadrate in distal view (see Upchurch et al., 2015:fig. 4; N.B., Upchurch et al.'s fig. 4A shows the distal end profile of the right humerus of *Mamenchisaurus youngi* incorrectly labelled as the left). *Rhomaleopakhus* possesses the same distal end profile seen in other CMTs (Fig. 8B): however, several non-CMTs also possess this state and, in any case, it is potentially the plesiomorphic eusauropod condition (Mannion et al., 2019a). In *Rhomaleopakhus*, the lateral third of the flat distal end surface is quite strongly beveled (~30° relative to the plane lying perpendicular to the proximodistal long-axis of the

FIGURE 7. Right humerus of *Rhomaleopakhus turpanensis* gen. et sp. nov. (IVPP V11121-1; holotype). **A**, anterior view; **B**, lateral view. **Abbreviations**: **dpc**, deltopectoral crest; **l.adp**, lateral anterodistal process; **m.adp**, medial anterodistal process; **mt**, medial tuber. Note that it was not possible to remove the humerus from its cradle at the time these photographs were taken, so obtaining images of the posterior and medial surfaces was not possible. Scale bar equals 200 mm.

humerus) (Fig. 7A): as a result, it faces laterodistally. This feature, however, does not seem to have a clear phylogenetic significance; it occurs sporadically in distantly related taxa such as *Amargasaurus*, *Anhuilong*, *Haestasaurus*, *Limaysaurus*, *Mamenchisaurus youngi*, and *Saltasaurus* (Ouyang and Ye, 2002; Upchurch et al., 2015; Ren et al., 2018; Mannion et al., 2019a). The supracondylar (= olecranon or cuboid) fossa, and the medial and lateral ridges that bound it on the distal part of the posterior surface of the shaft, are partially obscured by the packing material upon which the humerus rests (Fig. 8B). However, this fossa is not deep, unlike those of *Giraffatitan* and several somphospondylans (Upchurch et al., 2004a, 2015; D'Emic, 2012), and the associated ridges are broadly rounded transversely rather than acute.

Ulna—The ulna is complete apart from a small amount of material missing from the proximal end (Figs. 6, 9A–F). It is extremely robust, with one of the highest proximal end maximum width to proximodistal length ratios (0.50) of any sauropod, although *Opisthocoelicaudia* has a ratio of 0.51 (Table S2 in Supplemental Data 1). The expanded proximal end is triradiate because of the presence of well-developed anterolateral, anteromedial, and posteromedial processes. As in other sauropods, the anterolateral and anteromedial processes define a deep concavity that receives the proximal end of the radius (Wilson and Sereno, 1998). In proximal view (Fig. 9E), the ulna of *Rhomaleopakhus* has a 'V'-shaped profile, rather than the 'T'-shape seen in several somphospondylans (Upchurch et al., 2015). The angle between the anteromedial and anterolateral
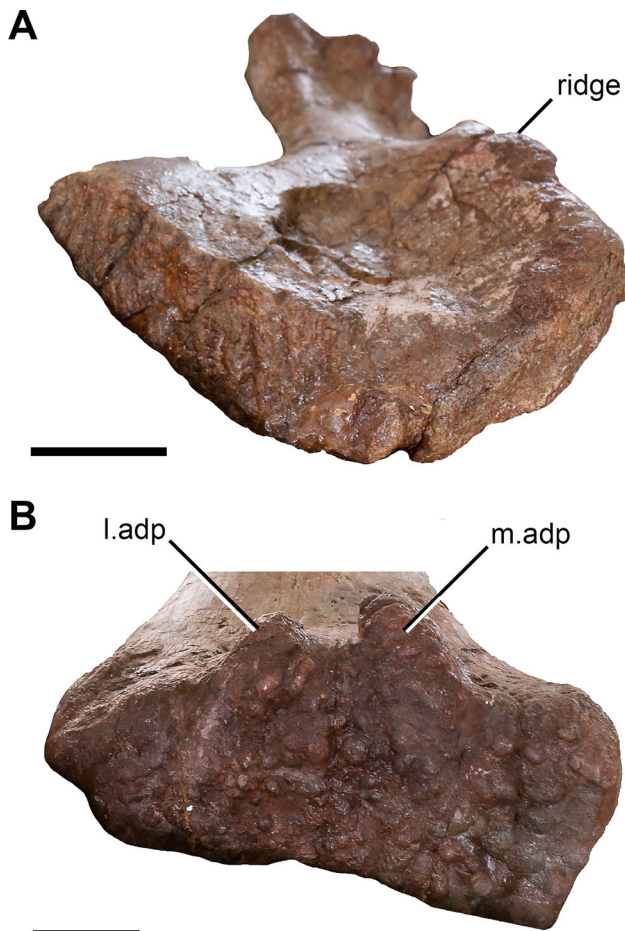
A

ridge

B

l.adp   m.adp

FIGURE 8. Right humerus of *Rhomaleopakhus turpanensis* gen. et sp. nov. (IVPP V11121-1; holotype). **A**, proximal end view (damaged); **B**, distal end view. **Abbreviations**: **l.adp**, lateral anterodistal process; **m.adp**, medial anterodistal process. Scale bars equal 100 mm.

processes is ~70°, which is the derived state (i.e., less than 80°) that occurs in most sauropods (including *Chuanjiesaurus*, *Mamenchisaurus youngi*, and *Klamelisaurus*), except some non-neosauropods, such as *Shunosaurus*, *Omeisaurus tianfuensis*, *Anhuilong*, *Huangshanlong*, *Bellusaurus*, and *Cetiosaurus*, as well as several titanosaurs, in which this angle is greater than 80° and often approaches 90° (Huang et al., 2014; Tschopp et al., 2015a; Poropat et al., 2016; Ren et al., 2018; Moore et al., 2020). In *Rhomaleopakhus*, the anteromedial to anterolateral process length ratio (sensu Upchurch et al., 2015) is 1.72 (N.B., the measurements in Table 3 give a ratio of 1.25, but these are the maximum lengths of the processes, not their lengths measured to the intersection of process long-axes, as defined by Upchurch et al. [2015:fig. 13A]). This ratio typically ranges between 1.6–1.8 in non-neosauropod eusauropods (e.g., *Vulcanodon*, *Cetiosauriscus*, *Ferganasaurus*), 1.0–1.3 in most diplodocoids and non-titanosauriform macronarians, and >1.5 in titanosauriforms (with values >1.6 in titanosaurs such as *Opisthocoelicaudia* and ≥2.0 in *Epachthosaurus* and *Cedarosaurus*) (Upchurch et al., 2015:table 2). The anteromedial process of the proximal end of the *Rhomaleopakhus* ulna has a strongly concave articular surface (Fig. 9A–D), as also occurs in many titanosaurs (Upchurch, 1995, 1998), several non-neosauropod eusauropods such as *Janenschia* and *Haestasaurus* (Bonaparte et al., 2000; Upchurch et al., 2015; Mannion et al., 2019a), and in a more

shallowly concave form in *Chuanjiesaurus* (Sekiya, 2011). Dong (1997) stated that the olecranon process is relatively low in *Rhomaleopakhus*, although this region is moderately projected, which is emphasized by the concave proximal surface of the ante-romedial process. Similarly developed olecranon processes are seen in *Mamenchisaurus youngi* (Ouyang and Ye, 2002:fig. 36), *Chuanjiesaurus* (Sekiya, 2011:fig. 40), *Haestasaurus* (Upchurch et al., 2015), *Janenschia* (Bonaparte et al., 2000; Mannion et al., 2019a), and several titanosaurs (Upchurch, 1995; Wilson and Carrano, 1999; Upchurch et al., 2004a). In *Rhomaleopakhus*, the posteromedially directed process of the proximal end creates a concavity on the posteromedial surface that does not fade out until approximately the midlength of the element, whereas the lateral surface is flat or slightly convex anteroposteriorly. In horizontal cross-section, the proximal portion of the ulna retains the triradiate configuration, but by midlength it is elliptical, with the long-axis of this ellipse oriented anteromedially. There is a prominent ridge for a ligamentous attachment to the radius, located on the anteromedial surface of the shaft at ~100 mm above the distal end. The distal end of the ulna is expanded both anteroposteriorly and transversely relative to the shaft. In distal view (Fig. 9F), the margins of this surface are strongly convex laterally and posteriorly, but slightly concave anteromedially, resulting in a comma-shaped distal profile, as is typical for most non-titanosaurian sauropods (Upchurch et al., 2015). The distal articular surface is mildly convex anteroposteriorly and transversely.

Radius—The radius is complete and is 63% of the length of the humerus. This is broadly similar to the condition in many other sauropods, which tend to have values ≥65% (Yates and Kitching, 2003; Mannion et al., 2013). For example, this value is ~66% in *Mamenchisaurus youngi* (Ouyang and Ye, 2002) and ranges from 65–76% in specimens referred to *Omeisaurus* (He et al., 1988; Ren et al., 2018). By contrast, this ratio is reduced in titanosauriforms (Mannion et al., 2013) and many CMTs (Ren et al., 2018), with particularly low values of 58% and 50% in *Huangshanlong* and *Anhuilong*, respectively (Huang et al., 2014; Ren et al., 2018). The radius of *Rhomaleopakhus* is a robust element with expanded proximal and distal ends relative to the shaft (Dong, 1997) (Fig. 9G–J). The maximum widths of the proximal and distal ends are subequal, the proximal end transverse width to radius proximodistal length ratio is 0.31, and the distal end is ~1.3 times as wide as the shaft at its midlength (Table 3). The proximal end surface is flat, with a central shallow concavity and a slightly convex portion around both its anterior and lateral margins. In proximal view (Fig. 9K), the radius has a 'D'-shaped profile, comprising a straight posterior margin (that becomes mildly concave towards the medial corner), and strongly convex anterior and lateral margins. This proximal profile appears to be plesiomorphic for sauropods, contrasting with the derived subtriangular profile with pointed medial process seen in many titanosauriforms (Upchurch et al., 2015:fig. 9), and the anteroposteriorly narrow morphology that characterizes some turiasaurians (Mateus et al., 2014).

Approximately 100 mm below the mildly concave posteromedial margin of the proximal end, on the posterior surface, there is a prominent 100 mm long ridge that projects posteromedially. Titanosaurs, such as *Epachthosaurus*, *Rapetosaurus*, and *Saltasaurus*, usually have a ridge on the posterior surface of the radius that extends along much of the element's length (Curry Rogers, 2005, 2009; Mannion et al., 2013), and Ren et al. (2018: fig. 4C) described a 'lateral ridge' ('lr') on the proximal part of the *Anhuilong* radius. However, the morphology and position of the short, prominent and posteromedially directed ridge seen in *Rhomaleopakhus* appears to be unique and is provisionally regarded as an autapomorphy. The radius is twisted along its length such that the long-axis of the proximal articular surface is set at about 90° to that of the distal end. As a result, the posterior
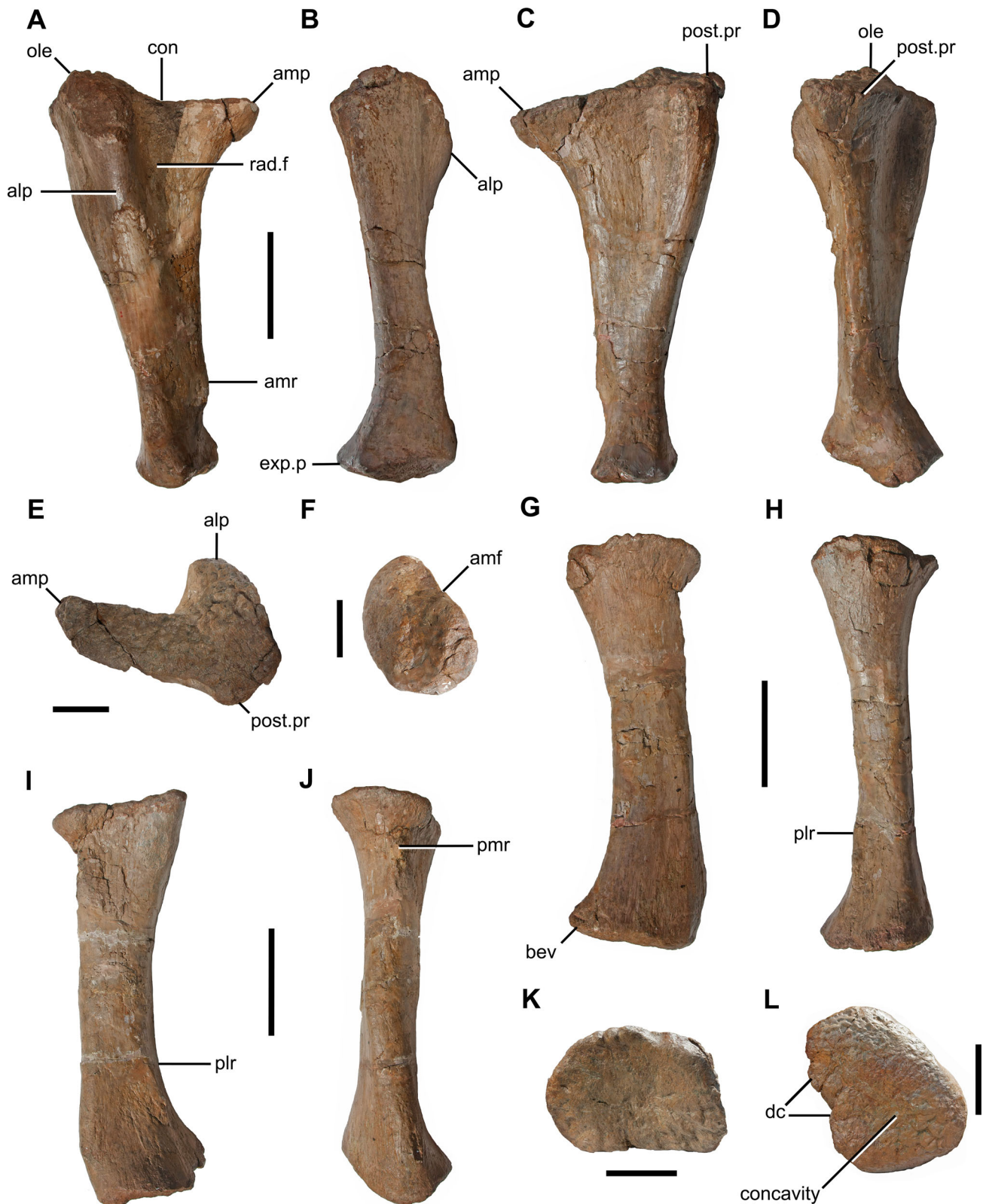
FIGURE 9. Right ulna and radius of *Rhomaleopakhus turpanensis*, gen. et sp. nov. (IVPP V11121-1; holotype). **A–F**, right ulna in anterior (**A**), lateral (**B**), posterior (**C**), posteromedial (**D**), proximal (**E**), and distal (**F**) views. **G–L**, right radius in anterior (**G**), lateral (**H**), posterior (**I**), medial (**J**), proximal (**K**), and distal (**L**) views. Note that in E, F, K, and L that anterior is towards the top of the page. **Abbreviations**: **alp**, anterolateral process of proximal ulna; **amf**, anteromedial fossa on distal ulna; **amp**, anteromedial process of proximal ulna; **amr**, anteromedial ridge on distal ulna; **bev**, beveled condyles of distal radius; **con**, concavity between olecranon and anteromedial processes on proximal ulna; **dc**, distal condyles; **exp.p**, posterior expansion of distal ulna; **ole**, olecranon process; **plr**, posterolateral ridge of distal radius; **pmr**, posteromedial ridge of proximal radius; **post.pr**., posterior process of proximal ulna; **rad.f**, radial fossa. Scale bars equal 200 mm (A–D, G–J) or 100 mm (E, F, K, L).

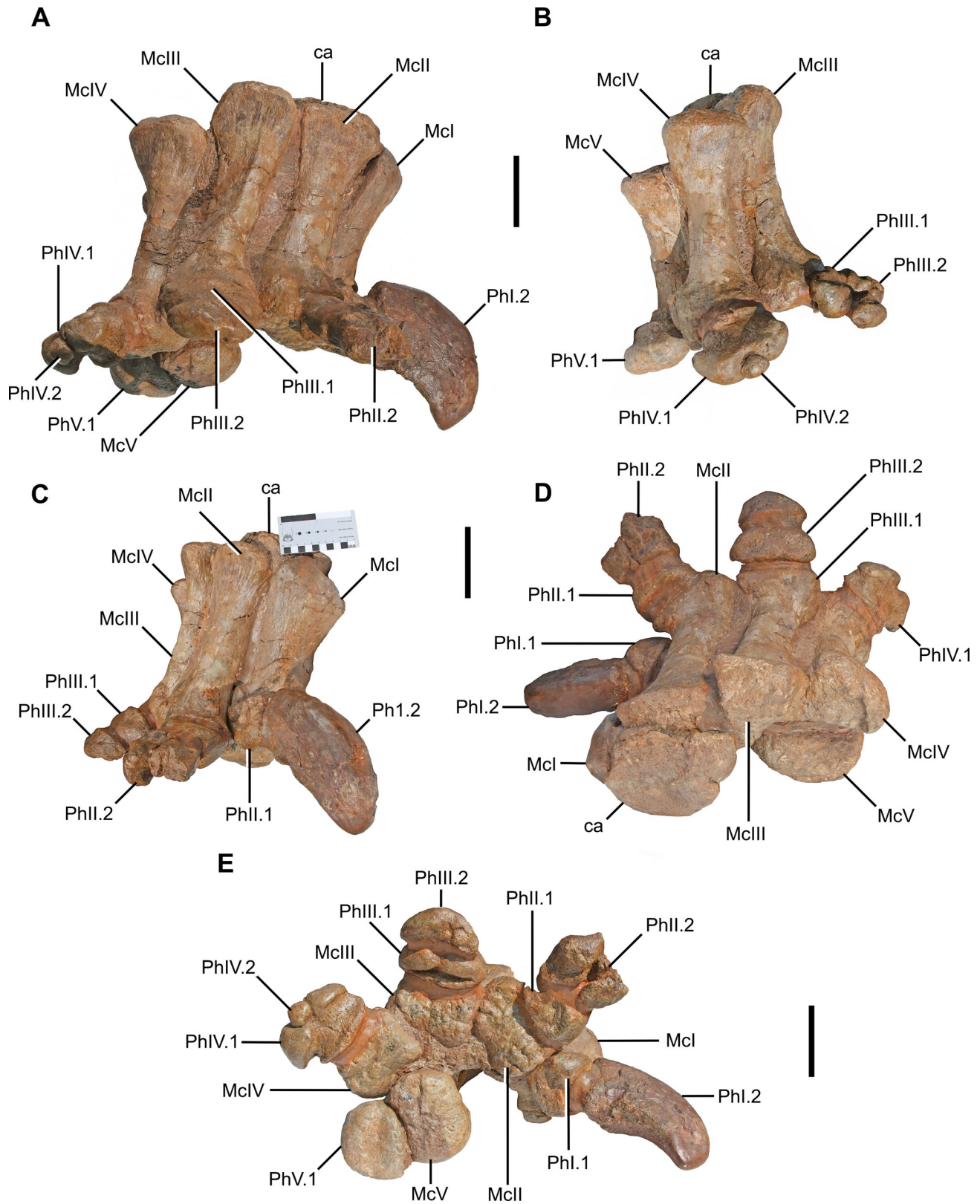FIGURE 10. Articulated right manus of *Rhomaleopakhus turpanensis*, gen. et sp. nov. (IVPP V11121-1; holotype). **A**, anterior view; **B**, anterolateral view; **C**, anteromedial view; **D**, proximal (dorsal) view; and **E**, distal (ventral) view. **Abbreviations**: **1–2**, phalanx number; **ca**, carpal; **I–V**, digit/meta-carpal number; **McX**, metacarpal (number); **PhX.Y**, phalanx (number). Scale bars equal 100 mm.

TABLE 3. Measurements of the right humerus, ulna, and radius of *Rhomaleopakhus turpanensis*, gen. et sp. nov. (IVPP V11121-1). **Abbreviations**: **ALPW**, Proximal end width on anterolateral process (ulna only); **AMPW**, Proximal end width on anteromedial process (ulna only); **DWAP**, anteroposterior width of distal end; **DWPM**, width across distal end taken perpendicular to maximum width; **DWM**, maximum width across distal end; **PW**, proximal end transverse width; **PWAP**, proximal end anteroposterior width. All measurements in mm.

Element	Length	PW	AMPW	ALPW	PWAP	DWM	DWPM	DWAP
Humerus	1240	566	–	–	–	474	–	–
Ulna	785	–	393	314	—	245	168	–
Radius	785	247	–	–	175	245	–	182

TABLE 4. Measurements of the right manus of *Rhomaleopakhus turpanensis*, gen. et sp. nov. (IVPP V11121-1). **Abbreviations**: **APW**, anteroposterior width; **H**, height; **W**, width. All measurements in mm.

Element	Medial length	Lateral length	Proximal end H	Proximal end W	Proximal end APW	Distal end H	Distal end W
Carpal	–	–	–	172	139	–	–
Metacarpal I	217	195	–	–	–	–	–
Metacarpal II	312	324	–	–	–	123	–
Metacarpal III	299	326	123	119	–	–	114
Metacarpal IV	278	302	143	145	–	121	142
Metacarpal V	276	–	–	150	88	94	136
Phalanx I–1	–	70	–	–	–	–	–
Phalanx I–2	–	224	134	–	–	–	–
Phalanx II–1	–	45	–	103	–	–	–
Phalanx II–2	–	–	–	–	–	–	–
Phalanx III–1	–	27	–	132	–	–	–
Phalanx III–2	–	45	–	114	–	–	–
Phalanx IV–1	–	65	–	134	–	–	–
Phalanx IV–2	–	20	–	33	–	–	–
Phalanx V–1	–	52	–	116	–	–	–

surface of the shaft turns to face laterally as it approaches the distal end. Such torsion of the radius is rare among sauropods (Mannion et al., 2013), although it has also been observed in the somphospondylan *Huabeisaurus* (D'Emic et al., 2013) and a few titanosaurs (e.g., *Epachthosaurus* – Poropat et al., 2016; *Malawisaurus* – Gomani, 2005; *Rapetosaurus* – Curry Rogers, 2009). At midlength, the cross-section through the shaft is elliptical in *Rhomaleopakhus*, with the radius being wider transversely than anteroposteriorly. There is a prominent vertical ridge on the posterolateral surface, located at approximately one-fifth of element length from the distal end. This matches the prominent ridge on the anteromedial surface of the shaft of the ulna, close to the distal end, suggesting that these two ridges marked the location of a strong interosseous ligament (Upchurch et al., 2004a).

In medial view (Fig. 9J), the distal end surface is set at an oblique angle to the long axis of the shaft such that it slopes anteroproximally (N.B., this would be proximolateral beveling of the distal end, in anterior view, if the radius was not twisted through 90° along its length). As a result, the distal end surface is set at ~15° to the plane perpendicular to the proximodistal long-axis of the radius. Non-neosauropod eusauropods (such as *Shunosaurus* and *Mamenchisaurus*), and at least some rebbachisaurids, display no such beveling of the distal radius, whereas turiasaurians and several titanosaurs have angles of ~25° or higher (Wilson, 2002; Mannion et al., 2019a). The degree of distal radial beveling in *Rhomaleopakhus* is similar to that seen in several non-neosauropod eusauropods, including *Omeisaurus tianfuensis*, *Chuanjiesaurus*, and *Jobaria*, as well as some neosauropods such as *Diplodocus* and *Giraffatitan* (Mannion et al., 2019a). In *Rhomaleopakhus*, beveling of the distal end extends uniformly across the entire articular surface, as occurs in some titanosaurs such as *Opisthocoelicaudia* and *Saltasaurus* (Wilson, 2002; Mannion et al., 2013; Upchurch et al., 2015). This contrasts with the more typical form of distal beveling in other sauropods,

in which the medial half of the distal end surface is perpendicular to the long-axis of the shaft, such that the beveled section is limited to the lateral half (Mannion et al., 2013; Upchurch et al., 2015). The distal end has a 'D'-shaped outline (Fig. 9L), with the derived, nearly straight posterior (= lateral because of shaft torsion) margin observed in other sauropod radii, rather than the plesiomorphic convex margin that occurs in non-sauropod sauropodomorphs (Wilson & Sereno, 1998). In fact, this posterior distal margin is mildly concave between the posterolateral and posteromedial 'condyles.' Such distal radial condyles were first discussed by D'Emic (2012, 2013), and their wider distribution among sauropods was further investigated by Upchurch et al. (2015). According to the latter, such condyles tend to occur in neosauropods, but with several reversals in, for example, some titanosaurs. Laterally, the distal surface of the *Rhomaleopakhus* radius is mildly convex, whereas the central and medial portions are markedly concave: this contrasts with the uniformly convex distal surfaces seen in nearly all other sauropods (Janensch, 1961; Upchurch et al., 2004a). Ren et al. (2018) described the distal end surface of the radius of *Anhuilong* as also being flat over most of its extent, with a convex area placed posteriorly and medially. Thus, while *Rhomaleopakhus* and *Anhuilong* potentially share the unusual flattening of the distal articular surface, the location of the residual convex area differs. Consequently, this concavity is regarded as an autapomorphy of *Rhomaleopakhus*.

Manus—The right manus is virtually complete, including one carpal element, five metacarpals, and two phalanges per digit except for digit V (see below) (Fig. 10). These elements are preserved in articulation, but many details are obscured by matrix (especially the 'palmar' surfaces of the metacarpals – see below for definitions of the orientations of the latter).

A large, flat, block-like carpal is situated above metacarpals I and II (Fig. 10A, D) (N.B., Dong [1997] stated that this element also articulated with metacarpal III, but this is not supported
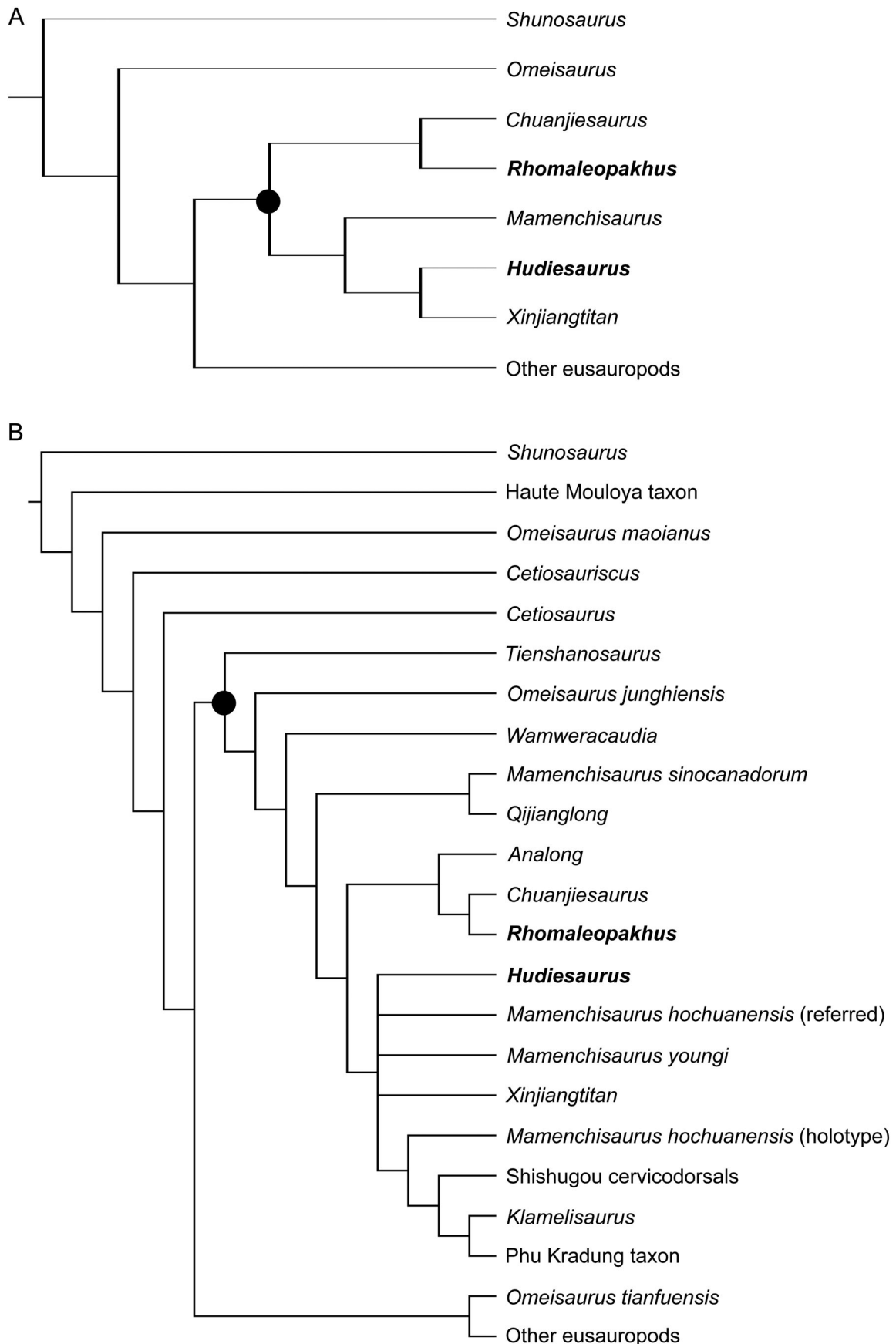
FIGURE 11. Phylogenetic relationships of *Hudiesaurus sinojapanorum* and *Rhomaleopakhus turpanensis*, gen. et sp. nov. **A**, topology based on EWP and EIW analyses of the Mannion et al. (2019a, b) matrix, with *Wamweracaudia* pruned a posteriori; **B**, topology based on EIW analysis of Moore et al. (2020) matrix. In both topologies, *Hudiesaurus* and *Rhomaleopakhus* are in bold font, the highlighted node represents 'Core *Mamenchisaurus*-like taxa' (CMTs), and eusauropods more derived than CMTs have been collapsed into a single lineage.

by our observations of the specimen). Possession of block-like carpals is a synapomorphy of Eusauropoda according to Wilson and Sereno (1998), contrasting with the carpals of non-sauropod sauropodomorphs, which tend to have proximodistally more rounded margins, and proximal and distal surfaces that are less parallel (Yates, 2007). Sauropods have often been interpreted as possessing ossified distal carpals only (e.g., Gauthier, 1986; Wilson and Sereno, 1998; Upchurch et al., 2004a), although an ossified proximal carpal is probably present in at least 'Bothriospondylus madagascariensis' and Apatosaurus (Läng and Goussard, 2007; Tschopp et al., 2015b). The Rhomaleopakhus carpal resembles the 'medial distal carpal' in Camarasaurus (Tschopp et al., 2015b). With the exception of Apatosaurus (Hatcher, 1902; Gilmore, 1936), the largest carpal in the sauropod wrist is generally placed over metacarpals I and II and articulates closely with them. This element could represent: a single enlarged distal carpal I; a fusion of distal carpals I and II; or the fusion of the intermedium, one or two centrales, and distal carpal I (as proposed for 'Bothriospondylus madagascariensis' by Läng and Goussard, 2007). If the latter interpretation is correct, then we cannot regard the carpal of Rhomaleopakhus as being either a proximal or distal carpal since it would be a composite with contributions from each of the three rows of carpals found in the plesiomorphic archosaurian wrist.

The margins of the Rhomaleopakhus carpal are damaged, such that its outline can only be estimated as subcircular to elliptical, with the long axis running transversely. The approximate transverse:anteroposterior width ratio is 1.23, similar to the values seen in several non-neosauropod eusauropods such as Shunosaurus and turiasaurians, but differing from the higher values (>1.4) observed in many neosauropods (Royo-Torres et al., 2014; Mannion et al., 2017). The proximal surface of the carpal is irregularly flat, with a slight convexity near the posterior and lateral margins. The posterolateral edge has a small vertical groove, suggesting that this portion is possibly a small medial part of a more lateral carpal, perhaps supporting the view that this large medial element is a composite structure (Läng and Goussard, 2007). The distal surface of the carpal cannot be examined because of the presence of matrix and the proximal ends of the metacarpals.

The true number of ossified carpals in Rhomaleopakhus cannot be determined. Sauropods appear to show a trend towards loss and/or fusion of carpals through their evolutionary history, with five and three-to-four elements in the early-diverging taxa 'Bothriospondylus madagascariensis' and Shunosaurus, respectively, two in non-neosauropod eusauropods and non-titanosauriform macronarians, one in diplodocids (such as Apatosaurus and Diplodocus) and Giraffatitan, and complete loss in some titanosaurs such as Alamosaurus and Opisthocoelicaudia (Janensch, 1961; Upchurch, 1998; Upchurch et al., 2004a; Apesteguía, 2005; Remes, 2008; Tschopp et al., 2015b). The single carpal in Apatosaurus (Gilmore, 1936; Bonnan, 2003) is placed centrally over metacarpals II–IV and has a proximal surface that conforms closely to the distal ends of the ulna and radius (Tschopp et al., 2015b). Although it is possible that Rhomaleopakhus only possessed one carpal and that this taxon differed from Apatosaurus in having this placed medially over metacarpals I and II, we consider it more likely that there was at least one additional (lateral) carpal placed over metacarpal III (as in Mamenchisaurus youngi: Ouyang and Ye, 2002) or metacarpal V (as in Camarasaurus, Atlasaurus, and possibly Argyrosaurus: Apesteguía, 2005; Tschopp et al., 2015b). This view is supported by the possible presence of a small portion of a more lateral carpal (as described above) which, if correctly identified, would suggest that the wrist of Rhomaleopakhus most closely resembled that of Mamenchisaurus youngi (Ouyang and Ye, 2002).

The stout metacarpals have a semicircular or horseshoe-shaped arrangement with their long axes oriented vertically (Fig. 10); this is a eusauropod synapomorphy (Upchurch, 1995, 1998; Yates, 2007; McPhee et al., 2014; Apaldetti et al., 2018). The arc of a circle covered by this metacarpal arcade is ~270°, as occurs in neosauropods (Upchurch, 1998; Wilson and Sereno, 1998; Bonnan, 2003; Apesteguía, 2005; Remes, 2008) and several taxa close to the neosauropod radiation, such as Mamenchisaurus youngi (Ouyang and Ye, 2002) and 'Bothriospondylus madagascariensis' (Läng and Goussard, 2007). This contrasts with the apparently less strongly curved arcades (~90–180°) seen in other non-neosauropod eusauropods, such as Omeisaurus tianfuensis (Bonnan, 2003), Shunosaurus (ZDM T5402; PU pers. observ., 1995), and possibly Ferganasaurus (Alifanov and Averianov, 2003) (N.B., we are skeptical about the accuracy of the reconstruction of the manus of the latter based on, for example, an anomalous arrangement of the metacarpals as reconstructed in distal end view: see Alifanov and Averianov, 2003:fig. 9C). The vertically oriented metacarpals, in a 'tubular colonnade,' make conventional directional anatomical terms ambiguous unless care is taken to define them (e.g., see Upchurch, 1994). Here, we treat the metacarpals as if they were laid on a flat surface side-by-side. As such, 'lateral,' 'medial,' 'dorsal,' and 'ventral' refer to surfaces on the shafts of the metacarpals, rather than how these surfaces would face in the articulated manus. As a result, the dorsal surfaces face outwards, ventral surfaces face towards the center of the tubular colonnade, and metacarpals typically contact each other via portions of their lateral and medial surfaces. In correct articulation, the phalanges are placed in a more conventional orientation, with their ventral surfaces facing approximately downwards. Therefore, no additional definitions are required for phalanges, although it should be borne in mind that, for example, the medial surface of the pollex claw would have faced posteriorly or posteromedially in life with respect to the sagittal plane of the animal (Fig. 10).

The proximal ends of metacarpals I and II in Rhomaleopakhus are obscured by the overlying carpal. In anterior view (Fig. 10A), the proximal ends of metacarpals I–III are level with each other, whereas that of metacarpal IV is displaced distally. The proximal end of metacarpal V is, in turn, displaced distally with respect to metacarpal IV. These displacements of metacarpals IV and V are presumably the result of post-mortem distortion rather than an unusual morphology possessed by the living animal. In metacarpals III–V, the exposed proximal end surfaces are generally flat and mildly rugose.

Metacarpal I is short compared with the other metacarpals (e.g., it is only 0.67 of the averaged length of metacarpals II and III: Table 4) and shorter than the ungual on digit I. Such a relatively short metacarpal I is the plesiomorphic state that occurs in non-sauropod sauropodomorphs, non-neosauropod eusauropods (such as Shunosaurus, Omeisaurus tianfuensis, and Mamenchisaurus youngi), and, to a lesser extent, in diplodocines (Table S2 in Supplemental Data 1). In Rhomaleopakhus, metacarpal I is substantially longer along its medial margin than on its lateral one (Table 4): this reflects the beveling of the distal end relative to the long-axis of the shaft. This condition is a derived state that occurs in most eusauropods except Shunosaurus, with a reversal to the plesiomorphic state in most titanosauriforms (Wilson, 2002; Mannion et al., 2013). As in Chuanjiesaurus (Sekiya, 2011), Turiasaurus (CPT-1195-1210; PU and PDM pers. observ., 2009), and many neosauropods (Wilson, 2002), the distal end of metacarpal I is not divided into two distinct condyles.

In dorsal view, the proximal end of metacarpal II is strongly expanded to overhang the medial surface of its shaft (Fig. 10A, C). This feature is absent in taxa such as Mamenchisaurus youngi (Ouyang and Ye, 2002:fig. 38B), Apatosaurus ajax (Upchurch et al., 2004b:pl. 8, fig. D), and Camarasaurus (Tschopp et al., 2015b: fig. 11), but a medial process appears to

be developed to some extent in *Ferganasaurus* (Alifanov and Averianov, 2003:figs. 9, 10), *Giraffatitan* (Janensch, 1961:194, fig. 1a), and *Alamosaurus* (Gilmore, 1946:fig. 10). A minimum shaft width to proximodistal length ratio of <0.2 in metacarpal II was proposed as a diagnostic character of *Chuanjiesaurus* by Sekiya (2011); however, this ratio is 0.19 in *Rhomaleopakhus*, similar to those of several other non-neosauropod eusauropods, such as *Omeisaurus tianfuensis*, *Mamenchisaurus youngi*, and *Turiasaurus* (Poropat et al., 2016).

The proximal articular surface of metacarpal III is subtriangular in outline (Fig. 10D). This element is the longest of the five metacarpals, as is the case in most eusauropods (Poropat et al., 2015a), although it only slightly exceeds the length of metacarpal II (Table 4). The length of metacarpal III is 0.42 of radius length, similar to the condition in taxa such as *Mamenchisaurus youngi* and *Apatosaurus*, but lower than the derived 0.45 ratio employed as a synapomorphy of Macronaria by Wilson and Sereno (1998; Table S2 in Supplemental Data 1). Its proximal end lacks the mediolaterally expanded morphology that characterizes brachiosaurids, as well as *Atlasaurus* and *Jobaria* (Mannion et al., 2017).

Metacarpal IV also has a subtriangular proximal end but differs from metacarpal III by possessing a ventromedially directed palmar process (Fig. 10D). Unlike the metacarpal IVs of several brachiosaurids and a few titanosaurs, that of *Rhomaleopakhus* lacks the chevron-shaped proximal end profile that wraps around the proximal end of metacarpal V (D'Emic, 2012; Mannion et al., 2013).

The proximal end of metacarpal V is semicircular to slightly subrectangular in outline, with a flattened medial surface that articulates with metacarpal IV (Fig. 10D). Metacarpal V is twisted along its length such that the long-axes of its proximal and distal ends lie at ~90° to each other, and this degree of twisting has also been reported in *Ferganasaurus* (Alifanov and Averianov, 2003). Some torsion of metacarpal V also occurs in neosauropods but is less extreme than in *Rhomaleopakhus* and *Ferganasaurus* (Apesteguía, 2005; Bedwell and Trexler, 2005; Tschopp et al., 2015b). For example, in *Camarasaurus* and *Diplodocus* the amount of torsion is ~25–30° (Bedwell and Trexler, 2005; Tschopp et al., 2015b), and in the titanosaur *Epachthosaurus* it is ~45° (UNPSJB-PV 920; PU and PDM pers. observ., 2013).

The phalanges are hyper-extended such that they lie on the dorsodistal parts of each metacarpal, except in metacarpal I where the phalanx obscures the distal end (resulting in the distal end surfaces being visible in metacarpals II–V) (Fig. 10E). In general, the distal articular surfaces of the metacarpals are expanded dorsoventrally, and especially transversely, and have a rounded subrectangular outline. These surfaces are gently saddle-shaped, with mild midline grooves between slightly expanded lateral and medial condyles. The ventral portions of the distal ends are flattened and have a rugose texture. Generally, the distal articular surfaces do not extend onto the dorsal surfaces of the shafts: this is a derived state seen in titanosauriforms (Gimenez, 1992; Salgado et al., 1997; Apesteguía, 2005; D'Emic, 2012; Mannion et al., 2013) that also occurs convergently in rebbachisaurids (Mannion et al., 2019a). *Rhomaleopakhus* lacks the additional flanges, close to the distal ends of the metacarpals, that helped bind them together in some titanosaurs (Apesteguía, 2005).

Dong (1997) stated that IVPP V11121-1 has a phalangeal formula of 2-2-2-1-1; however, it is actually 2-2-2-2-1 (Fig. 10E). Retention of two phalanges on manual digit IV occurs in early-branching sauropods such as *Shunosaurus*, but in most neosauropods the phalangeal formula has been reduced to 2-2-2-1-1, 2-2-1-1-1, or 2-1-1-1-1 (in diplodocoids and early-diverging macronarians), or the phalanges are completely lost (apart from a rudimentary phalanx IV-1) in titanosaurs such as *Epachthosaurus*, *Alamosaurus*, and *Opisthocoelicaudia*

(Gilmore, 1946; Borsuk-Białynicka, 1977; Salgado et al., 1997; Bonnan, 2003; Martínez et al., 2004; Upchurch et al., 2004a, b; Mannion et al., 2013; Poropat et al., 2015b; Tschopp et al., 2015b). The phalanges (except for the ungual of digit I) of *Rhomaleopakhus* are wider transversely than they are proximodistally, which is a eusauropod synapomorphy (Wilson, 2002; Upchurch et al., 2004a, 2007b; Yates, 2007). The phalanges in the proximal row have flattened or mildly concave ventral surfaces. These phalanges are also expanded transversely at their distal ends, so that they are wider at this point than they are at midlength.

Phalanx I-1 is subrectangular in dorsal view, decreasing only slightly in proximodistal length towards its medial margin. Similar subrectangular manual phalanx I-1s are seen in several other non-neosauropod eusauropods, such as *Ferganasaurus* (Alifanov and Averianov, 2003:fig. 11) and *Omeisaurus tianfuensis* (He et al., 1988:pl. XIV, fig. 6), as well as the titanosauriform *Giraffatitan* (Janensch, 1961). Thus, *Rhomaleopakhus* retains the plesiomorphic manual phalanx I-1 dorsal profile, rather than the derived trapezoidal outline seen in *Turiasaurus* (Mannion et al., 2019a) and *Jobaria* (Läng and Goussard, 2007), or the even more strongly wedge-shaped outline seen in several diplodocids and the non-titanosauriform eusauropod specimen MfN MB.R. 2093 (previously referred to *Janenschia* but removed from that genus by Mannion et al. [2019a]) (Upchurch et al., 2004a; Tschopp et al., 2015b). The proximal and distal ends of phalanx I-1 are obscured by the metacarpal and ungual respectively, but the general outline of the transverse cross-section is an irregular 'D'-shape, with rounded medial, dorsal, and lateral surfaces, and a flattened ventral surface. There is no lappet-like projection from the proximodorsal margin. Such a lappet occurs as the plesiomorphic condition in early-branching eusauropods such as *Shunosaurus*, *Omeisaurus tianfuensis*, *Turiasaurus*, and *Zby*, but is absent in most neosauropods (Mannion et al., 2019a). Distally, the phalanx terminates in well-developed, rounded lateral and medial condyles.

Phalanx I-2 is a large, robust ungual that is transversely compressed. As in most other sauropods, this ungual is much longer than phalanx I-1 (Fig. 10E), whereas in *Giraffatitan* the two elements are subequal in length (Janensch, 1922). In dorsal view, the proximal articular surface of the *Rhomaleopakhus* ungual is approximately perpendicular to the long axis of the claw: this is the plesiomorphic state, whereas in neosauropods (e.g., *Apatosaurus*—Upchurch et al., 2004b; *Camarasaurus*—Tschopp et al., 2015b; *Giraffatitan*—Janensch, 1961) this surface is set at an oblique angle to the long-axis such that it faces proximolaterally. The *Rhomaleopakhus* ungual bears a groove on each of the lateral and medial surfaces, with the former being positioned lower than the latter. The ventral side merges smoothly into the medial surface but meets the lateral surface at a sharper edge.

Phalanx II-1 is subrectangular in dorsal view. The medial, lateral, and dorsal surfaces round smoothly into each other, although the medial edge meets the ventral surface at a slightly more acute angle than the lateral edge. The ventral surface is nearly flat. Phalanx II-2 is larger than phalanx II-1 (Table 4) (contra Dong, 1997) but seems to have a pathological distal termination. It appears damaged and ends irregularly, with a cavity running down the central part of its ventral surface (Fig. 10E).

Phalanx III-1 is large and dorsoventrally compressed, with two distinct distal condyles. Whereas the dorsal surface meets the proximal and distal end surfaces at an obtuse angle in lateral or medial views, the articular surfaces expand ventrally to make the ventral surface concave proximodistally. In dorsal view, this element narrows slightly in transverse width towards its distal end. Phalanx III-2 is similar to phalanx III-1, but is slightly smaller, with its distal end rounding transversely in dorsal view so that it curves into the corners of the proximal

end. It is therefore more semicircular, rather than rectangular, in dorsal profile. This element is also bowed upwards in distal end view.

Phalanx IV-1 is large, dorsoventrally compressed, and subrectangular in dorsal outline. The medial condyle is large and rounded, and projects more distally than the lateral one. In dorsal view, the medial margin is mildly concave, whereas the lateral one is straighter. This element tapers slightly transversely towards the distal end in dorsal view. Phalanx IV-2 is a very small, flattened hemisphere of bone that sits in the intercondylar groove on the distal end of phalanx IV-1. The dorsal and ventral surfaces are slightly concave longitudinally because of the expansion of both ends. The lateral condyle of the distal end is enlarged dorsoventrally, but the medial condyle is indistinct.

Phalanx V-1 is large, subrectangular, and dorsoventrally compressed. The dorsal and ventral surfaces are slightly concave longitudinally because of the expansion of the proximal end. The element tapers in dorsoventral thickness towards its distal end. The distal surface is generally convex both dorsoventrally and transversely, with little division into two separate condyles. Thus, this phalanx in *Rhomaleopakhus* still resembles the other proximal phalanges, as it does in several other sauropods such as *Apatosaurus* (Upchurch et al., 2004b): this contrasts with phalanx V-1 of *Camarasaurus*, which is very irregular and rather different from the other proximal phalanges (Tschopp et al., 2015b).

PHYLOGENETIC ANALYSES

Datasets and Analytical Approach

In order to assess the phylogenetic relationships of *Hudiesaurus* and *Rhomaleopakhus*, we scored them for modified versions of two recent data matrices. Mannion et al. (2013) developed a titanosauriform-focused data matrix of 63 taxa scored for 279 characters that was expanded upon in subsequent iterations (Upchurch et al., 2015; Poropat et al., 2016; Mannion et al., 2017), with the version published by González Riga et al. (2018) consisting of 84 taxa scored for 423 characters. Two parallel versions of this 2018 data matrix have substantially augmented the dataset. Mannion et al. (2019a, b) incorporated a large number of additional characters, as well as a broader sampling of eusauropods (especially diplodocoids), such that this version of the data matrix comprises 124 taxa scored for 548 characters. Moore et al. (2020) incorporated a large number of non-neosauropod eusauropods (especially East Asian CMTs) and made several modifications to existing characters and scorings, as well as adding characters. This version of the data matrix consists of 103 taxa scored for 436 characters. It is beyond the scope of this study to combine these two matrices. Given that the Mannion et al. (2019a, b) version is better suited to evaluating the broader phylogenetic positions of *Hudiesaurus* and *Rhomaleopakhus* within Eusauropoda, whereas the Moore et al. (2020) version is more appropriate for testing their relationships with other East Asian Jurassic taxa, we use both matrices.

In addition to *Hudiesaurus* and *Rhomaleopakhus*, we incorporated *Xinjiangtitan shanshanesis* into both matrices, based on information presented in Wu et al. (2013) and Zhang et al. (2020). A small number of character score changes were made to the *Mamenchisaurus* OTU in the Mannion et al. (2019a, b) matrix. Mannion et al. (2019a) also modified Character (C) 373 such that it was inapplicable to some taxa; however, this character is revised here so that it is applicable to all taxa, as was the case in earlier versions of the matrix (Poropat et al., 2016; Mannion et al., 2017; González Riga et al., 2018). These revisions are documented in Supplementary Data 1. Moore et al. (2020) made five characters inactive and added revised versions of

four of these to the end of the matrix. Here we follow Moore et al. (2020) in treating C14, 20, 122, and 130 as inactive in that version of the matrix. The fifth inactive character in that matrix (C413) was not revised by Moore et al. (2020): this pertains to whether a vertical groove and ridge structure is present on the posterolateral surface of the distal shaft of the ulna and was originally proposed as a feature of turiasaurs (Royo-Torres et al., 2006). However, the reinterpretation of the orientation of the antebrachium of *Turiasaurus* by Mateus et al. (2014) means that this feature was misinterpreted. As such, following suggestions by previous authors that this character should not be included (e.g., Royo-Torres et al., 2017; Moore et al., 2020), it is here replaced in both versions of the matrix by the following:

C413. Manus, arc of a circle covered by the proximal ends of the metacarpals in articulation: <180° (0); ≥180° (usually close to 270°), forming a 'tubular' manus (1) (Wilson & Sereno, 1998; modified here).

We also added three further characters to the end of both versions of the dataset, such that they are C549–551 in the Mannion et al. (2019a, b) matrix, and C442–444 in the Moore et al. (2020) matrix:

C549/C442. Middle–posterior cervical and anterior-most dorsal neural arches, prezygapophyseal articular surfaces: flat or gently concave (0); strongly convex mediolaterally (1) (Upchurch, 1995, 1998; modified here);

C550/C443. Manual phalanx I-2 (ungual), proximal articular surface: approximately perpendicular to the long axis of the ungual (0); beveled so that it faces proximolaterally (1) (new character);

C551/C444. Manual digit IV, number of phalanges: two or more (0); one or fewer (1) (new character: based on Upchurch, 1998; Wilson and Sereno, 1998; Wilson, 2002; note that titanosaurs that have lost their manual phalanges are not scored for this character).

Multistate characters were ordered where appropriate (e.g., see Upchurch, 1998; Brazeau, 2011), with 18 such characters in the Mannion et al. (2019a, b) matrix (C11, 14, 15, 27, 40, 51, 104, 122, 147, 148, 195, 205, 259, 297, 426, 435, 472, and 510) and 16 in the Moore et al. (2020) version (C11, 14, 15, 27, 40, 51, 104, 147, 148, 177, 195, 205, 259, 430, 432, and 438). Following previous iterations of these datasets, several unstable taxa were excluded a priori from analyses using both matrices (*Astrophocaudia*, *Australodocus*, *Brontomerus*, *Fukuititan*, *Fusuisaurus*, *Liubangosaurus*, *Malarguesaurus*, and *Mongolosaurus*), with *Mamenchisaurus constructus* and *Xianshanosaurus* also excluded from analyses using the Moore et al. (2020) matrix.

Both matrices were analyzed in a maximum parsimony framework, using equal weighting (EWP) and extended implied weighting (EIW) of characters. For the latter (see Goloboff et al., 2018), we used a k-value of 12, following Moore et al. (2020). In EWP and EIW analyses, we first applied the 'Stabilize Consensus' option in the 'New Technology Search' in TNT v. 1.5 (Goloboff et al., 2008; Goloboff and Catalano, 2016). Searches employed sectorial searches, drift, and tree fusing, with the consensus stabilized five times. The MPTs resulting from each of these runs were then used as the starting topologies for 'Traditional Searches', using Tree Bisection-Reconstruction (see Mannion et al., 2013 for further discussion of this protocol).

The revised data matrices are provided as TNT files (Supplementary Data 2 and 3 for Mannion et al. and Moore et al. respectively), with stored settings for assigning characters as ordered or inactive.

Phylogenetic Results

Analysis of the Mannion et al. (2019a, b) matrix under EWP produces 3168 most parsimonious trees (MPTs) with lengths of

2681 steps (Consistency Index [CI] = 0.217, Retention Index [RI] = 0.594). Other than around the base of Neosauropoda, resolution is high across much of the topology, with *Hudiesaurus* and *Xinjiangtitan* recovered in a polytomy with the CMTs *Mamenchisaurus* and *Wamweracaudia* (Bremer value = 2), with *Rhomaleopakhus* + *Chuanjiesaurus* as the sister taxon of this clade (Bremer value = 1). The *Chuanjiesaurus* OTU in this matrix is now a composite taxon following the removal of the referred specimen (renamed *Analong*) from this genus by Ren et al. (2020): however, we do not believe that this has had a significant impact on our results because the *Chuanjiesaurus* and *Analong* character state scores would differ in only one scorable character in this data set if they were revised to form two separate OTUs. A posteriori pruning of *Wamweracaudia* from the trees resolves *Hudiesaurus* and *Xinjiangtitan* as sister taxa (Fig. 11A). Applying EIW to this dataset results in 2376 MPTs of 115.3 steps (CI = 0.215, RI = 0.590) and produces identical interrelationships among the CMTs as the EWP analysis.

Analysis of the Moore et al. (2020) matrix under EWP produces 18,240 MPTs with lengths of 2042 steps (CI = 0.231, RI = 0.578). Resolution is poor in some parts of the topology, but *Hudiesaurus*, *Rhomaleopakhus*, and *Xinjiangtitan* are recovered as CMTs (Bremer values = 1). *Rhomaleopakhus* is recovered in a polytomy with *Analong*, *Chuanjiesaurus*, *Mamenchisaurus sinocanadorum*, and *Qijianglong*, with this clade the sister taxon to *Mamenchisaurus hochuanensis* (type). *Hudiesaurus* and *Xinjiangtitan* lie outside of this clade, forming a large polytomy with other CMTs. The Pruned Trees option highlights the 'Shishigou cervicodorsals' OTU as one of the most unstable taxa: a posteriori exclusion of this OTU from the MPTs recovers *Hudiesaurus* and *Xinjiangtitan* in a polytomy with *Klamelisaurus*, *Mamenchisaurus youngi*, the referred specimen of *Mamenchisaurus hochuanensis*, and the 'Phu Kradong' taxon. A majority rule consensus indicates that *Hudiesaurus* and *Xinjiangtitan* are sister taxa in 76% of the MPTs, whilst *Rhomaleopakhus* and *Chuanjiesaurus* are sister taxa in 69% of the MPTs. Application of EIW to this dataset results in 70 MPTs of length 90.1 steps (CI = 0.230, RI = 0.575) and produces a well-resolved topology that is broadly the same as that recovered by Moore et al. (2020:fig. 26). *Hudiesaurus*, *Rhomaleopakhus*, and *Xinjiangtitan* are all recovered as CMTs (Fig. 11B). *Rhomaleopakhus* is recovered as the sister taxon to *Chuanjiesaurus*, forming a clade with *Analong*. This grouping is in turn the sister taxon to a speciose clade that includes *Hudiesaurus* and *Xinjiangtitan*. The latter two taxa are part of a polytomy with *Mamenchisaurus youngi* and the referred specimen of *Mamenchisaurus hochuanensis* that lies outside of a clade including *Mamenchisaurus hochuanensis* (type) and *Klamelisaurus* (Fig. 11B).

DISCUSSION

Relationships, Systematics, and Taxonomy

All of our analyses recover *Hudiesaurus* as a CMT, with most placing it as the sister taxon to *Xinjiangtitan*. Although details vary (Fig. 11) these two taxa tend to lie in a clade with *Klamelisaurus*, the referred specimen of *Mamenchisaurus hochuanensis*, and *Mamenchisaurus youngi*. Given the extreme incompleteness of *Hudiesaurus*, it is likely that its position within a CMT clade is strongly determined by apomorphies it shares with the more complete *Xinjiangtitan*. The current study has elucidated two hitherto unrecognized synapomorphies uniting these two taxa: a distinct ridge bounding the posterior part of the dorsal margin of the lateral pneumatic opening; and the combined presence of a horizontal accessory lamina and anterodorsally oriented SPDL-like strut, creating a 'V'-shaped arrangement within the SDF of the posterior-most cervical.

This sister-taxon relationship, combined with the close geographic proximity and unusually large size of *Hudiesaurus* and *Xinjiangtitan*, raises the issue of whether they should be synonymized as a single species, assigned to a single genus containing two species, or retained as distinct genera. Both taxa were found in Shanshan County in the Turpan Basin (Dong, 1997; Wu et al., 2013): based on the latitudinal and longitudinal coordinates of their approximate localities (taken from The Paleobiology Database – https://paleobiodb.org), they were found ~34 km apart. Dong (1997) estimated that *Hudiesaurus* was around 29–30 m long and regarded it as being the largest sauropod known from Asia at that time. Part of this estimate was based on the size of the forelimb (now removed from *Hudiesaurus* and assigned to the new genus *Rhomaleopakhus*), but comparisons of centrum height and total vertebral height suggest that the *Hudiesaurus* vertebra is ~70–80% the size of Cv18 of *Xinjiangtitan* (compare Table 1 here with Zhang et al., 2020: table S1). *Xinjiangtitan* is also very large, having a body length estimated at 32.6 m (Wu et al., 2013) and a neck length of ~14.5 m (Zhang et al., 2020). Despite these superficial similarities and two detailed synapomorphies, there are a number of differences between *Xinjiangtitan* and *Hudiesaurus*, which is remarkable given that they can only be compared using the posterior-most cervical vertebra. *Xinjiangtitan* lacks the five autapomorphies of *Hudiesaurus* listed in our revised diagnosis, and this remains true even when we look for these features at other points in the cervicodorsal region of the former taxon. At least four other differences are present: (1) the centrum is transversely compressed in *Xinjiangtitan* (though this might reflect postmortem distortion) and dorsoventrally compressed in *Hudiesaurus*; (2) the vertical TPRL of *Hudiesaurus* is absent in *Xinjiangtitan*; (3) the CPRL bifurcates dorsally in *Xinjiangtitan*, but not in *Hudiesaurus*; and (4) the CPOL bifurcates dorsally in *Hudiesaurus*, but not in *Xinjiangtitan*. Three of the diagnostic characters of *Xinjiangtitan* proposed by Wu et al. (2013) pertain to posterior-most cervical vertebrae: a ventral midline keel on the penultimate cervical; a semicircular process developed at the posterior end of the ventral surface of the centrum; and relatively elongated posterior cervical vertebrae. The first of these character states is now known to occur in several other CMTs, including *Euhelopus*, *Mamenchisaurus hochuanensis* (CCG V 20401; PU and PMB pers. observ., 2010), and *Klamelisaurus* (see above). The posterior semicircular process is certainly absent in *Hudiesaurus*, but it has recently been reinterpreted as a taphonomic artifact in *Xinjiangtitan* by Zhang et al. (2020). The FAEIs for the posterior cervical vertebrae of *Xinjiangtitan* do not appear to be unusually high relative to those in other CMTs (Table S1 in Supplemental Data 1; see also Zhang et al., 2020), but these values for the penultimate and last cervical vertebrae are somewhat higher than that for *Hudiesaurus*, potentially representing a genuine difference between these two taxa. Zhang et al. (2020) revised the diagnosis for *Xinjiangtitan* and listed five autapomorphies pertaining to cervical vertebrae. However, only one of these can be assessed in *Hudiesaurus*, and this is here recognized as the apomorphic ridge over the posterior dorsal margin of the lateral pneumatic opening. In summary, therefore, we conservatively estimate that there are at least nine taxonomically meaningful differences between *Hudiesaurus* and *Xinjiangtitan*. Tschopp et al. (2015a) employed two quantitative methods for establishing the boundaries between species and genera in a specimen-level phylogenetic analysis of diplodocids. We have not deployed these here because a specimen-level analysis of CMT phylogeny lies outside the scope of the current study, and because the extreme incompleteness of *Hudiesaurus* renders disparity-based approaches difficult to apply. Moreover, Tschopp et al. (2015a) cautioned against extrapolating the results of their diplodocid-focused study to other parts of the sauropod tree, noting

that any other specimen-level phylogenetic study would need to run its own quantitative analyses in order to estimate taxonomic boundaries. Nevertheless, the results of Tschopp et al. (2015a) allow us to put the differences between *Hudiesaurus* and *Xinjiangtitan* into a wider context. In particular, Tschopp et al. (2015a) found that well-established diplodocid species within the same genus had at least six character state differences, and separate genera at least 13. Given that there are at least nine differences between *Xinjiangtitan* and *Hudiesaurus* based on comparison of a single posterior-most cervical vertebra, and that five of these are currently unambiguous autapomorphies of *Hudiesaurus*, it is very likely that more complete material of the latter taxon would provide compelling support for retaining two separate genera. Stratigraphic differences do not always provide valid grounds for separating species or genera: nevertheless, the fact that *Xinjiangtitan* was recovered from the Qiketai Formation (Maisch et al., 2019) while *Hudiesaurus* was found in the overlying Kalazha Formation, lends additional support to the retention of their taxonomic separation.

The phylogenetic relationships of *Xinjiangtitan* have only been formally assessed by one previous study (Wu et al., 2013). The latter authors, using an updated version of the data matrix presented by Harris (2006), supported a sister-taxon relationship between *Xinjiangtitan* and a single OTU representing *Mamenchisaurus*. While this supports Wu et al.'s (2013) conclusion that *Xinjiangtitan* was referrable to Mamenchisauridae, this result is difficult to evaluate further given recent evidence for the para- or polyphyly of *Mamenchisaurus* relative to other CMTs (e.g., Sekiya, 2011; Moore et al., 2020). Moreover, as Wu et al. (2013) acknowledged, support for the *Xinjiangtitan* + *Mamenchisaurus* clade was weak, requiring only one extra tree length step for it to be disrupted. Zhang et al. (2020) provided a more detailed description of the *Xinjiangtitan* cervical series, although they did not evaluate this taxon's relationships via a formal phylogenetic analysis. They did present a detailed comparison of *Xinjiangtitan* with a series of other CMTs, including several *Mamenchisaurus* species and *Qijianglong*, but *Hudiesaurus* was not considered. Zhang et al. (2020) concluded that *Xinjiangtitan* is a member of Mamenchisauridae and proposed that it is most closely related to the CMT *Qijianglong*. A close relationship between the latter and *Xinjiangtitan* was supported by two character states: the SDF of posterior cervical vertebrae is divided into two areas by a subtle horizontal ridge; and a finger-like epipophysis is present in middle cervical vertebrae and projects beyond the posterior margin of the postzygapophysis (Zhang et al., 2020). However, as noted earlier, the horizontal accessory lamina within the SDF is also seen in *Hudiesaurus*, *Klamelisaurus*, and several other CMTs, as well as *Euhelopus*. Moreover, the form of the epipophysis in middle cervical vertebrae cannot be determined in *Hudiesaurus*, and the finger-like process is present in *Euhelopus* (Wilson and Upchurch, 2009) and CMTs such as *Mamenchisaurus hochuanensis* (CCG V 20401; PU and PMB pers. observ., 2010). Our phylogenetic results are in partial agreement with Wu et al. (2013) and Zhang et al. (2020): *Xinjiangtitan* is supported as a 'mamenchisaurid' or CMT as we term them here, and it is closely related to at least some *Mamenchisaurus* species (see above). The subclade of CMTs that includes *Hudiesaurus*, *Xinjiangtitan*, *Klamelisaurus*, the referred specimen of *Mamenchisaurus hochuanensis*, and *M. youngi* is characterized by: approximately 18 cervical vertebrae; a ventral midline keel within a transversely concave fossa on the centra of cervicodorsal vertebrae; shallowly bifurcate cervicodorsal neural spines (often with some form of midline tubercle); a horizontal accessory lamina in the SDF of posterior-most cervical vertebrae; and transversely convex prezygapophyseal articular facets. Moreover, the scabrous sheet-like lateral projections on the cervical SPRLs seen in *Klamelisaurus* (Moore et al., 2020) are potentially homologous with the

lateral branch of the SPRL in *Hudiesaurus*. Caution is required because several of the above character states occur convergently in several non-CMT lineages (e.g., turiasaurs) and, in particular, are known in one or more other CMTs and *Euhelopus*. For example, the latter genus possesses a ventral midline keel within a transversely concave fossa in the cervicodorsal region, a horizontal accessory lamina within the SDF, and a shallowly bifid neural spine with prominent midline tubercle (Wilson and Upchurch, 2009). One character state that tends to exclude taxa such as *Euhelopus* and *Qijianglong* from the *Hudiesaurus* + *Xinjiangtitan* + *Klamelisaurus* + *Mamenchisaurus* subclade is the number of cervical vertebrae, which is thought to be 18 in *M. hochuanensis*, *M. youngi*, and *Xinjiangtitan* (Ouyang and Ye, 2002; Zhang et al., 2020; PU and PMB pers. observ., 2010), and 17 in *Euhelopus* and *Qijianglong* (Wilson and Upchurch, 2009; Xing et al., 2015). However, as noted earlier, precise determination of cervical number is often difficult, and in any case the number of cervical vertebrae in *Hudiesaurus* and *Klamelisaurus* is currently unknown. Similarly, while we can confirm that *Euhelopus* retains plesiomorphically flat prezygapophyseal articular facets in the cervicodorsal region (Wilson and Upchurch, 2009), this character is usually difficult to assess in those CMTs that have not been observed firsthand because it is often not mentioned or clearly illustrated in the descriptive literature. In short, the recovery of *Hudiesaurus* as the sister taxon of *Xinjiangtitan*, and their placement within a CMT clade, appears relatively well supported. However, the fine-scale relationships within the CMT clade should be regarded as provisional pending collection and evaluation of further character data.

All of our analyses support a CMT placement for *Rhomaleopakhus*: this can be understood in the light of its apomorphically robust forearm elements and relatively plesiomorphic manus. As discussed below, a very robust ulna, enlarged olecranon, and concave profile to the articular surface of the ulnar anteromedial process, are derived character states that frequently co-occur in several sauropod lineages. These features would tend to place *Rhomaleopakhus* with later-branching titanosaurs, the apatosaurine *Brontosaurus*, a *Janenschia-Haestasaurus* clade, or within CMTs. *Rhomaleopakhus* shares a few other apomorphies with a number of somphospondylan taxa, including the strong torsion of the radial shaft, the beveling of the radial distal end occupying all of this surface rather than just the lateral half, and the distal articular surfaces of the metacarpals not extending onto the anterior surfaces of the shafts. However, positions close to *Brontosaurus* or within Titanosauria would require multiple reversals in humerus and manus structure. For example, the humerus of *Rhomaleopakhus* lacks several apomorphies found in diplodocoids and/or titanosaurs, such as the medial expansion of the deltopectoral crest, strong muscular attachment areas on the posterolateral surface, very reduced or absent lateral and medial anterodistal processes, and a very deep supracondylar fossa at the distal end of the posterior surface (Wilson, 2002; Upchurch et al., 2004a, 2015). The proportions of the carpal element and a metacarpal III to radius length ratio of less than 0.45 in *Rhomaleopakhus* are consistent with those of non-neosauropod or non-macronarian eusauropods. Retention of plesiomorphies such as a relatively short metacarpal I, manual ungual on digit I lacking a proximolaterally beveled articular surface, and two phalanges on manual digit II, increase support for *Rhomaleopakhus* lying outside Neosauropoda and are consistent with a position among earlier-branching eusauropods (Upchurch et al., 2004a; Mannion et al., 2019a). Thus, the most parsimonious positions for *Rhomaleopakhus* are those that lie outside of Neosauropoda, within non-neosauropod eusauropod clades with hyper-robust antebrachia such as CMTs.

Our phylogenetic results support a close affinity between *Rhomaleopakhus*, *Analong*, and *Chuanjiesaurus*. While this is an interesting result that deserves further investigation, above

we have noted some potentially close similarities between *Rhomaleopakhus* and *Anhuilong* (e.g., the apomorphic structure of the distal radius), which are not captured in current phylogenetic data sets. Thus, the relationships of *Rhomaleopakhus* within the CMT assemblage should be treated with caution.

Discovery of the *Hudiesaurus* cervical vertebra and *Rhomaleopakhus* forelimb only 1 km apart in the same formation, their very large size, and their potentially close phylogenetic affinity, suggests that Dong's (1997) proposal that they belong to the same taxon is not without merit. However, lack of anatomical overlap means that such a referral is not supported at present, and this issue can be resolved only through the recovery of more complete sauropod material from the Kalazha Formation. In addition, the observations that *Hudiesaurus* appears to be more closely related to *Xinjiangtitan* (with these sister taxa clustering with *Klamelisaurus* and some *Mamenchisaurus* species), and that *Rhomaleopakhus* is most closely related to *Chuanjiesaurus/Analong* (and/or perhaps *Anhuilong*), lends support to the proposal that the cervical vertebra and forelimb should be treated as separate taxa. Caution is required because the lack of anatomical overlap between *Hudiesaurus* and *Rhomaleopakhus* might have contributed to an artifactual separation of these OTUs in our phylogenetic trees. However, we note that *Hudiesaurus* clusters with taxa such as *Mamenchisaurus youngi* and *Klamelisaurus*, both of which preserve both cervicodorsal vertebrae and forelimbs. Thus, our data sets allow an indirect comparison of *Rhomaleopakhus* and *Hudiesaurus*. Our topologies indicate that *Rhomaleopakhus* lacks the forelimb features that support the *M. youngi* + *Klamelisaurus* clade, whereas *Hudiesaurus* shares cervicodorsal synapomorphies that place it within that clade: this implies that the forelimb of *Hudiesaurus* (if it were known) would probably differ from *Rhomaleopakhus*. Thus, despite geographic and stratigraphic proximity, and the lack of anatomical overlap, there is support for the erection of a new generic name for the forelimb originally assigned to *Hudiesaurus*.

The Evolution of Robust Antebrachia in Sauropods

Rhomaleopakhus is characterized by a very robust forelimb, especially the ulna and radius, raising questions regarding the evolutionary and biomechanical significance of this feature. The robusticities of sauropod humeri, ulnae, and radii, when quantified, lie on a spectrum with no distinct breaks (Table S2 in Supplemental Data 1), and so a division into 'robust' versus 'slender' is both arbitrary and an over-simplification. Nevertheless, several previous studies have discretized this variation and used it as the basis for phylogenetic characters (e.g., Wilson, 2002:C168). For example, Upchurch (1995) proposed that a robust ulna characterized titanosaurs, and Wilson (2002) regarded this as a synapomorphy uniting an *Isisaurus* + Saltasauridae clade (with homoplastic acquisition in *Mamenchisaurus*). For the purposes of discussion here, we define a 'robust' antebrachium as one in which the greatest proximal width to proximodistal length ratio is ≥0.4 for the ulna and ≥0.3 for the radius, and a 'hyper-robust' antebrachium as one in which these ratios are ≥0.45 for the ulna and ≥0.35 for the radius. By these definitions, robust antebrachia are present in at least some lessemsaurids, *Bellusaurus*, *Mamenchisaurus constructus*, *Apatosaurus louisae*, and *Brontosaurus excelsus*, and hyper-robust ones are present in the CMTs *Rhomaleopakhus*, *Anhuilong*, *Huangshanlong*, and several titanosaurs such as *Alamosaurus*, *Opisthocoelicaudia*, and *Patagotitan* (Table S2 in Supplemental Data 1). A few taxa do not fit neatly into these categories: *Haestasaurus* and *Janenschia* (which form a clade with *Bellusaurus* in Mannion et al. [2019a]) have a robust and hyper-robust ulna respectively, but slender radii (though that of *Janenschia* nearly qualifies as robust; Table S2 in Supplemental Data 1). Robust antebrachia have

therefore arisen on at least five occasions independently, three times in non-neosauropods (lessemsaurids, CMTs, and the *Janenschia* + *Haestasaurus* lineage that might also include *Bellusaurus*), and twice in neosauropods (apatosaurines and titanosaurs). Given current uncertainties concerning the relationships among titanosaurs (e.g., Gorscak and O'Connor, 2019; Mannion et al., 2019b; Carballido et al., 2020), it is probable that hyper-robust antebrachia evolved more than once within this clade alone, and this is supported by the morphometric analyses of Páramo et al. (2020).

A biomechanical argument can be made that links antebrachial robusticity to the extent to which sauropods employed bipedal rearing. Additional stresses would have been generated in the forelimb elements during the 'push off' phase, and again during the deceleration of the body as the animal lowered itself back onto all fours. This behavior can be linked to other aspects of antebrachial morphology, especially the enlarged olecranon of the ulna (which also occurs in stegosaurs: Galton and Upchurch, 2004; Maidment et al., 2008; Mateus et al., 2009). The enlarged olecranon increases the mechanical advantage of muscles that extend the antebrachium, and so is associated with the forearm being held in a more flexed orientation (Carrano, 2005; Garcia et al., 2015; Klinkhamer et al., 2019). Straightening of the lower forelimb would have provided some additional impetus to the upward motion of the anterior part of the body during bipedal rearing (Wilson and Carrano, 1999), as occurs in extant elephants (Mallison, 2011). It is likely that early sauropods, such as lessemsaurids, possessed flexed rather than truly columnar forelimbs, and may have continued to use bipedal rearing as part of their browsing strategy (McPhee et al., 2015, 2018). Titanosaurs, in particular, have been linked to bipedal rearing because of a number of anatomical features that might have facilitated this, such as loss of the hypantrum-hyposphene system, strong convexo-concave articulations between dorsal centra, and low neural spines, consistent with greater flexibility in the trunk region (Wilson and Carrano, 1999). The short tail, with strongly developed procoelous articulations, might have assisted in supporting titanosaurs during rearing, with the tail forming the third 'leg' of a tripod (Wilson and Carrano, 1999; Ibiricu et al., 2014). The shortening of the ischium, and the lateral flaring of the preacetabular process of the ilium, have also been linked to rearing in titanosaurs: for example, the latter could have helped to support the viscera (Borsuk-Białynicka, 1977). However, this iliac flaring is perhaps more plausibly related to aspects of quadrupedal locomotion (Mallison, 2011; Garcia et al., 2015). One major problem with inferences of bipedality/tripodal stance in titanosaurs (and also CMTs) is that they probably possessed more anteriorly placed whole-body centers of mass (COMs) (Bates et al., 2016), making it biomechanically more demanding to raise the front part of the body off the ground (Henderson, 2006; Mallison, 2011). Some other dinosaur groups also indicate that a robust antebrachium, an enlarged olecranon, and flexed forelimb, were not always associated with bipedal rearing. For example, these features are present in ceratopsid ornithischians, which also possessed anteriorly shifted COMs because of their very large and heavy crania (Maidment and Barrett, 2012; Maidment et al., 2014; Barrett and Maidment, 2017) – these animals would seem to be unlikely candidates for bipedal rearing. Thus, although bipedal rearing is potentially related to robust antebrachia in lessemsaurids and stegosaurs, a separate explanation is required for CMTs and titanosaurs.

An alternative explanation for robust antebrachia in CMTs and titanosaurs can be derived from estimates of COM position, and its relationship to the role of the forelimb in locomotion. Bates et al. (2016) used convex hull modelling techniques to estimate the relative masses of various body segments and COM position for 15 sauropods. This study found that COMs were

relatively more anteriorly placed in titanosaurs and *Mamenchisaurus* compared with non-neosauropod eusauropods, most diplodocoids, and early-branching macronarians. This anterior shift of the COM reflects a number of proportional changes acquired convergently in CMTs and titanosaurs, including increases in the relative masses of the neck and forelimb, and decreases in tail mass (Bates et al., 2016:tables S29 and S30). A more anteriorly placed COM would promote more robust forelimbs because of the greater proportion of body mass passing through them. However, the direction of causality here is uncertain—a relative increase in the mass of the forelimbs, and decreased roles for the hind limbs and anterior tail in locomotion, would bring the COM further forward (Bates et al., 2016). Moreover, the relationship between COM position and aspects of forelimb robusticity is complex: for example, Ullmann et al. (2017) argued that the more anteriorly placed COMs of titanosauriforms were associated with greater gracility of the humerus (at least with regard to its mediolateral dimensions) because of the biomechanics of a wide-gauge stance.

Although structurally different in detail, the forelimbs of both CMTs and titanosaurs possess features that would have increased their range of motion. For example, Remes's (2008) analysis of the biomechanical evolution of the sauropodomorph forelimb indicated that most sauropods would have had very little ability to protract the forelimb beyond the vertical. By contrast, a number of modifications to the CMT glenoid and proximal head of the humerus imply much greater ability to protract the limb (Remes, 2008). CMTs also have modifications to the distal ends of their humeri and proximal ends of their ulnae that suggest greater rotation at the elbow was feasible (Remes, 2008). Similarly, Wilson and Carrano (1999) identified modifications to the titanosaur forelimb that probably enhanced its range of motion, especially at the shoulder and elbow. Such features include: the medial deflection of the glenoid; enlarged muscle attachment areas on the humerus; joint surfaces at the elbow that apparently allowed an increased range of motion; and the complete loss of ossified carpals and manual phalanges (see also Otero, 2010; Klinkhamer et al., 2019). These features have been interpreted as indicating improved muscle moment arms that assisted with support of increased body mass passing through the forelimbs, more flexibility enabling increased maneuverability, greater forelimb protraction, and/or a wider stance (Wilson and Carrano, 1999; Carrano, 2005; Ullmann et al., 2017; Klinkhamer et al., 2019; Voegele et al., 2020).

Greater forelimb protraction would have assisted in manual pronation and increased stride length, allowing faster and/or more efficient locomotion (Remes, 2008; Lallensack et al., 2019). A faster moving forelimb, carrying a higher proportion of body mass because of a relatively anteriorly placed COM, would have experienced higher stresses as it impacted the substrate (e.g., Hutchinson, 2021). The enlarged olecranon associated with robust ulnae has been linked to the habitual use of a more flexed antebrachium (see above): holding the ulna and radius at a slanting, rather than vertical, angle with respect to the ground would have increased the bending moments in their shafts. Interestingly, elephants use a more columnar limb stance during walking, but gradually shift to an increasingly flexed posture as locomotion speeds increase (Hutchinson, 2021). This more flexed limb posture allows more 'bounce' in each stride, which brings biomechanical advantages at higher speeds (Hutchinson, 2021). In short, some CMTs and titanosaurs potentially had greater maneuverability and speed than other sauropods, but this came at the price of requiring a more robust antebrachium.

Despite the apparent relationships between neck length, tail length, the role of the forelimb in locomotion, forearm flexure, COM position, and antebrachial robusticity, there are exceptions to this pattern among sauropods that merit exploration. For example, the extent to which apatosaurines fit this pattern is more difficult to determine. These taxa have relatively massive necks, robust antebrachia, and a whole-body COM that is shifted anteriorly (at least in comparison with more gracile diplodocoids) (Bates et al., 2016). However, aside from the robust antebrachium and a medially deflected scapular glenoid (Wilson, 2002), apatosaurines lack many of the features seen in CMTs and titanosaurs that have been linked to increased protraction and flexibility. The titanosaur *Neuquensaurus* is even more problematic, having a hyper-robust antebrachium, but a relatively massive tail and posteriorly placed COM (Bates et al., 2016). This could be a genuine phenomenon, with saltasaurids possessing an extreme wide-gauge stance that required a posterior shift in COM position according to some workers (Ullmann et al., 2017; Páramo et al., 2020). However, an alternative explanation is that the mass of the *Neuquensaurus* tail was overestimated by Bates et al. (2016). In particular, although Bates et al. (2016) took vertebral pneumaticity into account when calculating CoM position, they did so only for the neck and thoracic regions. Yet, the tails of many titanosaurs generally (Mannion et al., 2013; Poropat et al., 2020), and those of saltasaurines in particular (Wilson, 2002; Powell, 2003; Wedel, 2003; Zurriaguz and Cerda, 2017; Zurriaguz et al., 2017), appear to have been highly pneumatized. In the tail of *Neuquensaurus*, the internal tissue structure is camerate in the centra, and camellate in the neural arches, spines, and transverse processes (Salgado et al., 2005; Zurriaguz and Cerda, 2017). This pneumatization persists throughout much of the tail (into even very posterior caudal vertebrae), and the air space proportion within middle caudal vertebrae is estimated at 25% (Zurriaguz and Cerda, 2017). Moreover, important hind limb retractors such as the M. caudofemoralis longus have been estimated to have originated on approximately the first 17 caudal vertebrae in early-branching titanosaurs (the plesiomorphic condition), on caudal vertebrae 1–9/10 in more nested titanosaurs, and solely on caudal vertebrae 1–8 in saltasaurines (Ibiricu et al., 2014). In short, *Neuquensaurus* is very likely to have had a lighter tail, with reduced anterior muscle mass and increased pneumatization, compared with those of non-saltasaurine titanosaurs. It seems probable, therefore, that Bates et al. (2016) overestimated the mass of the *Neuquensaurus* tail: if so, then its whole-body CoM would have been somewhat more anteriorly located in life, bringing this taxon more into line with our prediction based on its very robust antebrachium.

The above review raises the question as to why at least some CMTs and titanosaurs had more flexible forelimbs with a greater capacity for protraction. Interestingly, the modelling work of Mallison (2011) suggested that there would have been a trade-off between locomotion speed and rearing ability, with more anteriorly placed whole-body COMs aiding higher accelerations and maximum speeds, but making rearing more difficult. It is possible that some titanosaurs and CMTs reduced or gave up the ability to gain additional fodder via bipedal/tripodal rearing, in exchange for an even longer neck and the ability to move between patchily distributed resources more quickly and efficiently in order to increase food acquisition rates.

CONCLUSIONS

We demonstrate that the Late Jurassic Chinese sauropod *Hudiesaurus sinojapanorum* should be restricted to the posterior cervical vertebra, with no evidence to support the referral of either the previously attributed teeth or forelimb. *Hudiesaurus* is closely related to the 'core *Mamenchisaurus*-like taxon' (CMT) *Xinjiangtitan*, although differences between them indicate that separate genera should be retained at this time. The four teeth cannot be identified precisely, but the available evidence suggests that they are probably those of a CMT, potentially one closely related to *Mamenchisaurus sinocanadorum*.

The forelimb specimen is diagnosable on the basis of several autapomorphies and is named *Rhomaleopakhus turpanensis* herein. The latter taxon can safely be regarded as a CMT, with current evidence supporting a close relationship with *Chuanjiesaurus* and *Analong*.

Robust antebrachia are associated with an enlarged olecranon and a more flexed orientation of the lower forelimb. In lessemsaurids and stegosaurs, these features potentially reflect the continuing reliance on bipedal rearing as part of a frequently deployed food-gathering strategy. However, the more anteriorly placed whole-body COMs of several CMTs and titanosaurs, coupled with their often gigantic size, suggests that bipedal rearing is not an adequate explanation for robust antebrachia in these forms. Instead, it appears that a complex set of selective pressures (perhaps operating in an evolutionary cascade: Sander, 2013), resulted in the convergent evolution of larger necks and shorter tails, a more anteriorly placed whole-body COM, and an enhanced role for the forelimbs in locomotion. The more flexed position of the antebrachium in certain CMTs and titanosaurs might thus reflect the requirement for more flexibility at the elbow joint, rather than a tendency to use bipedal rearing. This habitually more flexed orientation, a greater proportion of the body mass passing through the forelimbs, and the higher stresses generated, are likely to have exposed the antebrachium to bending moments that could only be accommodated by increased robusticity. Thus, CMTs and titanosaurs potentially sacrificed the ability to augment food-gathering via bipedal rearing in exchange for higher locomotion speeds and reduced travel times between patchily distributed food sources.

ACKNOWLEDGMENTS

ORCID

Paul Upchurch http://orcid.org/0000-0002-8823-4164
Philip D. Mannion http://orcid.org/0000-0002-9361-6941
Paul M. Barrett http://orcid.org/0000-0003-0412-3000

LITERATURE CITED

Alifanov, V. R., and A. O. Averianov. 2003. *Ferganasaurus verzilini*, gen. et sp. nov., a new neosauropod (Dinosauria, Saurischia, Sauropoda) from the Middle Jurassic of Fergana Valley, Kirghizia. Journal of Vertebrate Paleontology 23:358–372.

Allain, R., and N. Aquesbi. 2008. Anatomy and phylogenetic relationships of *Tazoudasaurus naimi* (Dinosauria, Sauropoda) from the late Early Jurassic of Morocco. Geodiversitas 30:345–424.

Apaldetti, C., R. N. Martínez, I. A. Cerda, D. Pol, and O. Alcober. 2018. An early trend towards gigantism in Triassic sauropodomorph dinosaurs. Nature Ecology and Evolution 2:1227–1232.

Apesteguía, S. 2005. Evolution of the titanosaur metacarpus; pp. 321–345 in V. Tidwell and K. Carpenter (eds.), Thunder-lizards: The Sauropodomorph Dinosaurs. Indiana University Press, Bloomington and Indianapolis.

Barrett, P. M., and S. C. R. Maidment. 2017. The evolution of ornithischian quadrupedality. Journal of Iberian Geology 43:363–377. https://doi.org/10.1007/s41513-017-0036-0

Barrett, P. M., and P. Upchurch. 2005. Sauropodomorph diversity through time: paleoecological and macroevolutionary implications: pp. 125–151 in K. A. Curry Rogers and J. A. Wilson (eds.), The Sauropods: Evolution and Paleobiology. University of California Press, Berkeley.

Barrett, P. M., and X.-L. Wang. 2007. Basal titanosauriform (Dinosauria, Sauropoda) teeth from the Lower Cretaceous Yixian Formation of Liaoning Province, China. Palaeoworld 16:265–271.

Barrett, P. M., Y. Hasegawa, M. Manabe, S. Isaji, and H. Matsuoka. 2002. Sauropod dinosaurs from the Lower Cretaceous of Eastern Asia: taxonomic and biogeographic implications. Palaeontology 45:1197–1217.

Bates, K. T., P. D. Mannion, P. L. Falkingham, S. L. Brusatte, J. R. Hutchinson, A. Otero, W. I. Sellers, C. Sullivan, K. A. Stevens, and V. Allen. 2016. Temporal and phylogenetic evolution of the sauropod dinosaur body plan. Royal Society Open Science 3:150636. doi:10.1098/rsos.150636

Bedwell, M. W. Jr., and D. L. Trexler. 2005. First articulated manus of *Diplodocus carnegii*; pp. 302–320 in V. Tidwell and K. Carpenter (eds.), Thunder-lizards: The Sauropodomorph Dinosaurs. Indiana University Press, Bloomington and Indianapolis.

Bohlin, B. 1953. Reports from the Scientific Expedition to the North-Western Provinces of China Under Leadership of Dr. Sven Hedin. VI. Vertebrate Palaeontology 6: Fossil Reptiles from Mongolia and Kansu. Statens Etnografiska Museum, Stockholm, 113 pp.

Bonaparte, J. F. 1986. Les dinosaures (carnosaures, allosauridés, sauropodes, cétiosauridés) du Jurassique Moyen de Cerro Cóndor (Chubut, Argentine) (Part 2). Annales de Paléontologie (Vert.-Invert.) 72:325–386.

Bonaparte J. F., B. J. González Riga, and S. Apesteguía. 2006. *Ligabuesaurus leanzai* gen. et sp. nov. (Dinosauria, Sauropoda), a new titanosaur from the Lohan Cura Formation (Aptian, Lower Cretaceous) of Neuquén, Patagonia, Argentina. Cretaceous Research 27:364–376.

Bonaparte, J. F., W.-D., Heinrich, and R. Wild. 2000. Review of *Janenschia* Wild, with the description of a new sauropod from the Tendaguru beds of Tanzania and a discussion on the systematic value of procoelous caudal vertebrae in the Sauropoda. Palaeontographica, Abteilung A 256:25–76.

Bonnan, M. F. 2003. The evolution of manus shape in sauropod dinosaurs: implications for functional morphology, forelimb orientation, and phylogeny. Journal of Vertebrate Paleontology 23:595–613.

Borsuk-Białynicka, M. 1977. A new camarasaurid sauropod *Opisthocoelicaudia skarzynskii* gen. n., sp. n. from the Upper Cretaceous of Mongolia. Palaeontologica Polonica 37:5–63.

Brazeau, M. D. 2011. Problematic character coding methods in morphology and their effects. Biological Journal of the Linnean Society 104:489–498.

Britt, B. B., R. D. Scheetz, M. F. Whiting, and D. R. Wilhite. 2017. *Moabosaurus utahensis*, n. gen., n. sp., a new sauropod from the Early Cretaceous (Aptian) of North America. Contributions from the Museum of Paleontology, University of Michigan 32:189–243.

Calvo, J. O., and L. Salgado. 1995. *Rebbachisaurus tessonei* sp. nov. a new Sauropoda from the Albian-Cenomanian of Argentina; new evidence on the origin of the Diplodocidae. GAIA 11:13–33.

Canudo, J. I., J. I. Ruiz-Omenaca, J. L. Barco, and R. Royo-Torres. 2002. Saurópodos asiáticos en el Barremiense inferior (Cretácico inferior) de España. Ameghiniana 39:443–452.

Carballido, J. L., and D. Pol. 2010. The dentition of *Amygdalodon patagonicus* (Dinosauria: Sauropoda) and the dental evolution in basal sauropods. Comptes Rendus Palevol 9:83–93.

Carballido, J. L., M. Scheil, N. Knötschke, and P. M. Sander. 2020. The appendicular skeleton of the dwarf macronarian sauropod *Europasaurus holgeri* from the Late Jurassic of Germany and a

re-evaluation of its systematic affinities. Journal of Systematic Palaeontology 18:739–781.

Carballido, J. L., D. Pol, A. Otero, I. A. Cerda, L. Salgado, A. C. Garrido, J. Ramezani, N. R. Cúneo, and J. M. Krause. 2017. A new giant titanosaur sheds light on body mass evolution among sauropod dinosaurs. Proceedings of the Royal Society of London B 284:20171219. doi.org/10.1098/rspb.2017.1219

Carrano, M. T. 2005. The evolution of sauropod locomotion: morphological diversity of a secondarily quadrupedal radiation; pp. 229–251 in K. A. Curry Rogers and J. A. Wilson (eds.), The Sauropods: Evolution and Paleobiology. University of California Press, Berkeley.

Cerda, I. A. 2009. Consideraciones sobre la histogénesis de las costillas cervicales en los dinosaurios saurópodos. Ameghiniana 46:193–198.

Cerda, I. A., G. A. Casal, R. D. Martinez, and L. M. Ibiricu. 2015. Histological evidence for a supraspinous ligament in sauropod dinosaurs. Royal Society Open Science 2:150369. doi.org/10.1098/rsos.150369

Chapelle, K. E. J., and J. N. Choiniere. 2018. A revised cranial description of *Massospondylus carinatus* Owen (Dinosauria: Sauropodomorpha) based on computed tomographic scans and a review of cranial characters for basal Sauropodomorpha. PeerJ 6: e4224. doi.org/10.7717/peerj.4224

Chure, D. J., B. B. Britt, J. A. Whitlock, and J. A. Wilson. 2010. First complete sauropod dinosaur skull from the Cretaceous of the Americas and the evolution of sauropod dentition. Naturwissenschaften 97:379–391.

Curry Rogers, K. 2005. Titanosauria: a phylogenetic overview; pp. 50–103 in K. A. Curry Rogers and J. A. Wilson (eds.), The Sauropods: Evolution and Paleobiology. University of California Press, Berkeley.

Curry Rogers, K. A. 2009. The postcranial osteology of *Rapetosaurus krausei* (Sauropoda: Titanosauria) from the Late Cretaceous of Madagascar. Journal of Vertebrate Paleontology 29:1046–1086.

D'Emic, M. D. 2012. The early evolution of titanosauriform sauropod dinosaurs. Zoological Journal of the Linnean Society 166:624–671.

D'Emic, M. D. 2013. Revision of the sauropod dinosaurs of the Early Cretaceous Trinity Group, southern USA, with the description of a new genus. Journal of Systematic Palaeontology 11:707–726.

D'Emic, M. D., P. D. Mannion, P. Upchurch, R. B. J. Benson, Q. Pang, and Z. Cheng. 2013. Osteology of *Huabeisaurus allocotus* (Sauropoda: Titanosauriformes) from the Upper Cretaceous of China. PLoS ONE 8:e69375. doi.org/10.1371/journal.pone.0069375

Deng, S., S. Wang, Z. Yang, Y. Lu, X. Li, Q. Hu, C. An, D. Xi, and X. Wan. 2015. Comprehensive study of the Middle-Upper Jurassic strata in the Junggar Basin, Xinjiang. Acta Geoscientia Sinica 36:559–574.

Dong, Z. 1992. Dinosaurian Faunas of China. China Ocean Press, Beijing, 188 pp.

Dong, Z. 1997. A gigantic sauropod (*Hudiesaurus sinojapanorum*, gen. et sp. nov.) from the Turpan Basin, China; pp. 102–110 in Z. Dong (ed.), Sino-Japanese Silk Road Dinosaur Expedition. China Ocean Press, Beijing.

Eberth, D. A., D. B. Brinkman, P.-J. Chen, F.-T. Yuan, S.-Z. Wu, G. Li, and X.-S. Cheng. 2001. Sequence stratigraphy, paleoclimate patterns, and vertebrate fossil preservation in Jurassic-Cretaceous strata of the Junggar Basin, Xinjiang Autonomous Region, People's Republic of China. Canadian Journal of Earth Sciences 38:1627–1644.

Fang, Y., C. Wu, Y. Wang, L. Wang, Z. Guo, and H. Hu. 2016. Stratigraphic and sedimentary characteristics of the Upper Jurassic-Lower Cretaceous strata in the Junggar Basin, Central Asia: tectonic and climate implications. Journal of Asian Earth Sciences 129:294–308.

Galton, P. M., and P. Upchurch. 2004. Stegosauria; pp. 343–362 in D. B. Weishampel, P. Dodson, and H. Osmólska, (eds.), The Dinosauria (Second Edition). University of California Press, Berkeley.

García, R. A., L. Salgado, M. S. Fernández, I. A. Cerda, A. Paulina Carabajal, A. Otero, R. A. Coria, and L. E. Fiorelli. 2015. Paleobiology of titanosaurs: reproduction, development, histology, pneumaticity, locomotion and neuroanatomy from the South American fossil record. Ameghiniana 52:29–68.

Gauthier, J. 1986. Saurischian monophyly and the origin of birds. Memoirs of the Californian Academy of Sciences 8:1–55.

Gilmore, C. W. 1925. A nearly complete articulated skeleton of *Camarasaurus*, a saurischian dinosaur from the Dinosaur National Monument. Memoirs of the Carnegie Museum 10:347–384.

Gilmore, C. W. 1932. On a newly mounted skeleton of *Diplodocus* in the United States National Museum. Proceedings of the United States National Museum 81:1–21.

Gilmore, C. W. 1936. Osteology of *Apatosaurus* with special reference to specimens in the Carnegie Museum. Memoirs of the Carnegie Museum 11:175–300.

Gilmore, C. W. 1946. Reptilian fauna of the North Horn Formation of central Utah. United States Geological Survey Professional Paper 210C:1–52.

Gimenez, O. 1992. Estudio preliminar del miembro anrerior de los saur6podos titanosauridos. Ameghiniana 30:154.

Goloboff, P. A., and S. A. Catalano. 2016. TNT version 1.5, including a full implementation of phylogenetic morphometrics. Cladistics 32:221–238.

Goloboff, P. A., J. S. Farris, and K. C. Nixon. 2008. TNT, a free program for phylogenetic analysis. Cladistics 24:1–13.

Goloboff, P. A., A. Torres, and J. S. Arias. 2018. Weighted parsimony outperforms other methods of phylogenetic inference under models appropriate for morphology. Cladistics 34:407–437.

Gomani, E. M. 2005. Sauropod dinosaurs from the Early Cretaceous of Malawi, Africa. Palaeontologia Electronica 8(1):27A. https://palaeoelectronica.org/2005_1/gomani27/issue1_05.htm

González Riga, B. J., P. D. Mannion, S. F. Poropat, L. Ortiz David, and J. P. Coria. 2018. Osteology of the Late Cretaceous Argentinean sauropod dinosaur *Mendozasaurus neguyelap*: implications for basal titanosaur relationships. Zoological Journal of the Linnean Society 184:136–181.

Gorscak, E. and P. M. O'Connor. 2019. A new African Titanosaurian Sauropod Dinosaur from the middle Cretaceous Galula Formation (Mtuka Member), Rukwa Rift Basin, Southwestern Tanzania. PLoS ONE 14:e0211412.

Harris, J. D. 2006. The significance of *Suuwassea emilieae* (Dinosauria: Sauropoda) for flagellicaudatan intrarelationships and evolution. Journal of Systematic Palaeontology 4:185–198

Harris, J. D., and P. Dodson. 2004. A new diplodocoid sauropod dinosaur from the Upper Jurassic Morrison Formation of Montana, USA. Acta Palaeontologica Polonica 49:197–210.

Hatcher, J. B. 1901. *Diplodocus* (Marsh): its osteology, taxonomy, and probable habits, with a restoration of the skeleton. Memoirs of the Carnegie Museum 1:1–63.

Hatcher, J. B. 1902. Structure of the forelimb and manus of *Brontosaurus*. Annals of the Carnegie Museum 1:356–376.

He, X.-L., K. Li, and K.-J. Cai. 1988. The Middle Jurassic Dinosaur Fauna from Dashanpu, Zigong, Sichuan. Vol IV. Sauropod Dinosaurs (2). *Omeisaurus tianfuensis*. Sichuan Publishing House of Science and Technology, Chengdu. 143 pp. [In Chinese, English summary]

Henderson, D. M. 2006. Burly gaits: centers of mass, stability, and the trackways of sauropod dinosaurs. Journal of Vertebrate Paleontology 4:907–921.

Holwerda, F. M., D. Pol, and O. W. M. Rauhut. 2015. Using dental enamel wrinkling to define sauropod tooth morphotypes from the Cañadón Asfalto Formation, Patagonia, Argentina. PLoS ONE 10:e0118100. doi.org/10.1371/journal.pone.0118100

Huang, J.-D., H.-L. You, J.-T. Yang, and X.-X. Ren. 2014. A new sauropod dinosaur from the Middle Jurassic of Huangshan, Anhui Province. Vertebrata PalAsiatica 52:390–400.

Huene, F. von 1932. Die fossile Reptil-Ordnung Saurischia, ihre Entwicklung und Geschichte. Monographien zur Geologie und Palaeontologie 4:1–361.

Hutchinson, J. R. 2021. The evolutionary biomechanics of locomotor function in giant land animals. Journal of Experimental Biology 224: jeb217463. doi:10.1242/jeb.217463.

Ibiricu, L. M., M. C. Lamanna, and K. J. Lacovara. 2014. The influence of caudofemoral musculature on the titanosaurian (Saurischia: Sauropoda) tail skeleton: morphological and phylogenetic implications. Historical Biology 26:454–471.

Janensch, W. 1922. Das Handskelett von *Gigantosaurus robustus* u. *Brachiosaurus Brancai* aus den Tendaguru-Schichten Deutsch-Ostafrikas. Centralblatt für Mineralogie, Geologie und Paläontologie 15:464–480.

Janensch, W. 1929. Die Wirbelsäule der Gattung *Dicraeosaurus*. Palaeontographica (Supplement VII) 2:37–133.

Janensch, W. 1936. Ein aufgestelltes Skelett von *Dicraeosaurus hansemanni*. Palaeontographica (Supplement 7):299–308.

Janensch, W. 1961. Die gliedmaszen und gliedmaszengürtel der Sauropoden der Tendaguru-Schichten. Palaeontographica (Supplement VII) 3:177–235.

Jensen, J. A. 1988. A fourth new sauropod dinosaur from the Upper Jurassic of the Colorado Plateau and sauropod bipedalism. Great Basin Naturalist 48:121–145.

Klein, N., A. Christian, and P. M. Sander. 2012. Histology shows that elongated neck ribs in sauropod dinosaurs are ossified tendons. Biology Letters 8:1032–1035.

Klinkhamer, A. J., H. Mallison, S. F. Poropat, T. Sloan, and S. Wroe. 2019. Comparative three-dimensional moment arm analysis of the sauropod forelimb: implications for the transition to a wide-gauge stance in titanosaurs. Anatomical Record 302:794–817.

Ksepka, D. T., and M. A. Norell. 2006. *Erketu ellisoni*, a long-necked sauropod from Bor Guvé (Dornogov Aimag, Mongolia). American Museum Novitates 3508:1–16.

Lallensack, J. N., S. Ishigaki, A. Lagnaoui, M. Buchwitz, and O. Wings 2019. Forelimb orientation and locomotion of sauropod dinosaurs: insights from the ?Middle Jurassic Tafaytour tracksites (Argana Basin, Morocco). Journal of Vertebrate Paleontology 38:e1512501. doi.org/10.1080/02724634.2018.1512501

Läng, É., and F. Goussard. 2007. Redescription of the wrist and manus of ?*Bothriospondylus madagascariensis*: new data on carpus morphology in Sauropoda. Geodiversitas 29:549–560.

Li, L.-G., D.-Q. Li, H.-L. You, and P. Dodson. 2014. A new titanosaurian sauropod from the Hekou Group (Lower Cretaceous) of the Lanzhou-Minhe Basin, Gansu Province, China. PLoS ONE 9: e85979. doi.org/10.1371/journal.pone.0085979

Mahammed, F., E. Läng, L. Mami, L. Mekahli, M. Benhamou, B. Bouterfa, A. Kacemi, S. Chérief, H. Chaouati, and P. Taquet. 2005. The "Giant of Ksour", a Middle Jurassic sauropod dinosaur from Algeria. Comptes Rendus Palevol 4:707–714.

Maidment, S. C. R., and P. M. Barrett. 2012. Does morphological convergence imply functional similarity? A test using the evolution of quadrupedalism in ornithischian dinosaurs. Proceedings of the Royal Society B 279:3765–3771. https://doi.org/10.1098/rspb.2012.1040

Maidment, S. C. R., D. M. Henderson, and P. M. Barrett. 2014. What drove reversions to quadrupedality in ornithischian dinosaurs? Testing hypotheses using centre of mass modelling. Naturwissenschaften 101:989–1001. https://doi.org/10.1007/s00114-014-1239-2

Maidment, S. C. R., D. B. Norman, P. M. Barrett, and P. Upchurch. 2008. Systematics and phylogeny of Stegosauria (Dinosauria, Ornithischia). Journal of Systematic Palaeontology 6:367–407.

Maisch, M. W., and Matzke, A. T. 2019. First record of a eusauropod (Dinosauria: Sauropoda) from the Upper Jurassic Qigu Formation (southern Junggar Basin, China), and a reconsideration of late Jurassic sauropod diversity in Xinjiang. Neues Jahrbuch für Geologie und Paläontologie, Abhandlungen 291:109–117.

Mallison, H. 2011. Rearing giants: kinetic-dynamic modelling of sauropod bipedal and tripodal poses; pp. 237–250 in N. Klein, K. Remes, C. T. Gee, and P. M. Sander (eds.), Biology of the sauropod dinosaurs: understanding the life of giants. Indiana University Press, Bloomington.

Mannion, P. D. 2019. A turiasaurian sauropod dinosaur from the Early Cretaceous Wealden Supergroup of the United Kingdom. PeerJ 7: e6348.

Mannion, P. D., R. Allain, and O. Moine. 2017. The earliest known titanosauriform sauropod dinosaur and the evolution of Brachiosauridae. PeerJ 5:e3217. doi.org/10.7717/peerj.3217

Mannion, P. D., P. Upchurch, R. N. Barnes, and O. Mateus. 2013. Osteology of the Late Jurassic Portuguese sauropod dinosaur *Lusotitan atalaiensis* (Macronaria) and the evolutionary history of basal titanosauriforms. Zoological Journal of the Linnean Society 168:98–206.

Mannion, P. D., P. Upchurch, X. Jin, and W. Zheng. 2019b. New information on the Cretaceous sauropod dinosaurs of Zhejiang Province, China: impact on Laurasian titanosauriform phylogeny and biogeography. Royal Society Open Science 6:191057. doi.org/10.1098/rsos.191057

Mannion, P. D., P. Upchurch, D. Schwarz, and O. Wings. 2019a. Taxonomic affinities of the putative titanosaurs from the Late Jurassic Tendaguru Formation of Tanzania: phylogenetic and biogeographic implications for eusauropod dinosaur evolution. Zoological Journal of the Linnean Society 85:784–909.

Marsh, O. C. 1878. Principal characters of American Jurassic dinosaurs. Part I. American Journal of Science and Arts, Series 3 16:411–416.

Martinez, R. D., O. Gimenez, J. Rodriguez, M. Luna, and M. C. Lamanna. 2004. An articulated specimen of the basal titanosaurian (Dinosauria: Sauropoda) *Epachthosaurus sciuttoi* from the early Late Cretaceous Bajo Barreal Formation of Chubut province, Argentina. Journal of Vertebrate Paleontology 24:107–120.

Mateus, O., S. C. R. Maidment, and N. A. Christiansen. 2009. A new long-necked 'sauropod mimic' stegosaur and the evolution of the plated dinosaurs. Proceedings of the Royal Society of London B 276:1815–1821.

Mateus, O., P. D. Mannion, and P. Upchurch. 2014. *Zby atlanticus*, a new turiasaurian sauropod (Dinosauria, Eusauropoda) from the Late Jurassic of Portugal. Journal of Vertebrate Paleontology 34:618–634.

McIntosh, J. S. 1990. Sauropoda; pp. 345–401 in D. B. Weishampel, P. Dodson, and H. Ósmolska (eds.), The Dinosauria (First Edition). University California Press, Berkeley.

McPhee, B. W., A. M. Yates, J. N. Choiniere, and F. Abdala, 2014. The complete anatomy and phylogenetic relationships of *Antetonitrus ingenipes* (Sauropodiformes, Dinosauria): implications for the origins of Sauropoda. Zoological Journal of the Linnean Society 171:151–205.

McPhee, B. W., R. B. J. Benson, J. Botha-Brink, E. M. Bordy, and J. N. Choiniere. 2018. A giant dinosaur from the earliest Jurassic of South Africa and the transition to quadrupedality in early sauropodomorphs. Current Biology 28:3143–3151.

McPhee, B. W., M. F. Bonnan, A. M. Yates, J. Neveling, and J. N. Choiniere. 2015. A new basal sauropod from the pre-Toarcian Jurassic of South Africa: evidence of niche partitioning at the sauropodomorph–sauropod boundary? Scientific Reports 5:13224. doi.org/10.1038/srep13224

Moore, A. J., P. Upchurch, P. M. Barrett, J. M. Clark, and X. Xu. 2020. Osteology of *Klamelisaurus gobiensis* (Dinosauria: Eusauropoda) and the evolutionary history of Middle–Late Jurassic Chinese sauropods. Journal of Systematic Palaeontology 18:1299–1393.

Nesbitt, S. J., and M. R. Stocker. 2008. The vertebrate assemblage of the Late Triassic Canjilon Quarry (Northern New Mexico, USA), and the importance of apomorphy-based assemblage comparisons. Journal of Vertebrate Paleontology 28:1063–72.

Osborn, H. F., and C. C. Mook. 1921. *Camarasaurus, Amphicoelias*, and other sauropods of Cope. Memoirs of the American Museum of Natural History, New Series 3:247–387.

Ostrom, J. H., and J. S. McIntosh. 1966. Marsh's dinosaurs: the collection from Como Bluff. Vol. 1. Yale University Press, New Haven. 416 pp.

Otero, A. 2010. The appendicular skeleton of *Neuquensaurus*, a Late Cretaceous saltasaurine sauropod from Patagonia, Argentina. Acta Palaeontologica Polonica 55:399–426.

Otero, A. 2018. Forelimb musculature and osteological correlates in Sauropodomorpha (Dinosauria, Saurischia). PLoS ONE 13: e0198988.

Otero, A., J. L. Carballido and A. Pérez Moreno. 2020. The appendicular osteology of *Patagotitan mayorum* (Dinosauria, Sauropoda). Journal of Vertebrate Paleontology. doi.org/10.1080/02724634.2020.1793158.

Ouyang, H., and Y. Ye. 2002. The first mamenchisaurian skeleton with complete skull: *Mamenchisaurus youngi*. Sichuan Science and Technology Press, Chengdu, 111 pp.

Owen, R. 1842. Report on British fossil reptiles. Part II. Reports of the British Association for the Advancement of Science 11:60–204.

Páramo, A., P. Mocho, and F. Ortega. 2020. Three–dimensional analysis of the titanosaurian limb skeleton: implications for systematic analysis. Journal of Iberian Geology. doi.org/10.1007/s41513-020-00139-8

Peng, G., Y. Ye, Y. Gao, C. Shu, and S. Jiang. 2005. Jurassic dinosaur faunas in Zigong. Sichuan People's Publishing House, Chengdu, 236 pp.

Peyre de Fabrègues, C., R. Allain, and V. Barriel. 2015. Root causes of phylogenetic incongruence observed within basal sauropodomorph interrelationships. Zoological Journal of the Linnean Society 175:569–586.

Poropat, S. F., P. D. Mannion, P. Upchurch, S. A. Hocknull, B. P. Kear, and D. A. Elliot 2015a. Reassessment of the non-titanosaurian somphospondylan *Wintonotitan wattsi* (Dinosauria: Sauropoda: Titanosauriformes) from the mid-Cretaceous Winton Formation, Queensland, Australia. Papers in Palaeontology 1:59–106.

Poropat, S. F., P. Upchurch, P. D. Mannion, S. A. Hocknull, B. P., Kear, T. Sloan, G. H. K. Sinapius, and D. A. Elliott. 2015b. Revision of the

sauropod dinosaur *Diamantinasaurus matildae* Hocknull et al. 2009 from the middle Cretaceous of Australia: implications for Gondwanan titanosauriform dispersal. Gondwana Research 27:995–1033

Poropat, S. F., P. D. Mannion, P. Upchurch, T. R. Tischler, T. Sloan, G. H. K. Sinapius, J. A. Elliott and D. A. Elliott. 2020. Osteology of the wide-hipped titanosaurian sauropod dinosaur *Savannasaurus elliottorum* from the Upper Cretaceous Winton Formation of Queensland, Australia. Journal of Vertebrate Paleontology 40(3):e1786836.

Poropat, S. F., P. D. Mannion, P. Upchurch, S. A. Hocknull, B. P. Kear, M. Kundrat, T. R. Tischler, T. Sloan, G. H. K. Sinapius, J. A. Elliott, and D. A. Elliott. 2016. New Australian sauropods shed light on Cretaceous dinosaur palaeobiogeography. Scientific Reports 6:34467. doi.org/10.1038/srep34467

Powell, J. E. 2003. Revision of South American titanosaurid dinosaurs: palaeobiological, palaeobiogeographical and phylogenetic aspects. Records of the Queen Victoria Museum 111:1–173.

Rauhut, O. W. M., K. Remes, R. Fechner, G. Cladera, and P. Puerta. 2005. Discovery of a short-necked sauropod dinosaur from the Late Jurassic period of Patagonia. Nature 435:670–672.

Remes, K. 2008. Evolution of the pectoral girdle and forelimb in Sauropodomorpha (Dinosauria, Saurischia): osteology, myology, and function. Ph.D. Dissertation. Fakultät für Geowissenschaften, Ludwig-Maximilians-Universität, Munich. 355 pp.

Ren, X.-X., J.-D. Huang, and H.-L. You. 2018. The second mamenchisaurid dinosaur from the Middle Jurassic of Eastern China. Historical Biology 32:602–610.

Ren, X.-X., T. Sekiya, T. Wang, Z.-W. Yang, and H.-L. You. 2020. A revision of the referred specimen of *Chuanjiesaurus anaensis* Fang et al., 2000: a new early branching mamenchisaurid sauropod from the Middle Jurassic of China. Historical Biology. doi.org/10.1080/08912963.2020.1747450.

Royo-Torres, R., and P. Upchurch. 2012. The cranial anatomy of the sauropod *Turiasaurus riodevensis* and implications for its phylogenetic relationships. Journal of Systematic Palaeontology 10:553–583.

Royo-Torres, R., A. Cobos, and L. Alcalá. 2006. A giant European dinosaur and a new sauropod clade. Science 314:1925–1927.

Royo-Torres, R., P. Upchurch, J. I. Kirkland, D. D. DeBlieux, J. R. Foster, A. Cobos, and L. Alcalá. 2017. Descendants of the Jurassic turiasaurs from Iberia found refuge in the Early Cretaceous of western USA. Scientific Reports 7:14311. doi.org/10.1038/s41598-017-14677-2

Royo-Torres, R., P. Upchurch, P. D. Mannion, R. Mas, A. Cobos, F. Gasco, L. Alcala, and J. L. Sanz. 2014. The anatomy, phylogenetic relationships and stratigraphic position of the Tithonian–Berriasian Spanish sauropod dinosaur *Aragosaurus ischiaticus*. Zoological Journal of the Linnean Society 171:623–655.

Salgado, L., S. Apesteguia, and S. E. Heredia. 2005 A new specimen of *Neuquensaurus australis*, a Late Cretaceous saltasaurine titanosaur from north Patagonia. Journal of Vertebrate Paleontology 25:623–634.

Salgado, L., R. A. Coria, and J. O. Calvo. 1997. Evolution of titanosaurid sauropods. I: phylogenetic analysis based on the postcranial evidence. Ameghiniana 34:3–32.

Sander, P. M. 2013. An evolutionary cascade model for sauropod dinosaur gigantism–overview, update and tests. PLoS ONE 8:e78573. doi.org/10.1371/journal.pone.0078573

Sekiya, T. 2011. Re-examination of *Chuanjiesaurus anaensis* (Dinosauria: Sauropoda) from the Middle Jurassic Chuanjie Formation, Lufeng County, Yunnan Province, southwest China. Memoir of the Fukui Prefectural Dinosaur Museum 10:1–54.

Sereno, P. C., J. A. Wilson, L. M. Witmer, J. A. Whitlock, A. Maga, O. Ide, and T. A. Rowe. 2007. Structural extremes in a Cretaceous dinosaur. PLoS ONE 2:e1230. doi.org/10.1371/journal.pone.0001230

Sereno, P. C., A. L. Beck, D. B. Dutheil, H. C. E. Larsson, G. H. Lyon, B. Moussa, R. W. Sadleir, C. A. Sidor, D. J. Varricchio, G. P. Wilson, and J. A. Wilson. 1999. Cretaceous sauropods from the Sahara and the uneven rate of skeletal evolution among dinosaurs. Science 286:1342–1347.

Suteethorn, S., J. Le Loeuff, E. Buffetaut, V. Suteethorn, and K. Wongko. 2013. First evidence of a mamenchisaurid dinosaur from the Upper Jurassic-Lower Cretaceous Phu Kradung Formation of Thailand. Acta Palaeontologica Polonica 58:459–469.

Tschopp, E., and O. Mateus. 2013. The skull and neck of a new flagellicaudatan sauropod from the Morrison Formation and its implication for the evolution and ontogeny of diplodocid dinosaurs. Journal of Systematic Palaeontology 11:853–888.

Tschopp, E., O. Mateus, and R. B. J. Benson. 2015a. A specimen-level phylogenetic analysis and taxonomic revision of Diplodocidae (Dinosauria, Sauropoda). PeerJ 3:e857. doi.org/10.7717/peerj.857

Tschopp, E., O. Wings, T. Frauenfelder, and W. Brinkmann. 2015b. Articulated bone sets of manus and pedes of *Camarasaurus* (Sauropoda, Dinosauria). Palaeontologia Electronica 18(2):44A. https://palaeo-electronica.org/content/2015/1284-manus-and-pes-of-camarasaurus

Tsuihiji, T. 2004. The ligament system in the neck of *Rhea americana* and its implication for the bifurcated neural spines of sauropod dinosaurs. Journal of Vertebrate Paleontology 24:165–172.

Ullmann, P. V., M. F. Bonnan, and K. J. Lacovara. 2017. Characterizing the evolution of wide gauge features in stylopodial limb elements of titanosauriform sauropods via geometric morphometrics. Anatomical Record 300:1618–1635.

Upchurch, P. 1994. Manus claw function in sauropod dinosaurs. GAIA, 10:161–171.

Upchurch, P. 1995. The evolutionary history of sauropod dinosaurs. Philosophical Transactions of the Royal Society of London, Series B 349:365–390.

Upchurch, P. 1998. The phylogenetic relationships of sauropod dinosaurs. Zoological Journal of the Linnean Society 124:43–103.

Upchurch, P., and J. Martin, J. 2002. The Rutland *Cetiosaurus*: The anatomy and relationships of a Middle Jurassic British sauropod dinosaur. Palaeontology 45:1049–1074.

Upchurch, P., and J. Martin. 2003. The anatomy and taxonomy of *Cetiosaurus* (Saurischia: Sauropoda) from the Middle Jurassic of England. Journal of Vertebrate Paleontology 23:208–231.

Upchurch, P., P. M. Barrett, and P. Dodson. 2004a. Sauropoda; pp. 259–324 in D. B. Weishampel, P. Dodson, and H. Osmólska, (eds.), The Dinosauria (Second Edition). University of California Press, Berkeley.

Upchurch, P., P. M. Barrett, and P. M. Galton. 2007a. A phylogenetic analysis of basal sauropodomorph relationships: implications for the origin of sauropod dinosaurs. Special Papers in Palaeontology 77:57–90.

Upchurch, P., P. D. Mannion, and P. M. Barrett. 2011. Sauropod dinosaurs; pp. 476–525 In D. J. Batten (ed.), English Wealden Fossils. Palaeontology Association Field Guides to Fossils 14, Palaeontological Association, London.

Upchurch, P., P. D. Mannion, and M. P. Taylor. 2015. The anatomy and phylogenetic Relationships of "*Pelorosaurus*" *becklesii* (Neosauropoda, Macronaria) from the Early Cretaceous of England. PLoS ONE 10:e0125819. doi.org/10.1371/journal.pone.0125819

Upchurch, P., Y. Tomida, and P. M. Barrett. 2004b. A new specimen of *Apatosaurus ajax* (Sauropoda: Diplodocidae) from the Morrison Formation (Upper Jurassic) of Wyoming, USA. National Science Museum Monographs 26:1–108.

Upchurch, P., P. M. Barrett, X.-J. Zhao, and X. Xu. 2007b. A re-evaluation of *Chinshakiangosaurus chunghoensis* Ye vide Dong 1992 (Dinosauria, Sauropodomorpha): implications for cranial evolution in basal sauropod dinosaurs. Geological Magazine 144:247–262.

Voegele, K. K., P. V. Ullmann, M. C. Lamanna, and K. J. Lacovara. 2020. Appendicular myological reconstruction of the forelimb of the giant titanosaurian sauropod dinosaur *Dreadnoughtus schrani*. Journal of Anatomy 237:133–154.

Wang, S. E., and L. J. Gao. 2012. SHRIMP U-Pb dating of zircons from tuff of Jurassic Qigu Formation in Junggar Basin, Xinjiang. Geological Bulletin of China 31:503–509.

Wedel, M. J. 2003. The evolution of vertebral pneumaticity in sauropod dinosaurs. Journal of Vertebrate Paleontology 23:344–357.

Whitlock, J. A. 2011. A phylogenetic analysis of Diplodocoidea (Saurischia: Sauropoda). Zoological Journal of the Linnean Society 161:872–915.

Wilson, J. A. 1999. A nomenclature for vertebral laminae in sauropods and other saurischian dinosaurs. Journal of Vertebrate Paleontology 19:639–653.

Wilson, J. A. 2002. Sauropod dinosaur phylogeny: critique and cladistic analysis. Zoological Journal of the Linnean Society 136:217–276.

Wilson, J. A., and M. T. Carrano. 1999. Titanosaurs and the origin of 'wide-gauge' trackways: a biomechanical and systematic perspective on sauropod locomotion. Paleobiology 25:252–267.

Wilson, J. A., and P. C. Sereno. 1998. Early evolution and higher-level phylogeny of sauropod dinosaurs. Memoir of the Society of Vertebrate Paleontology 5:1–68.

Wilson, J. A., and P. Upchurch, 2003. A revision of *Titanosaurus* Lydekker (Dinosauria – Sauropoda), the first dinosaur genus with a "Gondwanan" distribution. Journal of Systematic Palaeontology 1:125–160.

Wilson, J. A., and P. Upchurch. 2009. Redescription and reassessment of the phylogenetic affinities of *Euhelopus zdanskyi* (Dinosauria: Sauropoda) from the Early Cretaceous of China. Journal of Systematic Palaeontology 7:199–239.

Wilson, J. A., M. D. D'Emic, T. Ikejiri, E. M. Moacdieh, and J. A. Whitlock. 2011. A nomenclature for vertebral fossae in sauropods and other saurischian dinosaurs. PLoS ONE 6:e17114. doi.org/10.1371/journal.pone.0017114

Wiman, C. 1929. Die Kriede-Dinosaurier aus Shantung. Palaeontologia Sinica Series C 6:1–67.

Wings, O., D. Schwarz-Wings, and D. W. Fowler. 2011. New sauropod material from the Late Jurassic part of the Shishugou Formation (Junggar Basin, Xinjiang,NW China). Neues Jahrbuch für Geologie und Paläontologie, Abhandlungen 262:129–150.

Wings, O., M. Rabi, J. Schneider, L. Schwermann, G. Sun, C.-F. Zhou, and W. Joyce. 2012. An enormous Jurassic turtle bone bed from the Turpan Basin of Xinjiang, China. Naturwissenschaften 99:925–935.

Wu, W.-H., C.-F. Zhou, O. Wings, T. Sekiya, and Z.-M. Dong. 2013. A new gigantic sauropod dinosaur from the Middle Jurassic of Shanshan, Xinjiang. Global Geology 32:437–446.

Xing, L, T. Miyashita, J. Zhang, D. Li, Y. Ye, T. Sekiya, F. Wang, and P. J. Currie. 2015. A new sauropod dinosaur from the Late Jurassic of China and the diversity, distribution, and relationships of mamench-isaurids. Journal of Vertebrate Paleontology 35:e889701. doi.org/ 10.1080/02724634.2014.889701

Xu, X., P. Upchurch, P. D. Mannion, P. M. Barrett, O. R. Regalado-Fernandez, J. Mo, J. Ma, and H. Liu. 2018. A new Middle Jurassic diplodocoid suggests an earlier dispersal and diversification of sauropod dinosaurs. Nature Communications 9:2300. doi.org/10.1038/s41467-018-05128-1

Yates, A. M. 2007. The first complete skull of the Triassic dinosaur *Melanorosaurus* Haughton (Sauropodomorpha: Anchisauria). Special Papers in Palaeontology 77:9–55.

Yates, A. M., and J. Kitching. 2003. The earliest known sauropod dinosaur and the first steps towards sauropod locomotion. Proceedings of the Royal Society of London B 270:1753–1758.

Ye, Y., Y.-H. Gao, and S. Jiang. 2005. A new genus of sauropod from Zigong, Sichuan. Vertebrata PalAsiatica 43:175–181.

Ye, Y., H. Ouyang, and Q.-M. Fu. 2001. New material of *Mamenchisaurus hochuanensis* from Zigong, Sichuan. Vertebrata PalAsiatica, 39:266–271.

Young, C. C. 1954. On a new sauropod from Yiping, Szechuan, China. Acta Paleontologica Sinica 2:355–369.

Young, C. C., and X.-J. Chao. 1972. *Mamenchisaurus hochuanensis* sp. nov. Institute of Vertebrate Paleontology and Paleoanthropology Monographs (Series A) 8:1–30.

Zhang, X.-Q., D.-Q. Li, Y. Xie, and H.-L. You. 2020. Redescription of the cervical vertebrae of the mamenchisaurid sauropod *Xinjiangtitan shanshanesis* Wu et al. 2013. Historical Biology 32(6):802–822.

Zhao, X.-J. 1980. Mesozoic vertebrate-bearing beds and stratigraphy of northern Xinjiang. Memoirs of the Institute of Vertebrate Paleontology and Paleoanthropology, Academica Sinica 16:1–120.

Zhao, X.-J. 1993. [A new mid-Jurassic sauropod (*Klamelisaurus gobiensis* gen. et sp. nov.) from Xinjiang, China]. Vertebrata PalAsiatica 31:132–138. [In Chinese with English summary]

Zurriaguz, V. L., and I. A. Cerda. 2017. Caudal pneumaticity in derived titanosaurs (Dinosauria: Sauropoda). Cretaceous Research 73:14–24.

Zurriaguz, V., A. Martinelli, G. W. Rougier, and M. D. Ezcurra. 2017. A saltasaurine titanosaur (Sauropoda: Titanosauriformes) from the Angostura Colorada Formation (upper Campanian, Cretaceous) of northwestern Patagonia, Argentina. Cretaceous Research 75:101–114.